CNES CENTRE NATIONAL D'ÉTUDES SPATIALES	**Orbital Systems Directorate** **Radiofrequency Department** Instrumentation Telemetry/Telecommand & Propagation Department **Non sensitive**	Réf : **DSO/RF/ITP-2020.0032915** Date : **27/08/2020** Edition : **2**, Révision : **0**

TECHNICAL NOTE
« IMPROVEMENT OF THE TROPOSPHERIC PROPAGATION INSTANTANEOUS AND STATISTICAL MODELS FOR EARTH-SPACE PATHS»

	Name, CNES entity	Date and Signature
Prepared by	**Xavier BOULANGER** **DSO/RF/ITP** **Specialist in RF Propagation in charge of tropospheric propagation thematic**	Boulanger Xavier 2021.04.14 14:59:19 +02'00'
Verified by	**Bouchra BENAMMAR** **DSO/RF/ITP** **Specialist in RF and Optical Propagation**	Benammar Bouchra Signature numérique de Benammar Bouchra DN : c=FR, o=CNES, ou=0002 775665912, ou=Agents CNES, 2.5.4.45=benammb@cnes.fr, cn=Benammar Bouchra Date : 2021.04.14 15:15:38 +02'00'
Authorised by	**Clément DUDAL** **Head of DSO/RF/ITP Division**	Dudal Clement Signature numérique de Dudal Clement DN : c=FR, o=CNES, ou=0002 775665912, ou=Agents CNES, 2.5.4.45=dudalc@cnes.fr, cn=Dudal Clement Date : 2021.04.14 16:19:38 +02'00'

INTERNAL/EXTERNAL DISTRIBUTION LIST			
CNES entity/ Company Organisation	**Name (+email address if external)**	**Observation for**	
		Action	**Information**
DSO/RF/D	D. PRADINES		x
DSO/RF/DA	C. LAPORTE		x
DSO/RF/ITP	ALL		x
DSO/NT/ST	ALL		x
ONERA	L. CASTANET (Laurent.Castanet@onera.fr)		x

INDEXATION

Authors: **Xavier BOULANGER**		
Title/Scope: This technical note describes CNES internal research activities on tropospheric propagation instantaneous and statistical models for Earth-Space paths between 1 and 350 GHz.		
Configuration management: **No**	Date:	By :
Contract : **Not applicable**		

MODIFICATION DIRECTORY

Issue	Date	Evolutions
1.0	**27/08/2020**	Creation
2.0	**27/01/2021**	Update of Section 2 with 30 years of ERA5 data Update of Section 4 • Update of the model of Section 4.1 with new data of Section 2 • New Section 4.2 Update of Section 5 • New section 5.1 • Update of the models of Section 5.2 with new data of Section 2 • New Section 5.3 Update of Section 6 • Update of the model of Section 6.1 with new data of Section 2 • New Section 6.2

TERMS, DEFINITIONS AND ABBREVIATIONS

Acronym : Abbreviation	Definition
CCDF	Complementary Cumulative Distribution Function
DEM	Digital Elevation Model
ECMWF	European Centre for Medium-Range Weather Forecasts
GEO	Geostationary Earth Orbit
ITU-R	International Telecommunication Union – Radiocommunication Sector
ILWC	Integrated Liquid Water Content (total columnar content of cloud liquid water)
ISL	Inter-Satellite Link
IWVC	Integrated Water Vapour Content (total columnar content of water vapour)
Ka-band	20-30 GHz (space communications)
Ku-band	10-14 GHz (space communications)
LEO	Low Earth Orbit
Q/V-band	40-50 GHz (space communications)
SG3	Study Group 3 of ITU-R
W-band	70-90 GHz (space communications)

VARIABLES MEMO

Variable	Definition	Unit
φ	Latitude	°N
λ	Longitude	°E
θ	Elevation	°
f	Frequency	GHz
p	Probability of exceedance (for a CCDF)	%
Z	Geometric height (above mean sea level)	km
H	Geopotential height (above mean sea level)	km
h_s	Height above mean sea level of the surface of the Earth	km
P	Total pressure	hPa
P_s	Total pressure at the surface of the Earth	hPa
$\overline{P_s}$	Mean of P_s for a given period (e.g. annual or monthly mean)	hPa
T	Temperature	K
T_s	Temperature at the surface of the Earth	K
$\overline{T_s}$	Mean of T_s for a given period (e.g. annual or monthly mean)	K
T_d	Dewpoint temperature	K
T_{d_s}	Dewpoint temperature at the surface of the Earth	K
RH	Relative humidity	%
RH_s	Relative humidity at the surface of the Earth	%
ρ_w	Water vapour density	g/m^3
ρ_{w_s}	Water vapour density at the surface of the Earth	g/m^3
$\overline{\rho_{w_s}}$	Mean of ρ_{w_s} for a given period (e.g. annual or monthly mean)	g/m^3
h_{VSC}	Water vapour scale height	km
$\overline{h_{VSC}}$	Mean of h_{VSC} for a given period (e.g. annual or monthly mean)	km
ρ_l	Cloud liquid water density	g/m^3
γ_o	Oxygen specific attenuation	dB/km
h_o	Oxygen equivalent height	km
A_O	Attenuation due to oxygen	dB
γ_w	Water vapour specific attenuation	dB/km
h_w	Water vapour equivalent height	km
K_V	Water vapour absorption coefficient	dB/(kg/m^2)
V	Total columnar content of water vapour (equivalent and equal to IWVC)	kg/m^2 (or mm)
A_W	Attenuation due to water vapour	dB
γ_c	Cloud liquid water specific attenuation	dB/km
K_l	Cloud liquid water specific attenuation coefficient	(dB/km)/(g/m^3)

K_L	Cloud liquid water absorption coefficient	dB/(kg/m^2)
L	Total columnar content of cloud liquid water (equivalent and equal to ILWVC)	kg/m^2 (or mm)
A_C	Attenuation due to clouds	dB

TABLE OF CONTENTS

1 INTRODUCTION

1.1 OBJECT AND CONTENT OF THE DOCUMENT

This technical note describes CNES internal research activities on tropospheric propagation instantaneous and statistical models for Earth-Space paths between 1 and 350 GHz. It presents revisions to the existing recommended prediction methods in Recommendation ITU-R P.676-12, Recommendation ITU-R P.835-6, Recommendation ITU-R P.836-6, Recommendation ITU-R P.840-8, and Recommendation ITU-R P.1510-1.

The content of this technical note is the following:

- Section 2 provides a methodology to derive the atmospheric profiles parameters from the up-to-date ECMWF reanalysis database: ERA5. New digital maps of the mean (annual, seasonal, monthly) vertical atmospheric profiles are computed. These maps will then be used to develop new prediction methods of oxygen, water vapour, and cloud attenuation.
- Section 3 gives a brief analysis on the impact of area on the surface of the Earth for regular latitude/longitude grids. This is a key point for the development and the global test of propagation models.
- Section 4 provides a framework for new prediction methods of the instantaneous oxygen attenuation and the statistical distribution of oxygen attenuation. In particular, the new maps of the mean annual vertical atmospheric profiles are used to develop a new model of the **oxygen equivalent height** from 1 to 350 GHz. The performances of the new models are assessed with a comparison to radiosounding observations.
- Section 5 provides a framework for new prediction methods of the instantaneous water vapour attenuation and the statistical distribution of water vapour attenuation. In particular, the new maps of the mean annual vertical atmospheric profiles are used to develop new models of the **water vapour equivalent height** and the **water vapour absorption coefficient** from 1 to 350 GHz. The performances of the new models are assessed with a comparison to radiosounding observations.
- Section 6 provides a framework for new prediction methods of the instantaneous cloud attenuation and the statistical distribution of cloud attenuation. In particular, the new maps of the mean annual vertical atmospheric profiles are used to develop a new model of the **cloud liquid water absorption coefficient** from 1 to 200 GHz. The performances of the new models are assessed with a comparison to radiosounding observations.

1.2 CONTEXT

This study falls within the tropospheric propagation thematic roadmaps of the division DSO/RF/ITP.

ITU-R SG3, and in particular Working Parties 3J and 3M, have recently approved several roadmaps on the improvement of the prediction methods of Earth-Space propagation. Among all ITU-R SG3 Recommendations, 4 are of interest:

- ITU-R P.676-12 which provides several models to derive attenuation by atmospheric gases
- ITU-R P.835-6 which provides a set of reference standard atmospheres
- ITU-R P.836-6 which provides digital maps of surface water vapour density and total columnar content of water vapour
- ITU-R P.840-8 which provides several models to derive attenuation due to clouds and fog

Several ITU-R SG3 Correspondence Groups (CG) have been established to work on these specific topics.

1.3 DOCUMENTATION

1.3.1 APPLICABLE DOCUMENTS

Reference	Title
AD 1 : FdR_Propa_RF_Tropo	Tropospheric propagation thematic roadmap, internal CNES document
AD 2 : Programme d'Intérêt Commun	Déclaration de lancement de la phase 2 du Programme d'Intérêt Commun (PIC) PERF: Propagation Electromagnétique Radio-Fréquence, 24/01/2020

1.3.2 REFERENCE DOCUMENTS

Reference	Title
RD 1 : ITU-R P.676-12	Recommendation ITU-R P.676-12, "Attenuation by atmospheric gases and related effects", Geneva, August 2019
RD 2 : ITU-R P.835-6	Recommendation ITU-R P.835-6, "Reference standard atmospheres", Geneva, December 2017
RD 3 : ITU-R P.836-6	Recommendation ITU-R P.836-6, "Water vapour: surface density and total columnar content", Geneva, December 2017
RD 4 : ITU-R P.840-8	Recommendation ITU-R P.840-8, "Attenuation due to clouds and fog" , Geneva, August 2019

2 NEW REFERENCE DATABASE OF ATMOSPHERIC PROFILES

MAIN OBJECTIVES OF THIS SECTION:

- Provide a methodology to derive the atmospheric profiles parameters from the new ECMWF reanalysis database: ERA5
- Provide new digital maps of the mean (annual, seasonal, monthly) vertical atmospheric profiles that will be used to develop new prediction methods of gaseous and cloud attenuation

2.1 DESCRIPTION OF THE ECMWF REANALYSIS DATABASE: ERA5

The following italic paragraphs have been extracted from [1]:

"ERA5 is the fifth generation ECMWF atmospheric reanalysis of the global climate. Reanalysis combines model data with observations from across the world into a globally complete and consistent dataset using the laws of physics. This principle, called data assimilation, is based on the method used by numerical weather prediction centres, where every so many hours (12 hours at ECMWF) a previous forecast is combined with newly available observations in an optimal way to produce a new best estimate of the state of the atmosphere, called analysis, from which an updated, improved forecast is issued. Reanalysis works in the same way, but at reduced resolution to allow for the provision of a dataset spanning back several decades. Reanalysis does not have the constraint of issuing timely forecasts, so there is more time to collect observations, and when going further back in time, to allow for the ingestion of improved versions of the original observations, which all benefit the quality of the reanalysis product.

The assimilation system is able to estimate biases between observations and to sift good-quality data from poor data. The laws of physics allow for estimates at locations where data coverage is low, such as for surface temperature in the Arctic. The provision of estimates at each grid point around the globe for each regular output time, over a long period, always using the same format, makes reanalysis a very convenient and popular dataset to work with.

The observing system has changed drastically over time, and although the assimilation system can resolve data holes, the initially much sparser networks will lead to less accurate estimates. For this reason, ERA5 includes an uncertainty estimate that provides guidance on where products are expected to be more and where less accurate.

When complete, ERA5 will contain a detailed record of the evolution of the global atmosphere from 1950 onwards with a total size of about 9 Petabytes. ERA5 will replace the ERA-Interim reanalysis, which is now 10 years old.

Although the analysis procedure considers chunks of data in a window of 12 hours in one go, ERA5 provides estimates for each hour of the day, worldwide. This is made possible by the 4D-Var assimilation method, which takes account of the exact timing of the observations and model evolution within the assimilation window. This hourly output resolution is quite an improvement with respect to ERA-Interim, and provides a more detailed evolution of particular weather events.

Variables are produced at the surface and on model levels but are also interpolated to three other level types: pressure levels, potential temperature levels and one potential vorticity level."

The full documentation can be found in [2].

2.1.1 DESCRIPTION OF THE PARAMETERS

Basically, ERA5 provides worldwide reanalysis data (single and pressure levels) with the following characteristics:

- Spatial resolution of 0.25° in both latitude and longitude,
- Temporal resolution of 1 h,
- 37 pressure levels (for pressure level data) with an upper altitude of about 45 km,
- Database extends from 1979. It will ultimately be extended from 1950.

Due to the size of data files, downloading global hourly profiles for several years is prohibitive; however, ECMWF also provides monthly averaged (global and by hour of the day) pressure level data, which is the data considered in this analysis. Among all the parameters available in the ERA5 monthly averaged data on pressure levels, the following five location-specific parameters are of interest in this analysis:

- **Pressure** (hPa): This parameter is the total barometric pressure fixed at 1, 2, 3, 5, 7, 10, 20, 30, 50, 70, 100, 125, 150, 175, 200, 225, 250, 300, 350, 400, 450, 500, 550, 600, 650, 700, 750, 775, 800, 825, 850, 875, 900, 925, 950, 975, and 1000 hPa.
- **Temperature** (K): This parameter is the temperature at each pressure level.
- **Specific humidity** ($kg \cdot kg^{-1}$): This parameter is the mass of water vapour per kilogram of moist air. The total mass of moist air is the sum of the dry air, water vapour, cloud liquid, cloud ice, rain, and falling snow.
- **Specific cloud liquid water content** ($kg \cdot kg^{-1}$): This parameter is the mass of cloud liquid water droplets per kilogram of the total mass of moist air. It represents the average value for a grid box. Water within clouds can be liquid or ice, or a combination of the two.
- **Geopotential** ($m^2 \cdot s^{-2}$): This parameter is the gravitational potential energy of a unit mass at each pressure level, relative to mean sea level. Geopotential is also the amount of work, against the force of gravity, to lift a unit mass to the height of that location above mean sea level. The geopotential height can be calculated by dividing the geopotential by the Earth's gravitational acceleration, g_0 (=9.80665 $m \cdot s^{-2}$). The geopotential height plays an important role in synoptic meteorology (analysis of weather patterns). Charts of geopotential height plotted at constant pressure levels (e.g., 300, 500, or 850 hPa) can be used to identify weather systems such as cyclones, anticyclones, troughs, and ridges. At the surface of the

Earth, this parameter shows the variations in geopotential (height) of the surface, and is often referred to as the orography.

2.1.2 SPATIAL REFERENCE SYSTEM

The ERA5 latitude and longitude are geodetic, rather than geocentric, and are referenced to the WGS-84 ellipsoid. The ERA5 geopotential height relative to mean sea level, H_{ERA}, is the ERA5 geopotential ($m^2 \cdot s^{-2}$) divided by 9.80665 $m \cdot s^{-2}$, where mean sea level is defined as the geoid specified by the U.S. National Geospatial-Intelligence Agency (NGA) Earth Gravitational Model EGM96.

2.1.3 CONVERSION OF GEOPOTENTIAL HEIGHT INTO GEOMETRIC HEIGHT

The variation of gravity with height must take into account the ellipsoidal shape of the Earth and the centrifugal force due to the Earth's rotation. The relationship between the geometric height Z (km) and the geopotential height H (km) is:

$$H = \frac{G(\varphi)R(\varphi)Z}{R(\varphi) + Z}$$

and

$$Z = \frac{R(\varphi)H}{G(\varphi)R(\varphi) - H}$$

where $G(\varphi) = \frac{g(\varphi)}{g_0}$ and $g_0 = 9.80665$ m $\cdot s^{-2}$.

$R(\varphi)$, the effective radius of the Earth vs latitude, φ, in the Smithsonian tables, accounts for the variations in the radius of the Earth and centrifugal force vs latitude. It is not the actual radius of the Earth at the given latitude. The Smithsonian radius increases from the equator to high latitudes; however, the actual radius of the Earth's ellipsoid is largest at the equator and smallest at the poles.

As the values for $R(\varphi)$ in the Smithsonian tables were obtained around 1949, the International Ellipsoid 1935 was used in the computations rather than the World Geodetic System 1984 (WGS-84) currently used with GPS receivers. Also, the Smithsonian tables used a value for $R(\varphi)$ (km) and $g(\varphi)$ ($m \cdot s^{-2}$) of:

$$R(\varphi) = \frac{2g(\varphi)}{-\left(\frac{\partial g(\varphi)}{\partial Z}\right)_{Z=0}}$$

where:

$$g(\varphi) = 9.80616 \times \left(1 - 0.0026373 \cdot \cos(2\varphi) + 0.0000059 \cdot \cos^2(2\varphi)\right)$$

and

$$-\left(\frac{\partial g(\varphi)}{\partial Z}\right)_{Z=0} = 3.085462 \times 10^{-3} + 2.27 \times 10^{-6} \cdot \cos(2\varphi) - 2 \times 10^{-9} \cdot \cos(4\varphi)$$

An alternative expression has been proposed by Mahoney[1] (personal communication), based on the WGS-84 geoid, which provides similar results to the values in the Smithsonian tables:

$$g(\varphi) = 9.780325 \frac{1 + 0.00193185 \cdot \sin^2(\varphi)}{\sqrt{1 - 0.00669435 \cdot \sin^2(\varphi)}}$$

and

$$R(\varphi) = \frac{6\,378.137}{1.006803 - 0.006706 \cdot \sin^2(\varphi)}$$

Since Mahoney's formulation is cited in WMO reference material, it is used in the following analysis.

2.1.4 CONVERSION OF SPECIFIC CONTENT INTO DENSITY

The computation of the moist air density, $\rho_{moistair}$ (kg·m^{-3}) is critically needed to convert both:

- specific humidity, q_w (kg·kg^{-1}) into water vapour density, ρ_w (g·m^{-3}), and
- specific cloud liquid water content, q_l (kg·kg^{-1}), into cloud liquid water density, ρ_l (g·m^{-3}),

The moist air density, $\rho_{moistair}$ (kg·m^{-3}) can be retrieved from:

$$\rho_{\text{moistair}} = \frac{P}{R_d T}\left(\frac{1 + w_w}{1 + w_w \frac{R_v}{R_d}}\right)$$

with:

- $R_d = 287.058$ J·kg^{-1}·K^{-1}
- $R_v = 461.52$ J·kg^{-1}·K^{-1}
- $w_w = \frac{q_w}{1-q_w}$
- P is the total pressure in Pa
- T is the temperature in K

Consequently,

$$\rho_w = 1000 \cdot q_w \cdot \rho_{moistair}$$

$$\rho_l = 1000 \cdot q_l \cdot \rho_{moistair}$$

[1] https://wahiduddin.net/calc/refs/measures_of_altitude_mahoney.html, equations (17) and (20).

2.2 DERIVATION OF NEW DIGITAL MAPS

According to the WMO definition of the climate normals, new worldwide digital maps of the mean (annual, seasonal, monthly) vertical atmospheric profiles have been derived from 30 years (from 1991 to 2020) of monthly averaged profiles. The maps consist of weighted means (by the number of days in the considered month) of a given parameter (temperature, water vapour density, cloud liquid water density and altitude) for a given pressure level.

Figure 2-1, Figure 2-2, and Figure 2-3 show the mean annual vertical profiles of temperature, water vapour density, and cloud liquid water density derived from the ERA5 monthly averaged database (1991-2020).

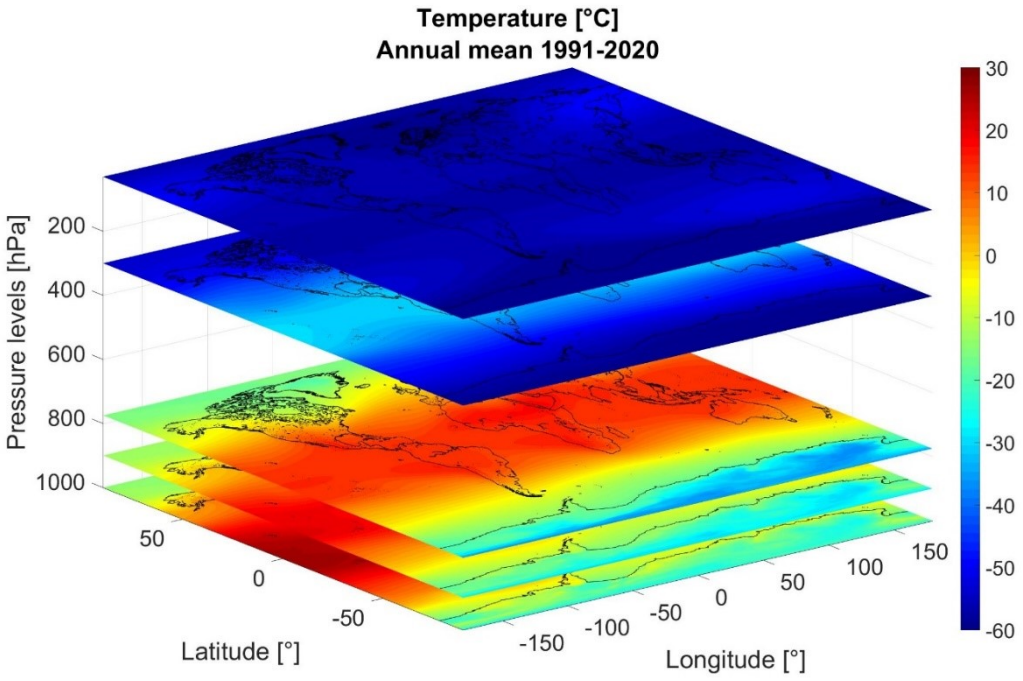

Figure 2-1 : Mean annual vertical profiles of temperature derived from the ERA5 monthly averaged database (1991-2020)

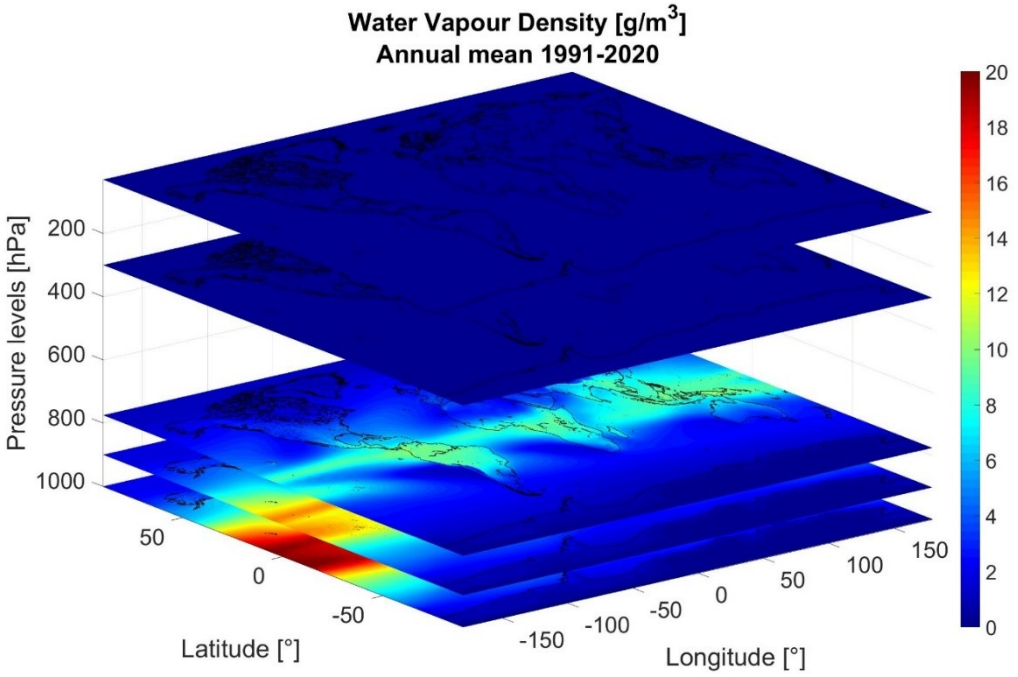

Figure 2-2 : Mean annual vertical profiles of water vapour density derived from the ERA5 monthly averaged database (1991-2020)

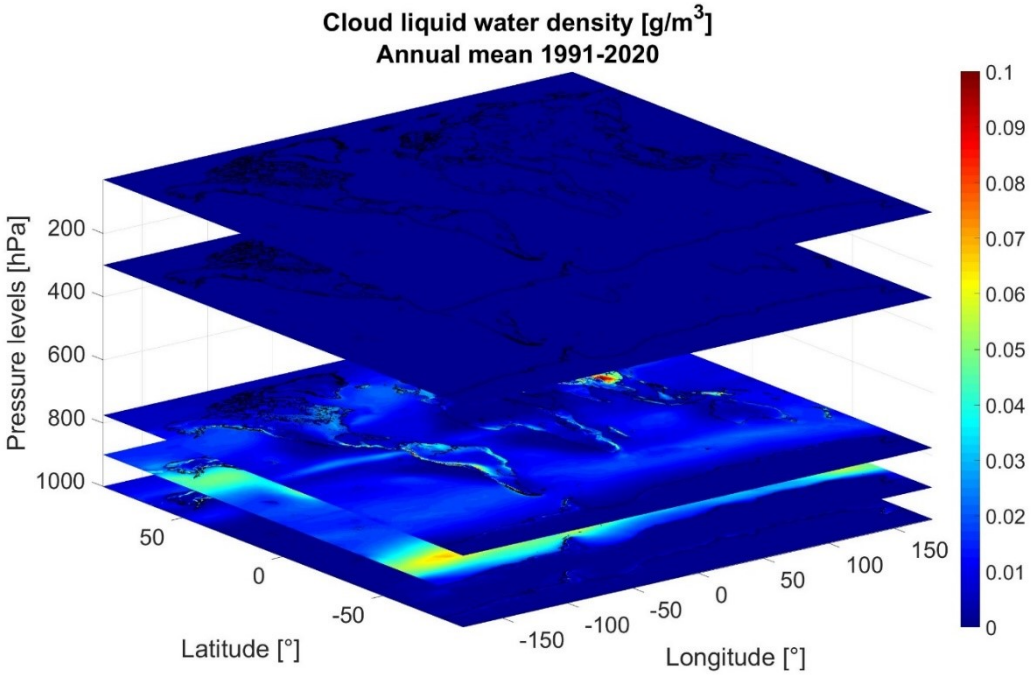

Figure 2-3 : Mean annual vertical profiles of cloud liquid water density derived from the ERA5 monthly averaged database (1991-2020)

3 IMPACT OF AREA ON THE SURFACE OF THE EARTH FOR REGULAR LATITUDE/LONGITUDE GRIDS

One of the main drawbacks of using regular grids in latitude and longitude for both the development and the test of global propagation prediction methods is the fact that the weight of each grid point is the same. However, the area on the surface of the Earth for a given grid cell is increasing from the equator to the poles. It means that the weight given to the grid point on the equator should be more important than over the poles. The area *A* (km) of a latitude(φ)-longitude(λ) rectangle is:

$$A = \frac{\pi}{180} \cdot R_E^2 \cdot \left|\sin\varphi_1 - \sin\varphi_2\right| \cdot \left|\lambda_1 - \lambda_2\right|$$

where R_E is the Earth radius.

For the WGS84 ellipsoid, the distance from the Earth's centre to a point on the spheroid surface at geodetic latitude φ is given by:

$$R_E = R_E(\varphi) = \sqrt{\frac{(a^2\cos\varphi)^2 + (b^2\sin\varphi)^2}{(a\cos\varphi)^2 + (b\sin\varphi)^2}}$$

where a = 6378.137 km and b = 6356.7523142 km.

It can be verified that $R_E(0) = a$ and $R_E(90) = b$.

Noting $\Delta\varphi = \varphi_1 - \varphi_2$ and $\Delta\lambda = \lambda_1 - \lambda_2$ the grid cell resolution in latitude and longitude respectively, the area *A* (km) for a given latitude φ can then be computed from:

$$A(\varphi) = \frac{\pi}{180} \cdot R_E^2(\varphi) \cdot \left|2\sin\frac{\Delta\varphi}{2}\cos\varphi\right| \cdot \left|\Delta\lambda\right|$$

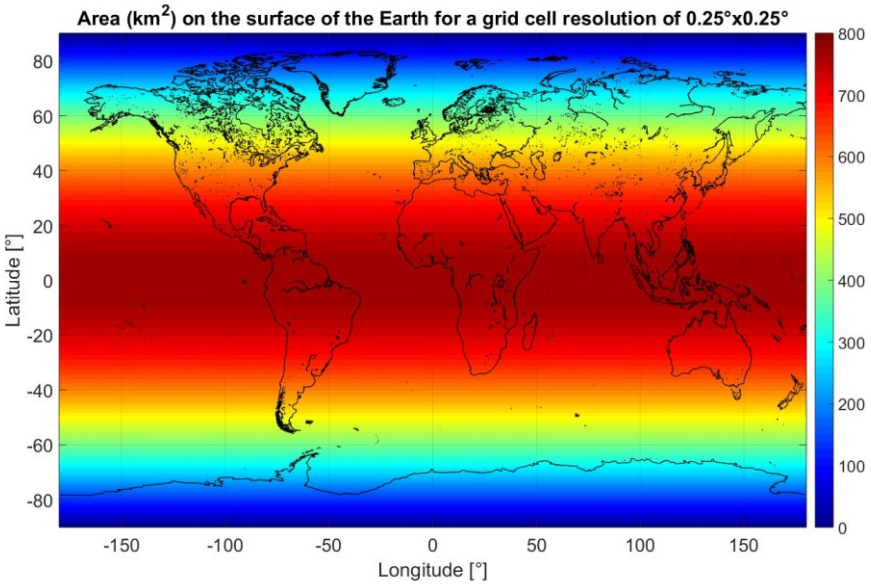

Figure 3-1 : Area (km²) on the surface of the Earth for a grid cell resolution of 0.25°x0.25°

4 NEW PREDICTION METHODS OF OXYGEN ATTENUATION

MAIN OBJECTIVES OF SECTION 4.1:

- Use of the new maps of the mean annual vertical atmospheric profiles to develop a new model of the **oxygen equivalent height** for the prediction of oxygen attenuation from surface meteorological parameters
- Verification and comparison of the performances of the new model with the prediction methods described in Section 2.2 of Annex 2 of Recommendations ITU-R P.676-11 and ITU-R P.676-12
- Test of the new model using radiosounding observations.

MAIN OBJECTIVES OF SECTION 4.2:

- Derivation of a new prediction method of the statistical distribution of oxygen attenuation
- Derivation of new digital maps of the surface pressure, surface temperature, surface relative humidity, and surface water vapour density for a worldwide application of the new prediction method in absence of local data

A block diagram of this Section is proposed in Figure 4-1.

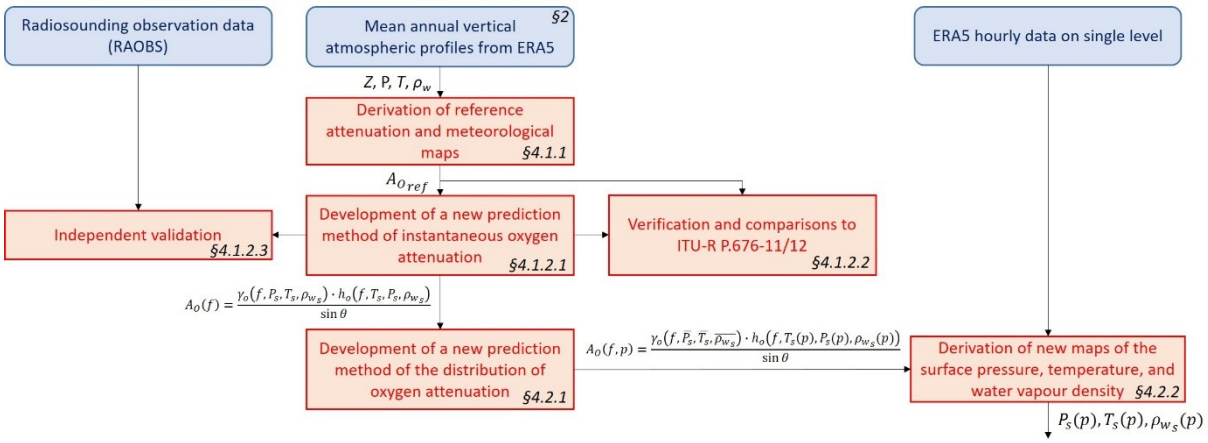

Figure 4-1 : Block diagram of Section 4

4.1 NEW PREDICTION METHOD OF THE INSTANTANEOUS OXYGEN ATTENUATION

4.1.1 METHODOLOGY TO DERIVE REFERENCE MAPS

Section 1 of Annex 1 of ITU-R P.676-12 [RD 1] is used to compute the oxygen specific attenuation profiles, $\gamma_o(Z)$, from the worldwide total pressure, $P(Z)$, temperature, $T(Z)$, and water vapour density, $\rho_w(Z)$, profiles given by the new maps of the mean annual vertical atmospheric profiles provided in Section 2.2 of this document.

Reference zenith oxygen attenuation maps, $A_{O_{ref}}$, are then derived from the integration of $\gamma_o(Z)$ along the profiles according to the methodology described in Section 2 of Annex 1 of ITU-R P.676-12 [RD 1]. This process has been performed **from 1 to 350 GHz** (validity range of Annex 2 of ITU-R P.676-12) with a frequency step of 1 GHz. The reference zenith oxygen attenuation maps at 20, 40, 50, and 80 GHz (frequencies currently used in SatCom systems) are shown in Figure 4-2.

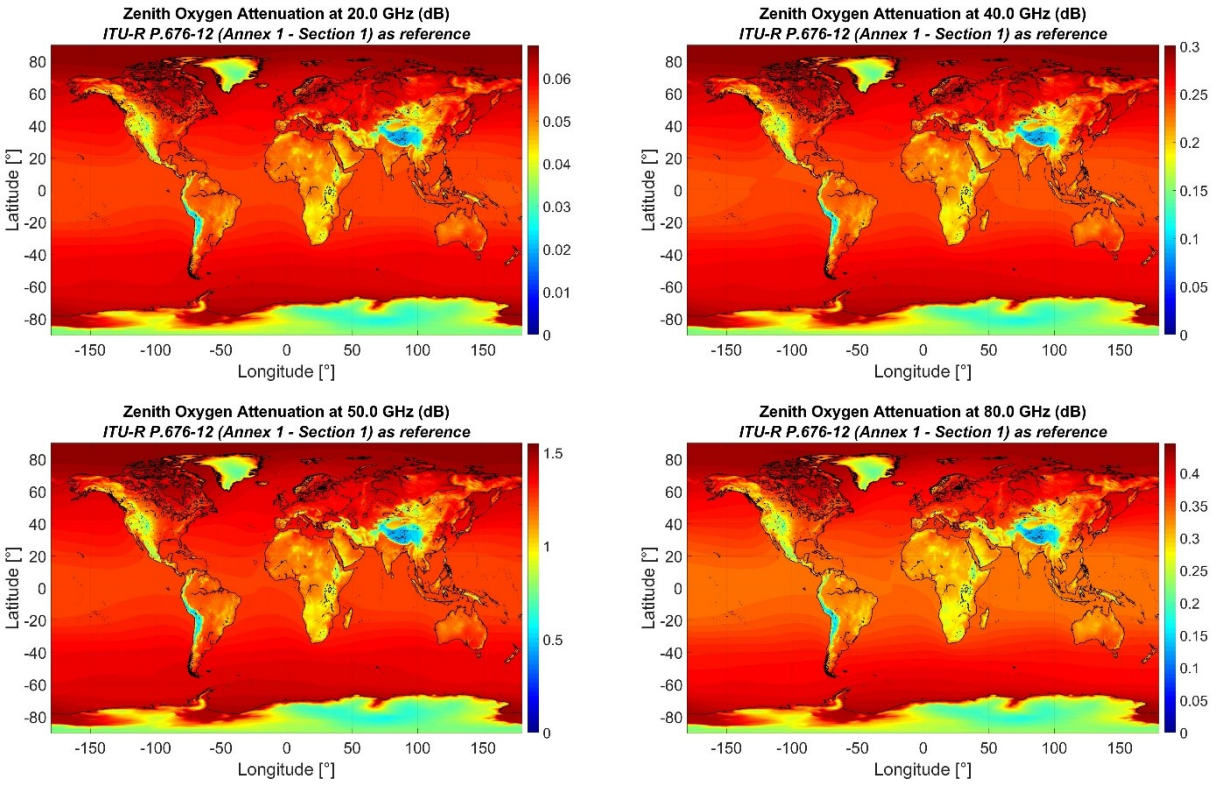

Figure 4-2 : Zenith Oxygen Attenuation at 20, 40, 50, and 80 GHz derived from the integration of the oxygen specific attenuation along the new ERA5 annual profiles by using Annex 1 of ITU-R P.676-12

4.1.2 NEW MODEL OF THE OXYGEN EQUIVALENT HEIGHT

4.1.2.1 DESCRIPTION

The idea is to propose a new model to compute the oxygen equivalent height, h_o (in km), such that oxygen attenuation can be easily derived from:

$$A_O = \frac{\gamma_{o_S} \cdot h_o}{\sin\theta}$$

where γ_{o_S} (in dB/km) is the oxygen specific attenuation at the surface of the Earth and θ the elevation angle (θ>5°).

The new proposed model has been derived by applying the following step-by-step procedure:

1. for each frequency, *f*, between 1 and 350 GHz, a global map of optimal values of $h_o(f)$, called $h_{o_{opt}}(f)$, is computed by dividing the reference zenith oxygen attenuation map, $A_{O_{ref}}(f)$, by the oxygen specific attenuation at the surface of the Earth, $\gamma_{o_S} = \gamma_o(f, P_s, T_s, \rho_{w_S})$, where P_s (hPa), T_s (K), and ρ_{w_S} (g/m^3) are the surface total pressure, temperature and water vapour density, respectively. It means that the following computation is performed:

$$h_{o_{opt}}(f) = \frac{A_{O_{ref}}(f)}{\gamma_o(f, P_s, T_s, \rho_{w_S})}$$

Examples at 20 GHz and 80 GHz are given below:

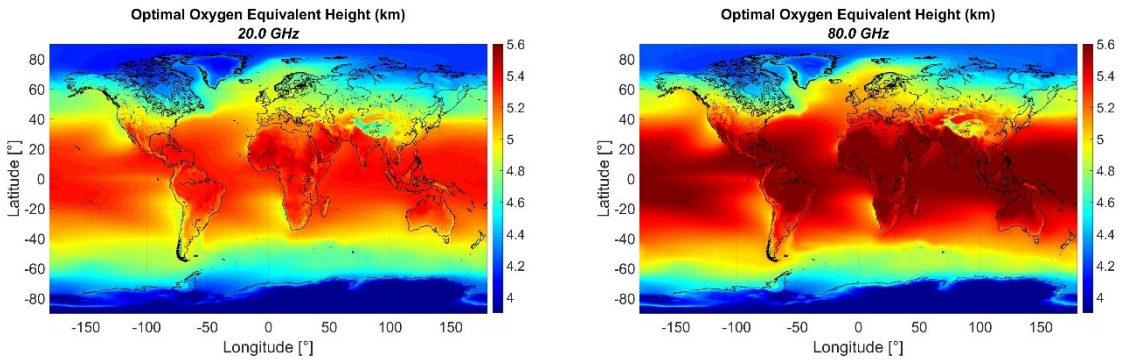

2. for each frequency, *f*, between 1 and 350 GHz, a linear relationship between $h_{o_{opt}}(f)$ and the surface total pressure, temperature and water vapour density is found. Four different models are tested:

   a. $h_{o_{opt}}(f) = h_{o_{opt}}(f, T_s) = a_o(f) + b_o(f) \cdot T_s$

   b. $h_{o_{opt}}(f) = h_{o_{opt}}(f, T_s, P_s) = a_o(f) + b_o(f) \cdot T_s + c_o(f) \cdot P_s$

   c. $h_{o_{opt}}(f) = h_{o_{opt}}(f, T_s, \rho_{w_S}) = a_o(f) + b_o(f) \cdot T_s + d_o(f) \cdot \rho_{w_S}$

d. $h_{o_{opt}}(f) = h_{o_{opt}}(f, T_s, P_s, \rho_{w_s}) = a_o(f) + b_o(f) \cdot T_s + c_o(f) \cdot P_s + d_o(f) \cdot \rho_{w_s}$

It has to be noticed that the linear regression has been performed by weighting each grid point (pixel) by the area on the surface of the Earth as explained in Section 3 of this document. Examples of the retrieval of the oxygen equivalent height (using model d.) are given below:

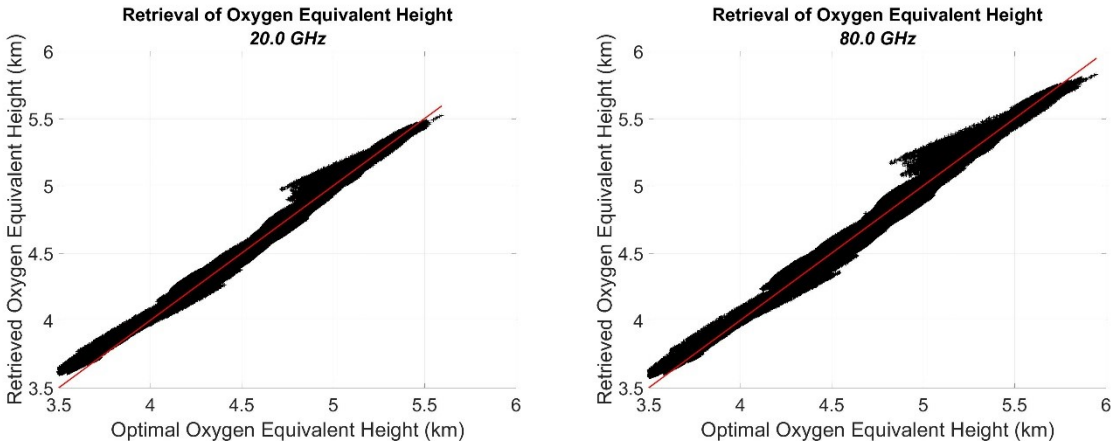

3. The absolute (in m) and relative (in %) RMS errors between the optimal oxygen equivalent height and the proposed models are computed

The results of the linear regressions are given in Figure 4-3 where the specific values of the coefficients a_o, b_o, c_o, and d_o are highlighted.

The absolute and relative RMS errors between the optimal oxygen equivalent height and the proposed models are shown in Figure 4-4. It can be observed that adding more surface parameters improves the global performances of the model.

Finally, for a given frequency, *f*, the final new prediction method of the instantaneous oxygen attenuation based on the oxygen equivalent height is:

$$A_O(f, P_s, T_s, \rho_{w_s}) = \frac{\gamma_o(f, P_s, T_s, \rho_{w_s}) \cdot h_o(f, T_s, P_s, \rho_{w_s})}{\sin\theta}$$

with $h_o(f, T_s, P_s, \rho_{w_s}) = a_o(f) + b_o(f) \cdot T_s + c_o(f) \cdot P_s + d_o(f) \cdot \rho_{w_s}$.

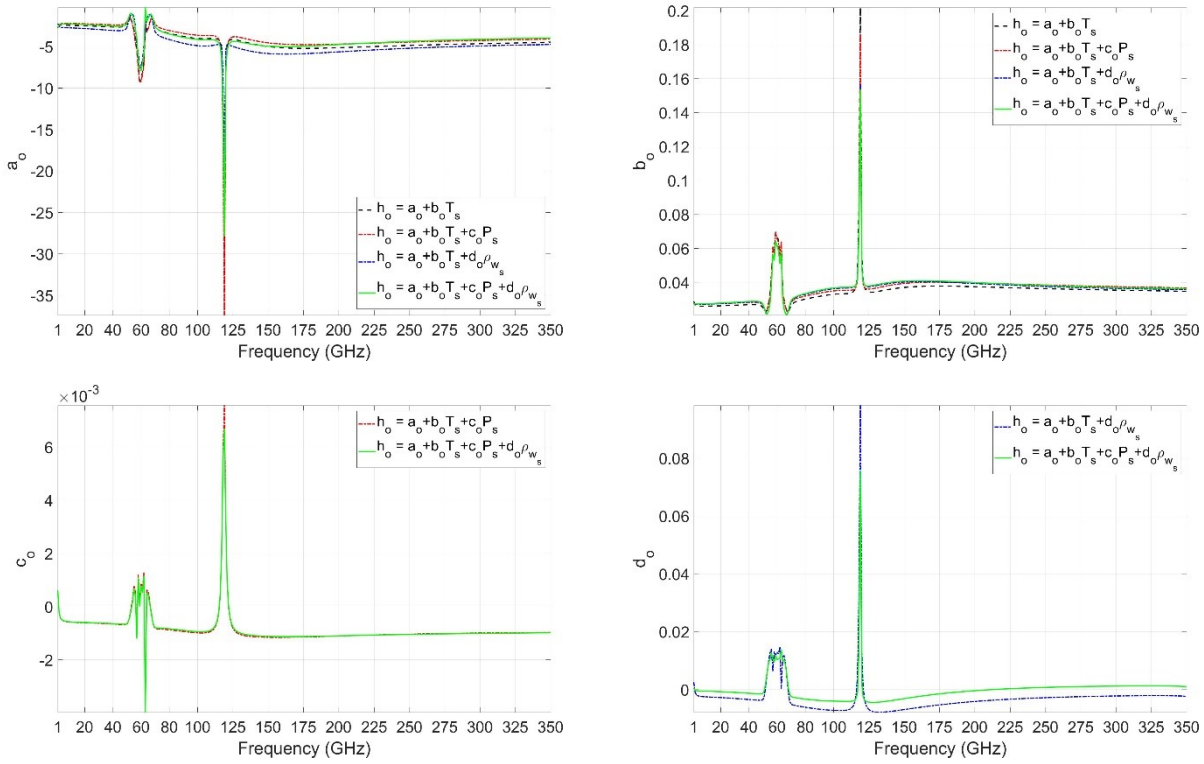

Figure 4-3 : a_o, b_o, c_o, and d_o coefficients of the new model of the oxygen equivalent height

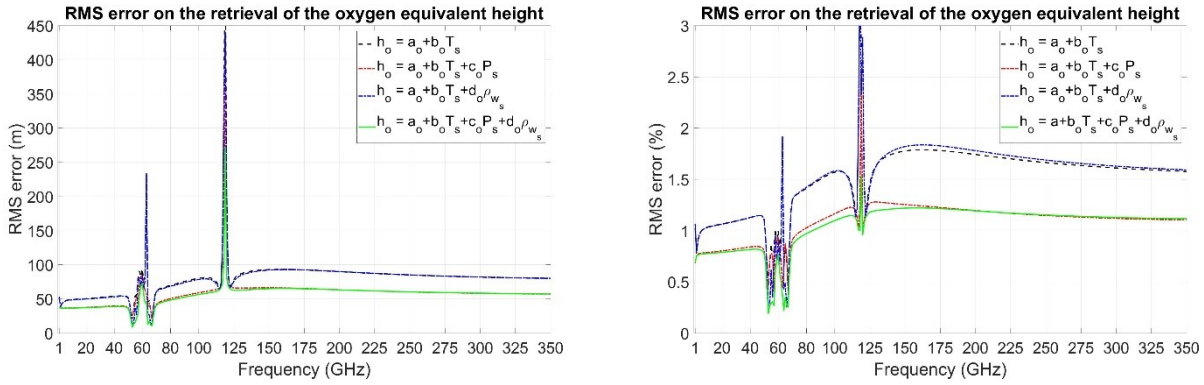

Figure 4-4 : Absolute (left) and relative (right) RMS errors of the new model of the oxygen equivalent height

4.1.2.2 VERIFICATION AND COMPARISONS TO ITU-R P.676-11 AND ITU-R P.676-12

The two prediction methods of Sections 2.2 of Annex 2 of ITU-R P.676-11 and ITU-R P.676-12 and the new model have been tested using the new mean annual maps provided in Section 2.2 of this document. First, the worldwide absolute and relative errors for the selected frequencies between 1 and 350 GHz are computed. Some illustrations of the relative errors at 20, 40, 50 and 80 GHz are shown in Figure 4-5. Finally, Figure 4-6 highlights the relative mean and RMS errors from 1 to 350 GHz. It can be observed that the new model performs largely better than Sections 2.2 of ITU-R P.676-11 and ITU-R P.676-12 over the full range of frequency from 1 to 350 GHz. Indeed, the relative RMS errors for ITU-R P.676-11 and ITU-R P.676-12 are around 9% and 6%, respectively, while for the new model, it is around 1%.

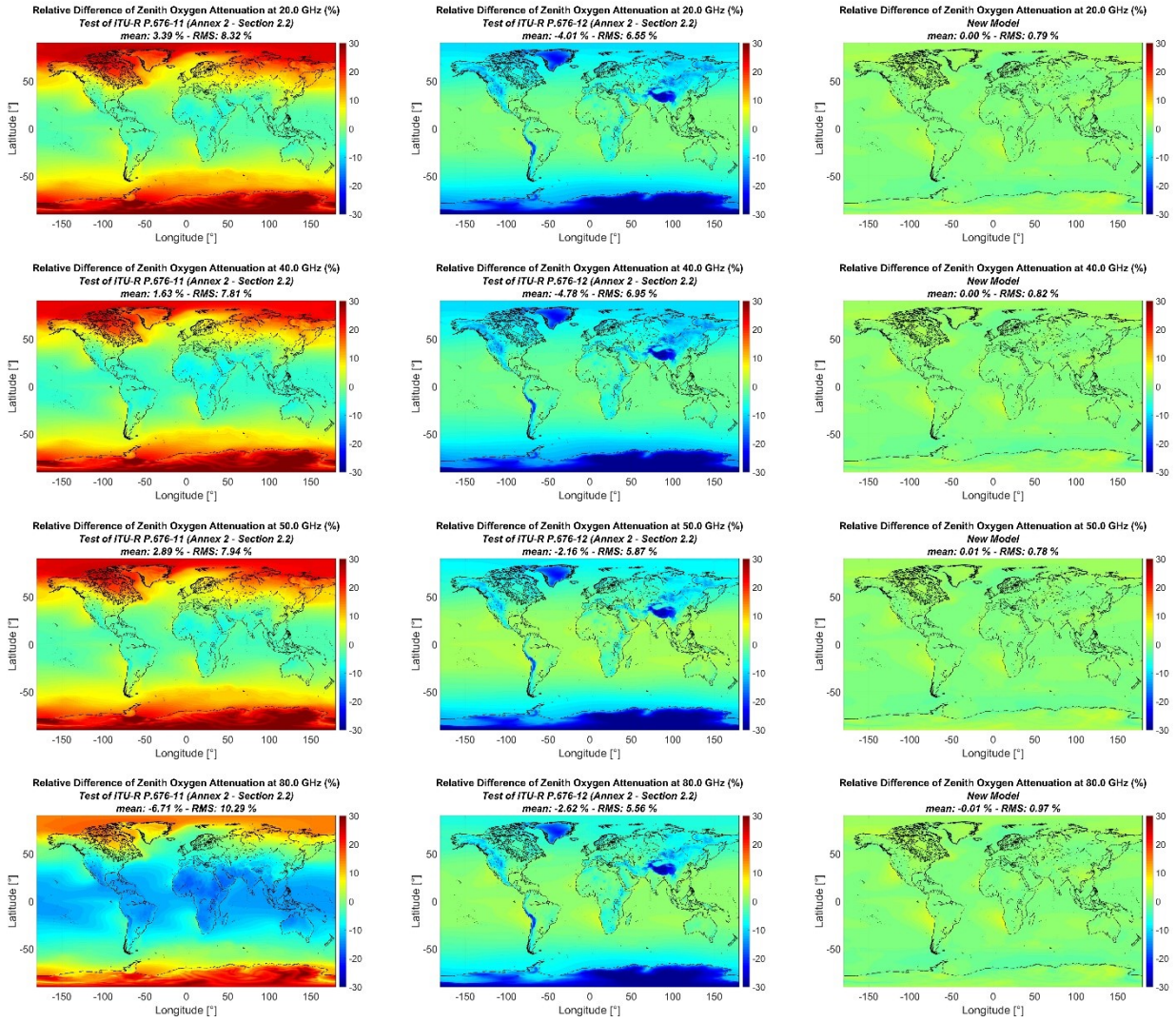

Figure 4-5 : Relative error of zenith oxygen attenuation
1st line: 20 GHz, 2nd line: 40 GHz, 3rd line: 50 GHz, 4th line: 80 GHz
1st column: ITU-R P.676-11, 2nd column: ITU-R P.676-12, 3rd column: new model

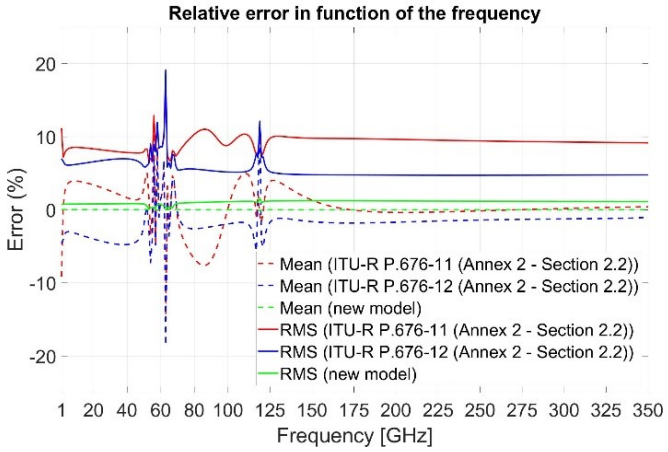

Figure 4-6 : Relative mean and RMS errors in function of the frequency

4.1.2.3 TEST USING RADIOSOUNDING OBSERVATIONS (RAOBS)

To test the performances of the new instantaneous oxygen attenuation prediction method with respect to Section 2.2 of Annex 2 of ITU-R P.676-12, concurrent surface total pressure, surface temperature, surface water vapour density and oxygen attenuation have been extracted from radiosounding observations (RAOBS) data. Ten years (2011-2020) of RAOBS on 24 different locations have been taken into account. As oxygen attenuation is not necessarily negligible above the tropopause, only RAOBS for which the highest altitude level is above 25 km have been considered. The table below highlights the main information on the RAOBS dataset. The total number of RAOBS used is 80698.

Country (NOAA ID)	Site	Latitude (°N)	Longitude (°E)	Altitude (m)	Total number of RAOBS	Number of RAOBS with the highest level above 25 km
AR	BUENOS-AIRES-EZEIZA	-34.82	-58.53	20	4930	3635
AT	GRAZ	47.00	15.43	347	3106	1254
BR	GALEAO-RIO	-22.82	-43.25	6	6650	1980
CI	ABIDJAN-PORT-BOUET	5.25	-3.93	8	5569	1713
CN	BEIJING-PEKING	39.93	116.28	55	6558	677
ES	MADRID-BARAJAS	40.47	-3.58	638	6449	5637
FR	BORDEAUX-MERIGNAC	44.83	-0.70	45	6413	3267
GA	LIBREVILLE-LEON-MBA	0.45	9.42	15	2206	1037
GF	CAYENNE-ROCHAMBEAU	4.83	-52.37	9	6851	2728
GP	POINTE-A-PITRE-RAIZET	16.27	-61.52	8	4667	2247
GR	ATHENS-HELLENKION	37.90	23.73	14	2479	853
IN	CALCUTTA-DUM-DUM	22.65	88.45	6	8056	3774
IN	DELHI-SAFDARJUNG	28.58	77.20	216	9499	1537
IT	MILANO-LINATE	45.43	9.28	103	7447	6946
MX	MEXICO-CITY	19.43	-99.07	2309	7353	5073
NO	NY-ALESUND-II	78.92	11.93	8	4615	4292
PT	LISBON-GAGO-COUTINHO	38.77	-9.13	105	3208	1808
RE	SAINT-DENIS	-20.88	55.52	20	3221	1408
SG	SINGAPORE-CHANGI	1.37	103.98	16	11635	3993
US	DENVER	39.77	-104.88	1611	7270	6772
US	FAIRBANKS	64.82	-147.87	135	7264	6888
US	LAS-VEGAS	36.05	-115.18	693	7209	6553
US	MCMURDO-USA-BASE	-77.85	166.67	34	5270	225
US	MIAMI-INTL-UNIV	25.75	-80.38	4	7455	6401

First, the relative mean (Figure 4-7) and RMS (Figure 4-8) errors have been computed for each site and each frequency from 1 to 350 GHz with a frequency step of 1 GHz. In both cases, the new model seems to perform better than Section 2.2 of Annex 2 of ITU-R P.676-12.

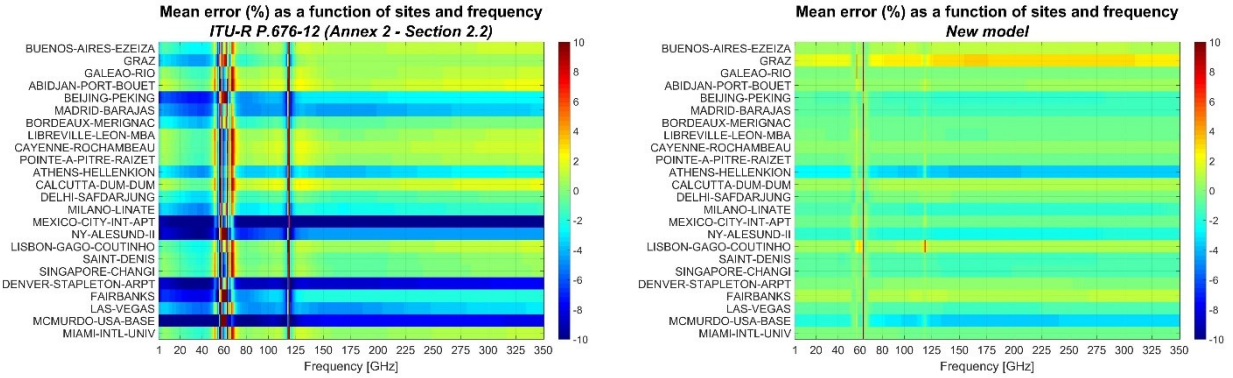

Figure 4-7 : Relative mean errors as a function of sites and frequency

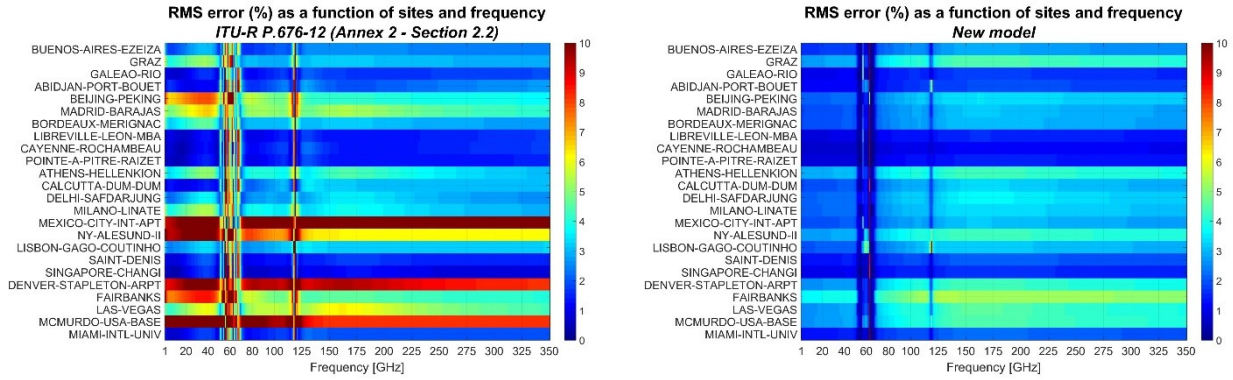

Figure 4-8 : Relative RMS errors as a function of sites and frequency

Second, the combined (for all sites) relative mean and RMS errors have been computed from 1 to 350 GHz with a frequency step of 1 GHz. The results are highlighted in Figure 4-9. It can be observed the new model performs better than Section 2.2 of Annex 2 of ITU-R P.676-12 over the full range of frequency from 1 to 350 GHz.

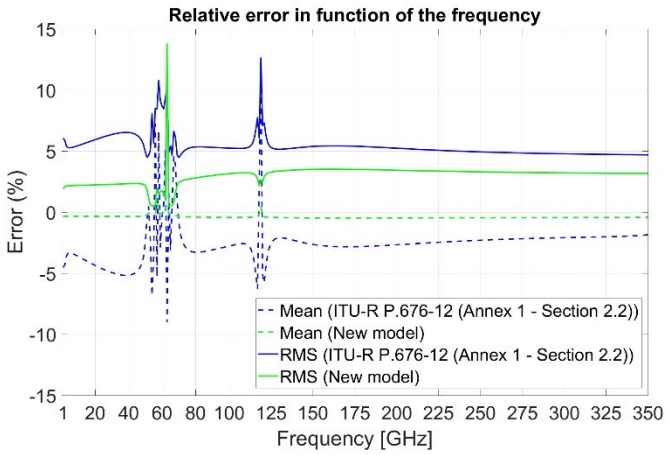

Figure 4-9 : Relative mean and RMS errors in function of the frequency

Third, the scatterplot of the retrieved oxygen attenuation vs. the reference oxygen attenuation is also a good performance indicator. The results at 20, 40, 80, and 150 GHz are shown in Figure 4-10. The straight black line represents the curve y=x. It can be then observed that the new model performs better than the in-force ITU-R prediction method which is in agreement with the results of Figure 4-9.

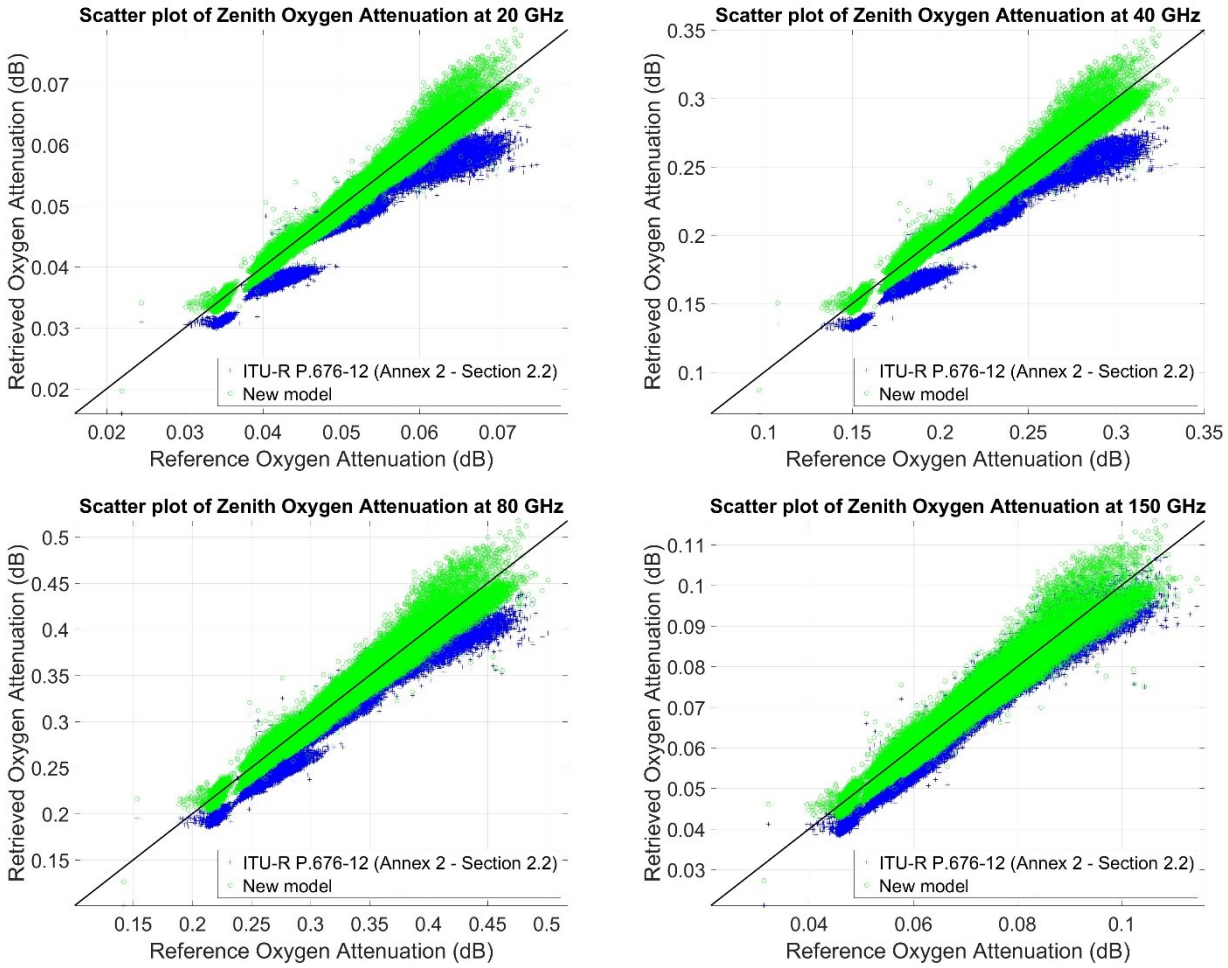

Figure 4-10 : Scatterplot of zenith oxygen attenuation

Finally, CCDF of oxygen attenuation (taking into account the full dataset, so disregarding the locations) have been computed. The results at 20, 40, 80, and 150 GHz are given in Figure 4-11. It can be observed a very good agreement of the new proposed model.

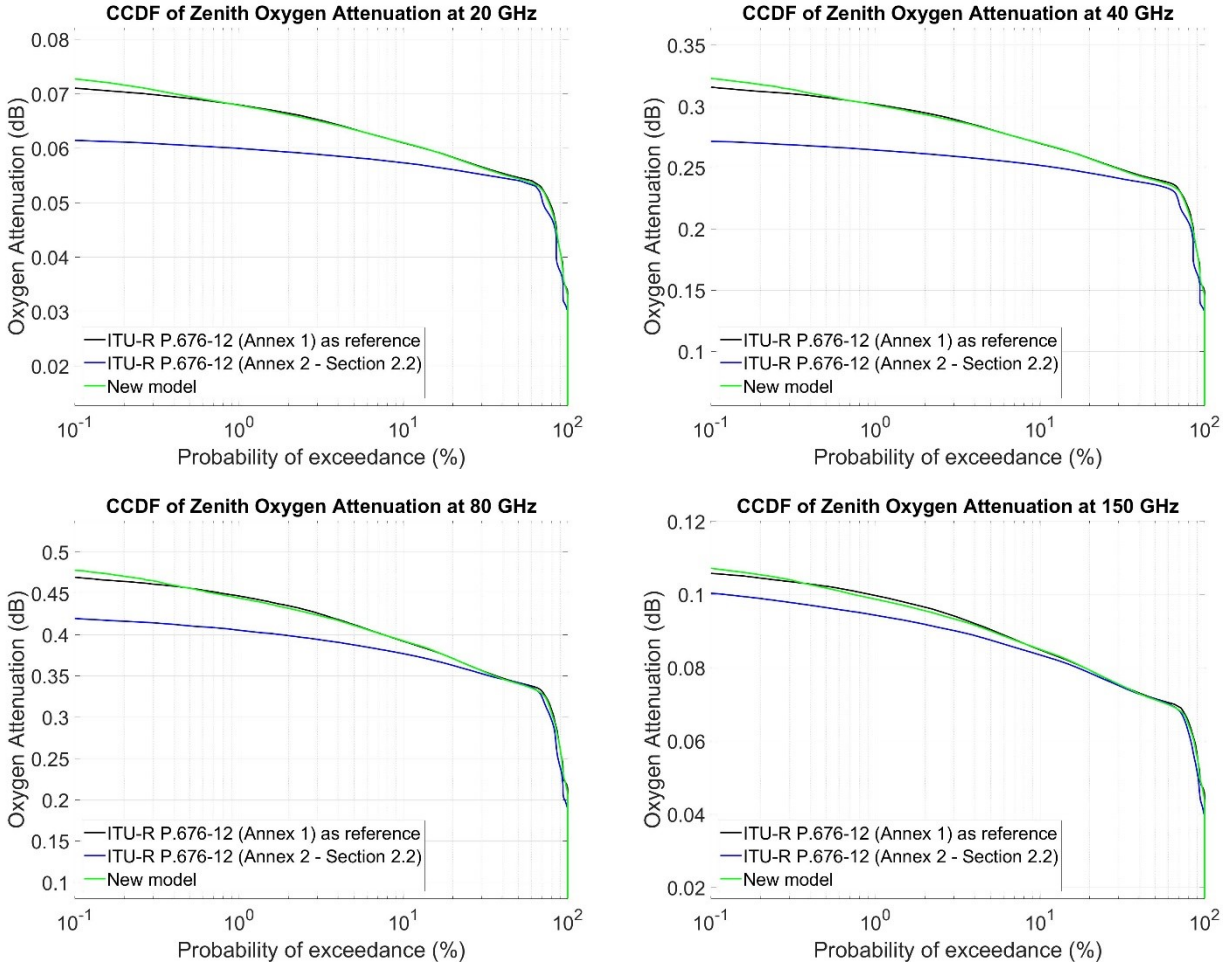

Figure 4-11 : CCDF of zenith oxygen attenuation

4.2 NEW PREDICTION METHOD OF THE STATISTICAL DISTRIBUTION OF OXYGEN ATTENUATION

4.2.1 DESCRIPTION

Recalling that the new prediction method of the instantaneous oxygen attenuation based on the oxygen equivalent height is (section 4.1.2.1):

$$A_O(f, P_s, T_s, \rho_{w_s}) = \frac{\gamma_o(f, P_s, T_s, \rho_{w_s}) \cdot h_o(f, T_s, P_s, \rho_{w_s})}{\sin\theta}$$

with $h_o(f, T_s, P_s, \rho_{w_s}) = a_o(f) + b_o(f) \cdot T_s + c_o(f) \cdot P_s + d_o(f) \cdot \rho_{w_s}$, it is not necessarily straightforward to define a new prediction method of the statistical distribution (CCDF) of oxygen attenuation $A_O(f, p)$ where *p* is the probability of exceedance (in %).

The proposed modelling of $A_O(f, p)$ is the following

$$A_O(f, p) = \frac{\gamma_o(f, \overline{P_s}, \overline{T_s}, \overline{\rho_{w_s}}) \cdot h_o(f, T_s(p), P_s(p), \rho_{w_s}(p))}{\sin\theta}$$

with $h_o(f, T_s(p), P_s(p), \rho_{w_s}(p)) = a_o(f) + b_o(f) \cdot T_s(p) + c_o(f) \cdot P_s(p) + d_o(f) \cdot \rho_{w_s}(p)$.

$\overline{P_s}$, $\overline{T_s}$, and $\overline{\rho_{w_s}}$ are respectively the mean of surface pressure, surface temperature and surface water vapour density over the period of interest (e.g. annual or monthly mean). $P_s(p)$, $T_s(p)$, and $\rho_{w_s}(p)$ represent respectively the CCDF of surface pressure, surface temperature and surface water vapour density over the same period of interest (e.g. annual or monthly CCDF), i.e. the values of P_s, T_s, and ρ_{w_s} exceeded for *p* % of the time.

Examples for some RAOBS sites are given in Figure 4-12 where the results coming from the instantaneous prediction method are compared with the results coming from the statistical prediction method. The black curve is the reference coming from the integration of the oxygen specific attenuation along the RAOBS profiles.

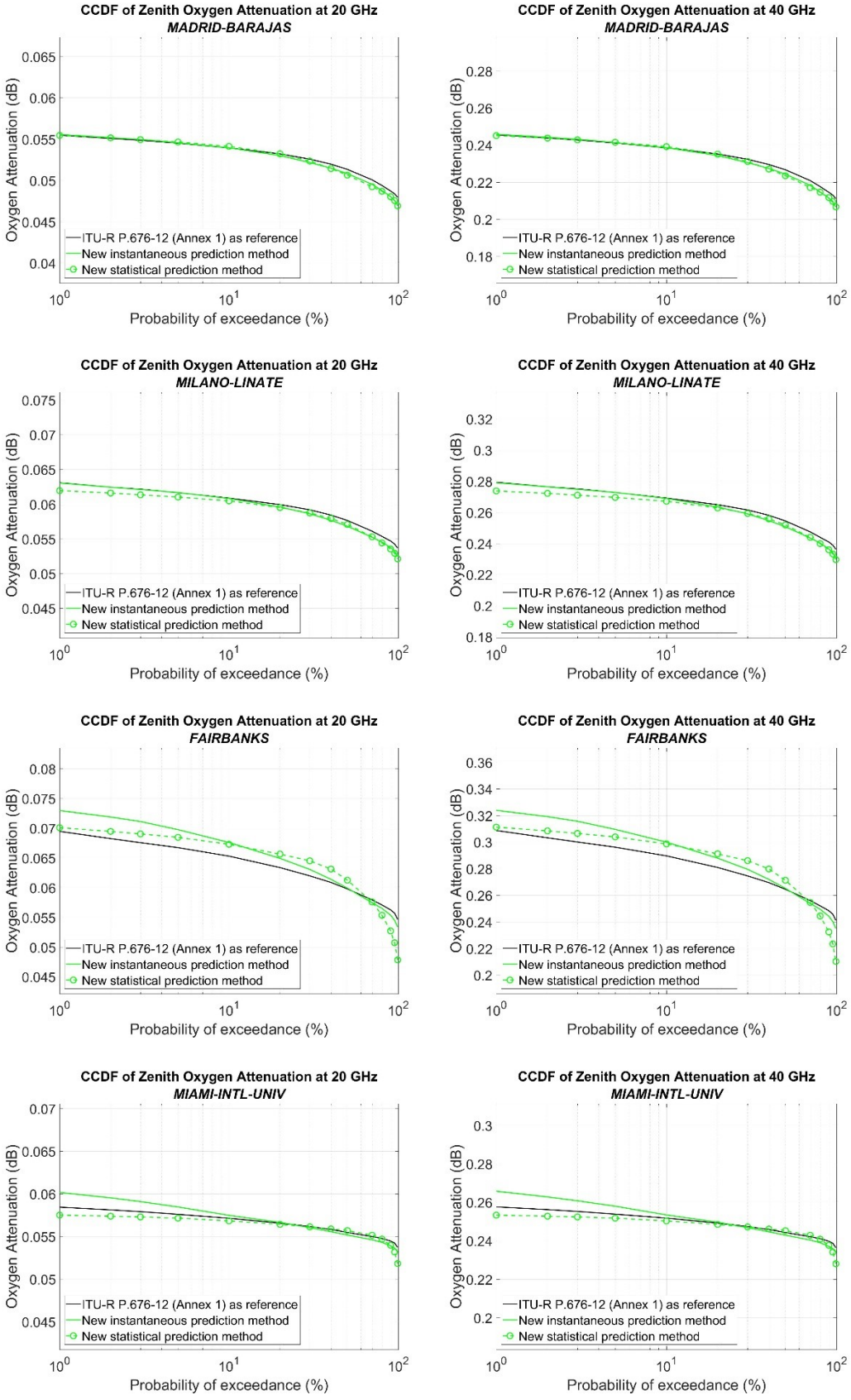

Figure 4-12 : Comparisons of instantaneous and statistical prediction methods of oxygen attenuation left: 20 GHz, right: 40 GHz

When local data of $P_s(p)$, $T_s(p)$, $\rho_{w_s}(p)$, $\overline{P_s}$, $\overline{T_s}$, and $\overline{\rho_{w_s}}$ are not available, the idea is now to provide to the user digital tabulated worldwide maps of $P_s(p)$, $T_s(p)$, $\rho_{w_s}(p)$, $\overline{P_s}$, $\overline{T_s}$, and $\overline{\rho_{w_s}}$ to be able to predict the CCDF of oxygen attenuation anywhere in the world. This is the goal of the next section.

4.2.2 DERIVATION OF NEW MAPS OF SURFACE PARAMETERS

In addition to the monthly averaged pressure level data described in Section 2, ERA5 also contains hourly reanalysis data on single level. As for pressure level data, the spatial resolution is 0.25° in both latitude and longitude. Among all the available parameters, the **surface pressure, P_s, the 2m temperature, T_s, and the 2m dewpoint temperature, T_{d_s}** might be of interest. In this document, the 2m temperature and the 2m dewpoint temperature will be considered as surface temperature and surface dewpoint temperature.

Extract from ERA5 website:

Surface pressure	Pa	This parameter is the pressure (force per unit area) of the atmosphere at the surface of land, sea and inland water. It is a measure of the weight of all the air in a column vertically above a point on the Earth's surface. Surface pressure is often used in combination with temperature to calculate air density. The strong variation of pressure with altitude makes it difficult to see the low and high pressure weather systems over mountainous areas, so mean sea level pressure, rather than surface pressure, is normally used for this purpose. The units of this parameter are Pascals (Pa). Surface pressure is often measured in hPa and sometimes is presented in the old units of millibars, mb (1 hPa = 1 mb= 100 Pa).
2m temperature	K	This parameter is the temperature of air at 2m above the surface of land, sea or inland waters. 2m temperature is calculated by interpolating between the lowest model level and the Earth's surface, taking account of the atmospheric conditions. This parameter has units of kelvin (K). Temperature measured in kelvin can be converted to degrees Celsius (°C) by subtracting 273.15.
2m dewpoint temperature	K	This parameter is the temperature to which the air, at 2 metres above the surface of the Earth, would have to be cooled for saturation to occur. It is a measure of the humidity of the air. Combined with temperature and pressure, it can be used to calculate the relative humidity. 2m dew point temperature is calculated by interpolating between the lowest model level and the Earth's surface, taking account of the atmospheric conditions. This parameter has units of kelvin (K). Temperature measured in kelvin can be converted to degrees Celsius (°C) by subtracting 273.15.

According to [3], temperature, *T*, and dewpoint temperature, T_d, can be used to derive the relative humidity, *RH* (in %):

$$RH = 100 \cdot \frac{f_1(t_d)}{f_1(t)}$$

with $f_1(X) = EF(\mathrm{P,t}) \cdot a_w \cdot e^{\left(b_w - \frac{X}{d_w}\right) \cdot \frac{X}{X + c_w}}$, $t_d = T_d - 273.15$, $t = T - 273.15$, and

$$\begin{cases} a_w = 6.1121 \\ b_w = 18.678 \\ c_w = 257.14 \\ d_w = 234.5 \\ EF(\mathrm{P},\mathrm{t}) = 1 + 10^{-4}[7.2 + \mathrm{P}\cdot(0.0320 + 5.9\cdot 10^{-6}\cdot t^2)] \end{cases}$$

Note that these equations (and the coefficients) are perfectly in line with Recommendation ITU-R P.453-14. Applying this framework to surface temperature, T_s, and surface dewpoint temperature, T_{d_s}, it resuts:

$$RH_s = 100\cdot\frac{e^{\left(b_w-\frac{t_{d_s}}{d_w}\right)\cdot\frac{t_{d_s}}{T_{d_s}+c_w}}}{e^{\left(b_w-\frac{t_s}{d_w}\right)\cdot\frac{t_s}{t_s+c_w}}} = 100\cdot e^{\left(b_w-\frac{t_{d_s}}{d_w}\right)\cdot\frac{t_{d_s}}{t_{d_s}+c_w}-\left(b_w-\frac{t_s}{d_w}\right)\cdot\frac{t_s}{t_s+c_w}}$$

With $t_{d_s} = T_{d_s} - 273.15$, $t_s = T_s - 273.15$, and

Then, RH_s is classically turned into the surface water vapour density, ρ_{w_s} (in g/m^3) using Recommendation ITU-R P.453-14:

$$\rho_{w_s} = \frac{RH_s\cdot e_s\cdot 216.7}{100\cdot T_s}$$

e_s being the surface water vapour saturation pressure, $e_s = f_1(t_s) = EF(P_s,t_s)\cdot a_w\cdot e^{\left(b_w-\frac{t_s}{d_w}\right)\cdot\frac{t_s}{t_s+c_w}}$.

Several new reference maps have then been derived from 30 years (1991-2020 that defines new climate normals) of ERA5 **hourly** data:

- The annual and monthly mean values of P_s (in hPa),
- The annual and monthly mean values of T_s (in K),
- The annual and monthly mean values of RH_s (in %),
- The annual and monthly mean values of ρ_{w_s} (in g/m^3),
- The annual and monthly standard deviation values of P_s (in hPa),
- The annual and monthly standard deviation values of T_s (in K),
- The annual and monthly standard deviation values of RH_s (in %),
- The annual and monthly standard deviation values of ρ_{w_s} (in g/m^3),
- The annual values of P_s (in hPa) exceeded for the probability levels of 0.001, 0.002, 0.003, 0.005, 0.01, 0.02, 0.03, 0.05, 0.1, 0.2, 0.3, 0.5, 1, 2, 3, 5, 10, 20, 30, 50, 60, 70, 80, 90, 95, and 99% of an average year,

- The monthly values of P_S (in hPa) exceeded for the probability levels of 0.01, 0.02, 0.03, 0.05, 0.1, 0.2, 0.3, 0.5, 1, 2, 3, 5, 10, 20, 30, 50, 60, 70, 80, 90, 95, and 99% of each average month.
- The annual values of T_S (in K) exceeded for the probability levels of 0.001, 0.002, 0.003, 0.005, 0.01, 0.02, 0.03, 0.05, 0.1, 0.2, 0.3, 0.5, 1, 2, 3, 5, 10, 20, 30, 50, 60, 70, 80, 90, 95, and 99% of an average year,
- The monthly values of T_S (in K) exceeded for the probability levels of 0.01, 0.02, 0.03, 0.05, 0.1, 0.2, 0.3, 0.5, 1, 2, 3, 5, 10, 20, 30, 50, 60, 70, 80, 90, 95, and 99% of each average month.
- The annual values of RH_S (in %) exceeded for the probability levels of 0.001, 0.002, 0.003, 0.005, 0.01, 0.02, 0.03, 0.05, 0.1, 0.2, 0.3, 0.5, 1, 2, 3, 5, 10, 20, 30, 50, 60, 70, 80, 90, 95, and 99% of an average year,
- The monthly values of RH_S (in %) exceeded for the probability levels of 0.01, 0.02, 0.03, 0.05, 0.1, 0.2, 0.3, 0.5, 1, 2, 3, 5, 10, 20, 30, 50, 60, 70, 80, 90, 95, and 99% of each average month.
- The annual values of ρ_{w_S} (in g/m^3) exceeded for the probability levels of 0.001, 0.002, 0.003, 0.005, 0.01, 0.02, 0.03, 0.05, 0.1, 0.2, 0.3, 0.5, 1, 2, 3, 5, 10, 20, 30, 50, 60, 70, 80, 90, 95, and 99% of an average year,
- The monthly values of ρ_{w_S} (in g/m^3) exceeded for the probability levels of 0.01, 0.02, 0.03, 0.05, 0.1, 0.2, 0.3, 0.5, 1, 2, 3, 5, 10, 20, 30, 50, 60, 70, 80, 90, 95, and 99% of each average month.

The latitude grid is from −90° N to +90° N in 0.25° steps, and the longitude grid is from −180° E to +180° E in 0.25° steps.

As an example Figure 4-13 shows the annual mean and standard deviation of ρ_{w_S} derived from 30 years (1991-2020) of ERA5 hourly reanalysis data.

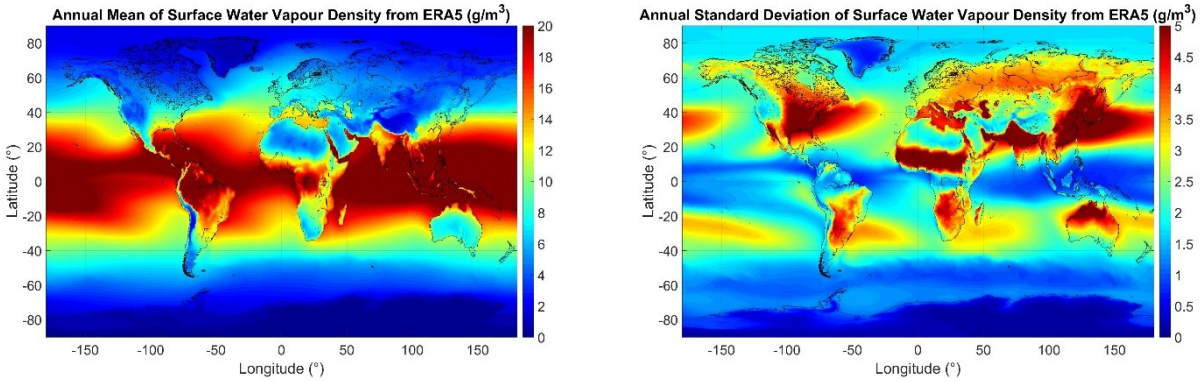

Figure 4-13 : Annual mean (left) and standard deviation (right) of surface water vapour density derived from ERA5 hourly reanalysis data (1991-2020)

Digital maps of surface water vapour density are provided in Recommendation ITU-R P.836-6. The main differences between the digital maps provided by ITU-R P.836-6 and this document are summarized in the table below:

Parameters related to surface water vapour density		**ITU-R P.836-6**	**This document**
Spatial resolution		**1.125°**	**0.25°**
Mean	Annual	Unavailable	Available
	Monthly	Unavailable	Available
Standard deviation	Annual	Unavailable	Available
	Monthly	Unavailable	Available
CCDF	Annual	Maps from 0.1% to 99%	Maps from 0.001% to 99%
	Monthly	Maps from 1% to 99%	Maps from 0.01% to 99%

Some illustrations of the differences of the annual surface water vapour density between ITU-R P.836-6 and the new ERA5 maps are shown in Figure 4-14 and Figure 4-15 respectively on a worldwide basis and over Europe for probabilities of exceedance equal to 0.1%, 1%, and 10%. No major difference can be observed but the impact of the new spatial resolution is clearly visible.

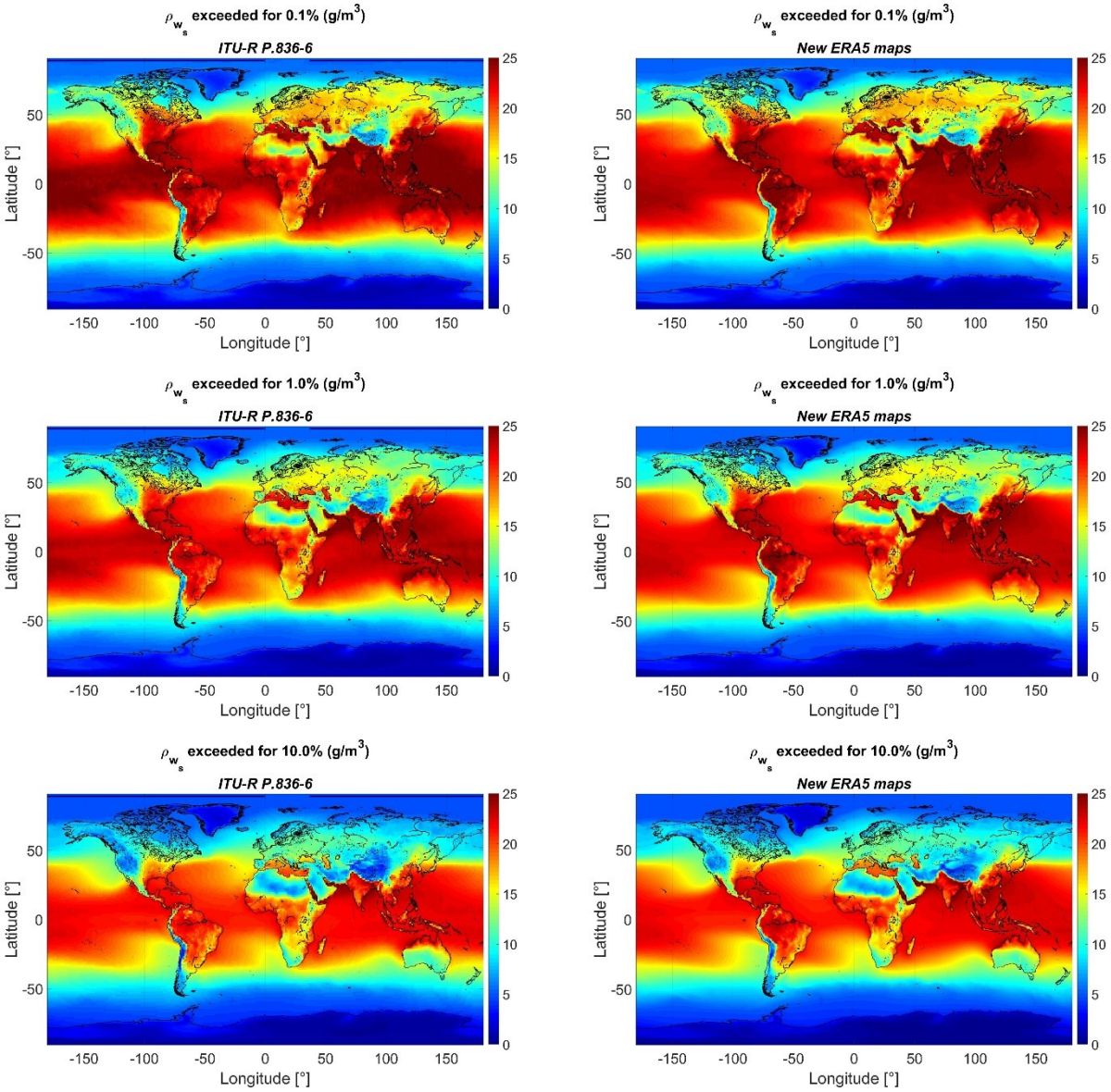

Figure 4-14 : Annual surface water vapour density
1st line: 0.1%, 2nd line: 1%, 3rd line: 10%
left: ITU-R P.836-6, right: new ERA5 maps

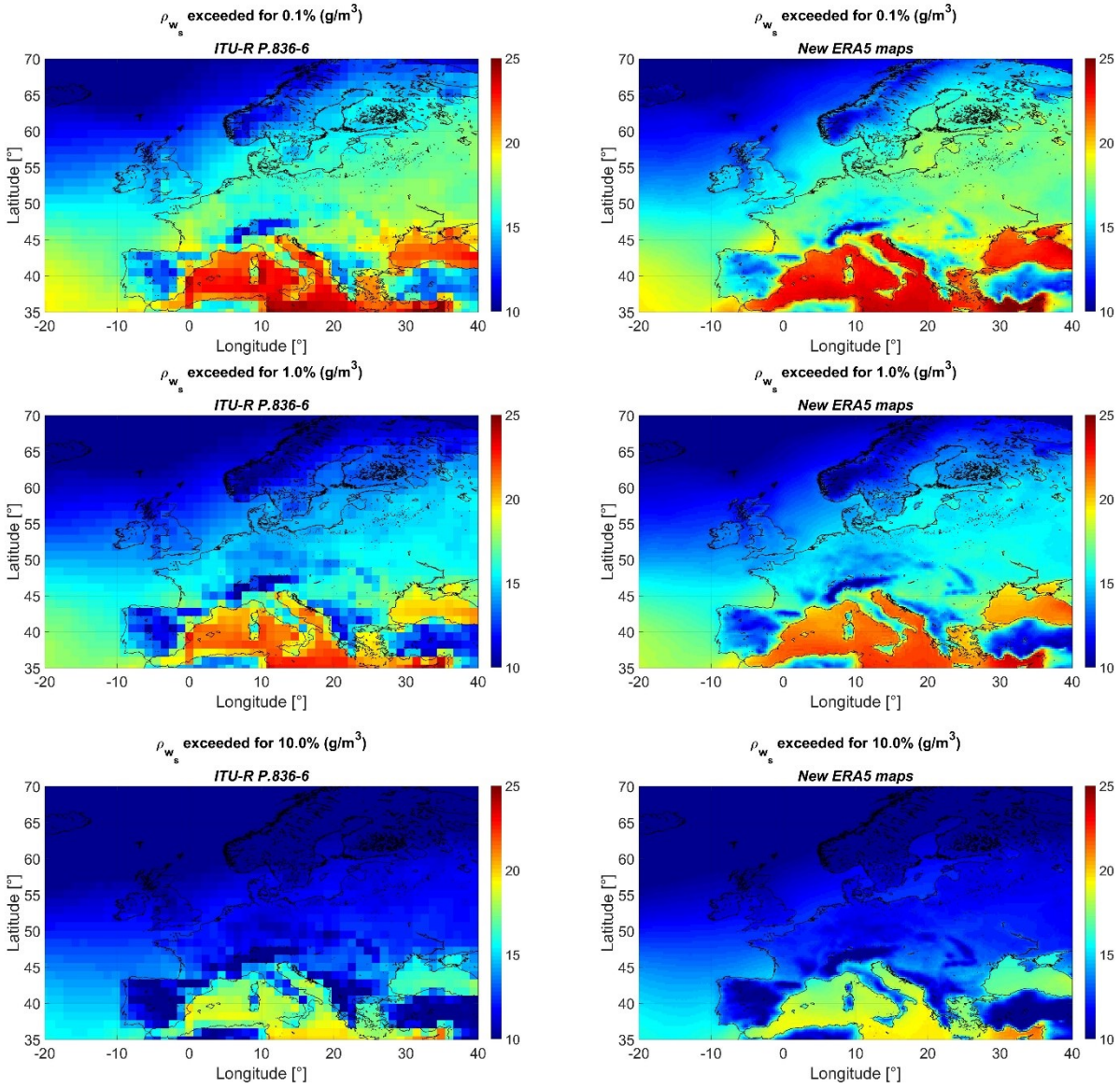

Figure 4-15 : Annual surface water vapour density (over Europe)
1st line: 0.1%, 2nd line: 1%, 3rd line: 10%
left: ITU-R P.836-6, right: new ERA5 maps

Five specific sites have then been selected to highlight the differences of the surface water vapour density over the full distribution. The results are shown in Figure 4-16. It can be observed that, globally, the new ERA5 maps tend to give higher density values than ITU-R P.836-6 while respecting the global behaviour. The new ERA5 maps should much better reproduce orographic effects.

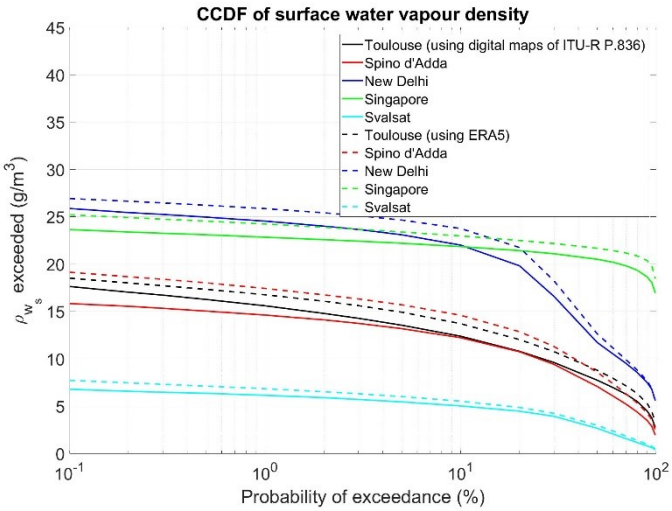

Figure 4-16 : CCDF of the surface water vapour density on the five specific locations

5 NEW PREDICTION METHODS OF WATER VAPOUR ATTENUATION

MAIN OBJECTIVES OF SECTION 5.1:

- Derivation of a new approach to use the water vapour scale height when predicting the statistical distribution of the surface water vapour density and the total columnar content of water vapour

MAIN OBJECTIVES OF SECTION 5.2:

- Use of the new maps of the mean annual vertical atmospheric profiles to develop:
    - a new model of the **water vapour equivalent height** for the prediction of water vapour attenuation from surface meteorological parameters
    - a new model of the **water vapour absorption coefficient** for the prediction of water vapour attenuation from the total columnar content of water vapour
- Verification and comparison of the performances of the new models with:
    - the prediction methods described in Section 2.2 of Annex 2 of Recommendations ITU-R P.676-11 and ITU-R P.676-12 (for the new model of the water vapour equivalent height)
    - the prediction methods described in Section 2.3 of Annex 2 of Recommendations ITU-R P.676-11 and ITU-R P.676-12 (for the new model of the water vapour absorption coefficient)
- Test of the new models using radiosounding observations.

MAIN OBJECTIVES OF SECTION 5.3:

- Derivation of a new prediction method of the statistical distribution of water vapour attenuation
- Derivation of new digital maps of the total columnar content of water vapour for a worldwide application of the new prediction method in absence of local data
- Derivation of new digital maps for the approximation of the statistics of the total columnar content of water vapour by a Weibull distribution

A block diagram of this Section is proposed in Figure 5-1.

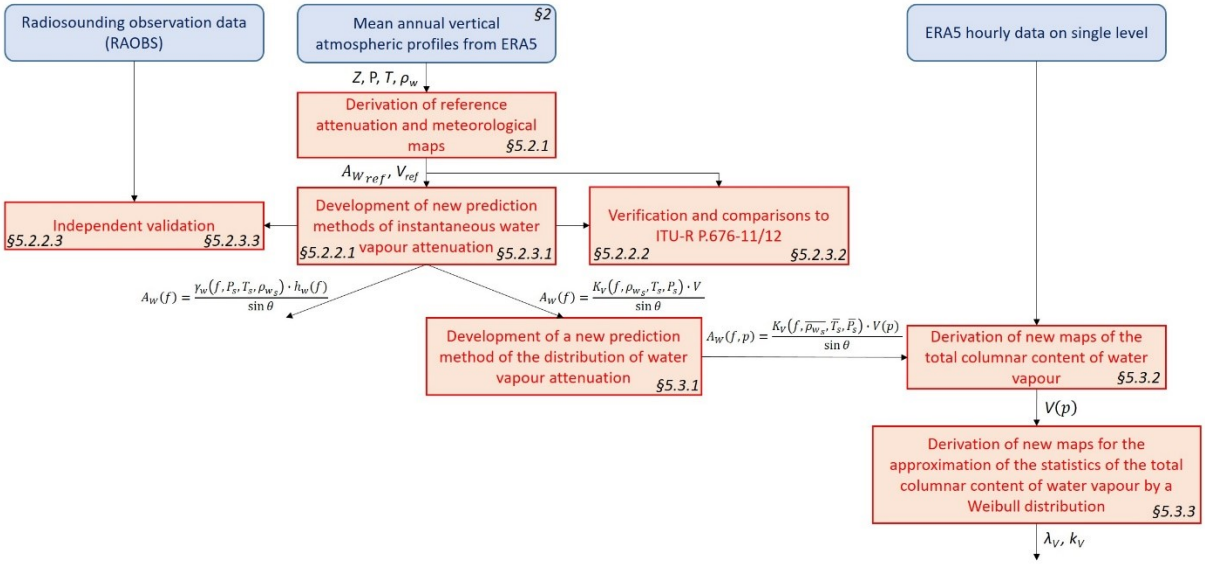

Figure 5-1 : Block diagram of Section 5

5.1 NEW APPROACH FOR THE USE OF THE WATER VAPOUR SCALE HEIGHT

It is commonly assumed that the vertical distribution of the water vapour density follows a decaying exponential function from the ground to the upper atmosphere:

$$\rho_w(Z) = \rho_{w_s} \cdot e^{-\frac{Z-h_s}{h_{VSC}}}$$

where ρ_{w_s} is the surface water vapour density, h_s is the height above mean sea level of the surface of the Earth of the point of interest (i.e. the level Z=h_s for which $\rho_w(Z = h_s) = \rho_{w_s}$), and h_{VSC} is the water vapour scale height.

Under this assumption, at any geometric height, Z, the total columnar content of water vapour, *V(Z)*, over the point of interest is:

$$V(Z) = \int_Z^{+\infty} \rho_w(z)dz = \int_Z^{+\infty} \rho_{w_s} \cdot e^{-\frac{z-h_s}{h_{VSC}}} dz = \rho_{w_s} \cdot h_{VSC} \cdot e^{-\frac{Z-h_s}{h_{VSC}}}$$

By denoting:

$$V_s = \int_{h_s}^{+\infty} \rho_w(z)dz = \rho_{w_s} \cdot h_{VSC}$$

Thus:

$$V(Z) = V_s \cdot e^{-\frac{Z-h_s}{h_{VSC}}}$$

Prediction methods of the statistical distribution of the surface water vapour density and the total columnar content of water vapour are proposed in the recommendation ITU-R P.836-6. Basically, for a given geometric height, Z, and a given probability of exceedance, *p*, the CCDF of the water vapour density, $\rho_w(Z,p)$, and the total columnar content, $V(Z,p)$, are given by:

$$\rho_w(Z,p) = \rho_{w_s}(p) \cdot e^{-\frac{Z-h_s}{h_{VSC}(p)}}$$

and

$$V(Z,p) = V_s(p) \cdot e^{-\frac{Z-h_s}{h_{VSC}(p)}}$$

Annual and monthly digital maps of $\rho_{w_s}(p)$, $V_s(p)$, and $h_{VSC}(p)$ are then provided to be able to derive the CCDF of both the water vapour density and the total columnar content of water vapour anywhere in the world.

A new approach is proposed in the following. Instead of using the full distribution of h_{VSC}, the practical idea is to only use the mean of h_{VSC}, $\overline{h_{VSC}} = E[h_{VSC}]$ (where *E*[] is the expectancy operator):

$$\rho_w(Z,p) = \rho_{w_s}(p) \cdot e^{-\frac{Z-h_s}{\overline{h_{VSC}}}}$$

and

$$V(Z,p) = V_s(p) \cdot e^{-\frac{Z-h_s}{\overline{h_{VSC}}}}$$

Under this assumption, $\overline{h_{VSC}}$ must be computed over the same reference period (e.g. on an annual or a monthly basis) than $\rho_w(Z,p)$ or $V(Z,p)$. It will be shown in Section 5.3.3 that this approach is more practical than the one given in Recommendation ITU-R P.836-6, especially when using an approximation for the distribution of the total columnar content of water vapour.

NB: Note that the total columnar content of water vapour is also known as the Integrated Water Vapour Content, *IWVC*.

To test the new approach, three sites (Milano, Singapore, and Fairbanks) have been extracted from the RAOBS dataset (see Section 5.2.3.3). The vertical profiles have been truncated to compute the CCDF of the water vapour density and the total columnar content of water vapour at three altitude levels h_s+100m, h_s+250m, and h_s+500m, h_s being the height of the surface of the Earth for the original RAOBS site of interest. Figure 5-2 and Figure 5-3 show the impact of the starting altitude on the CCDF of water vapour density and the total columnar content of water vapour, respectively. Not surprisingly, the water vapour values decrease when the starting altitude increase.

Finally, the two approaches for the retrieval of the CCDF of the water vapour density and the total columnar content of water vapour are compared in Figure 5-4 and Figure 5-5, respectively. It can be observed that none of the two approaches is perfect. The results seem to depend on the location of interest and on the starting altitude. However, the new proposed approach does not seem to degrade the results with respect to the first approach given in Recommendation ITU-R P.836-6.

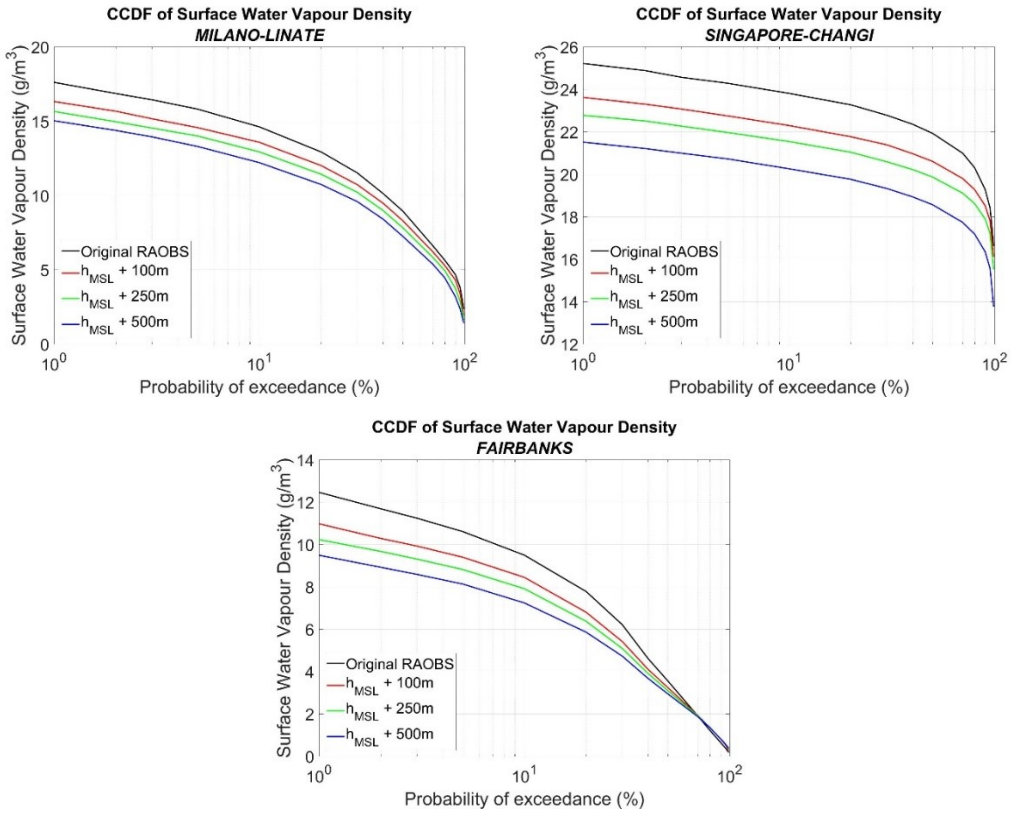

Figure 5-2 : Impact of starting altitude on the CCDF of water vapour density

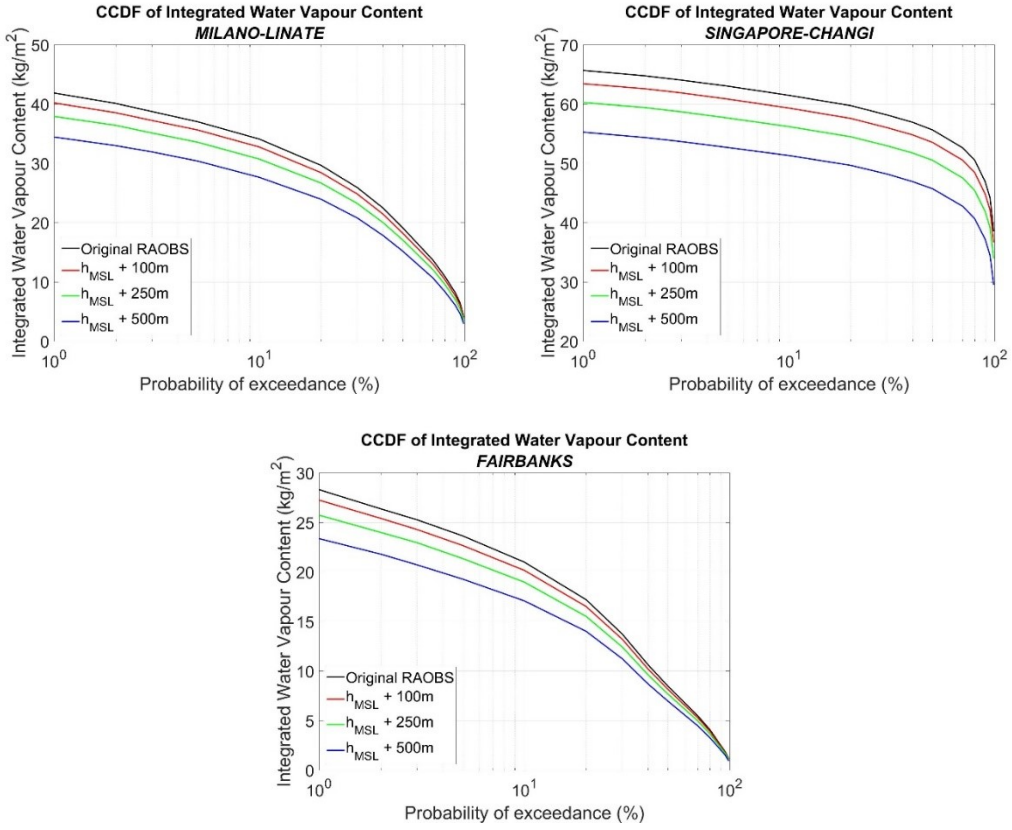

Figure 5-3 : Impact of starting altitude on the CCDF of IWVC

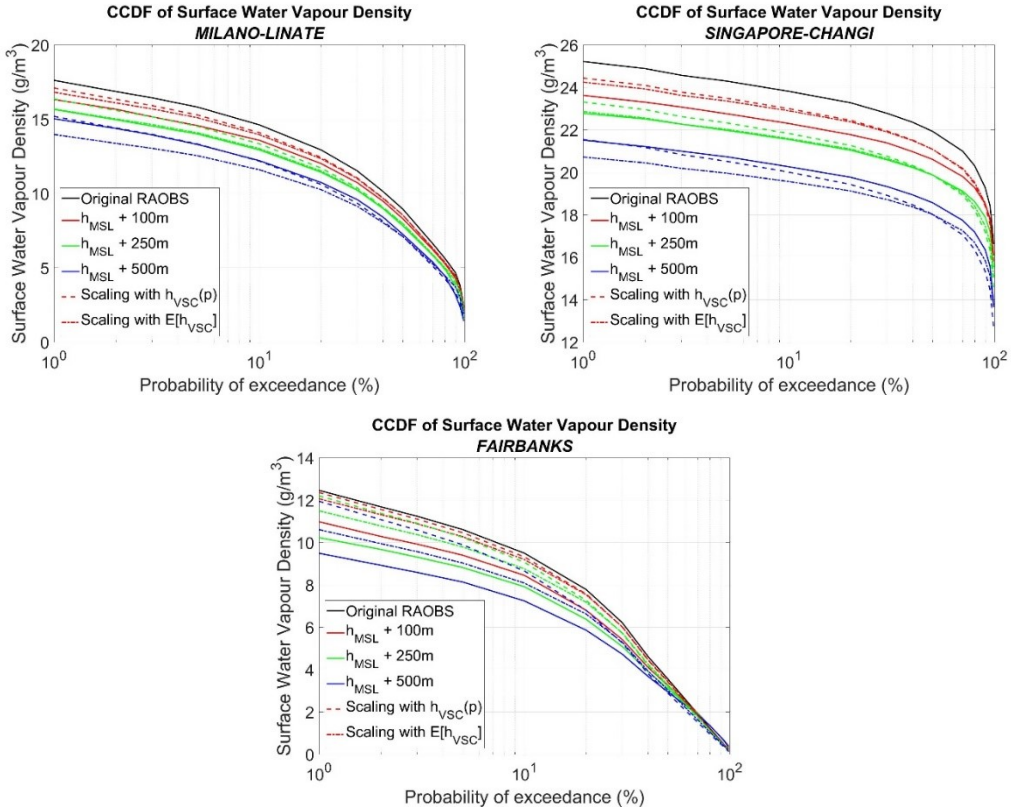

Figure 5-4 : Comparison of the two approaches for the retrieval of the CCDF of surface water vapour density

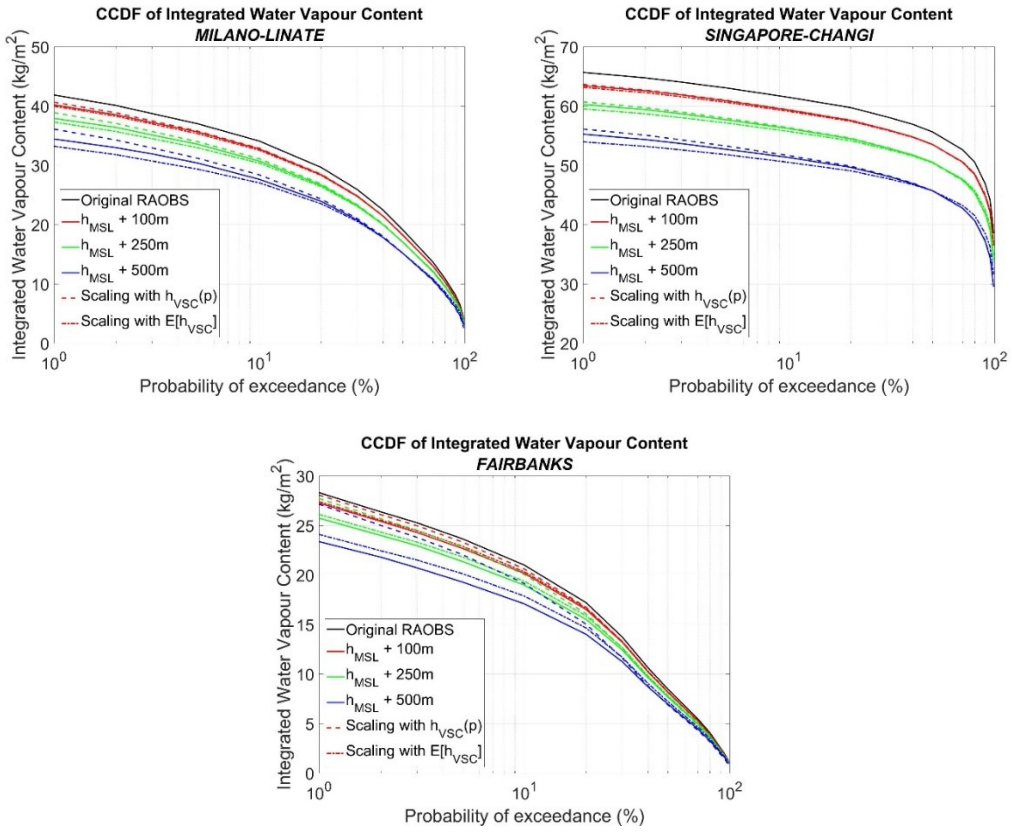

Figure 5-5 : Comparison of the two approaches for the retrieval of the CCDF of IWVC

5.2 NEW PREDICTION METHODS OF THE INSTANTANEOUS WATER VAPOUR ATTENUATION

5.2.1 METHODOLOGY TO DERIVE REFERENCE MAPS

Section 1 of Annex 1 of ITU-R P.676-12 [RD 1] is used to compute the water vapour specific attenuation profiles, $\gamma_w(Z)$, from the worldwide total pressure, $P(Z)$, temperature, $T(Z)$, and water vapour density, $\rho_w(Z)$, profiles given by the new maps of the mean annual vertical atmospheric profiles provided in Section 2.2 of this document.

Reference zenith water vapour attenuation maps, $A_{W_{ref}}$, are then derived from the integration of $\gamma_w(Z)$ along the profiles according to the methodology described in Section 2 of Annex 1 of ITU-R P.676-12 [RD 1]. This process has been performed **from 1 to 350 GHz** (validity range of Annex 2 of ITU-R P.676-12) with a frequency step of 1 GHz. The reference zenith water vapour attenuation maps at 20, 40, 50, and 80 GHz (frequencies currently used in SatCom systems) are shown in Figure 5-6.

The total columnar content of water vapour, *V*, is derived from the integration of $\rho_w(Z)$ along the profiles. The reference map is then noted V_{ref} and shown in Figure 5-7. We recall that the total columnar content of water vapour is also known as the Integrated Water Vapour Content, *IWVC*.

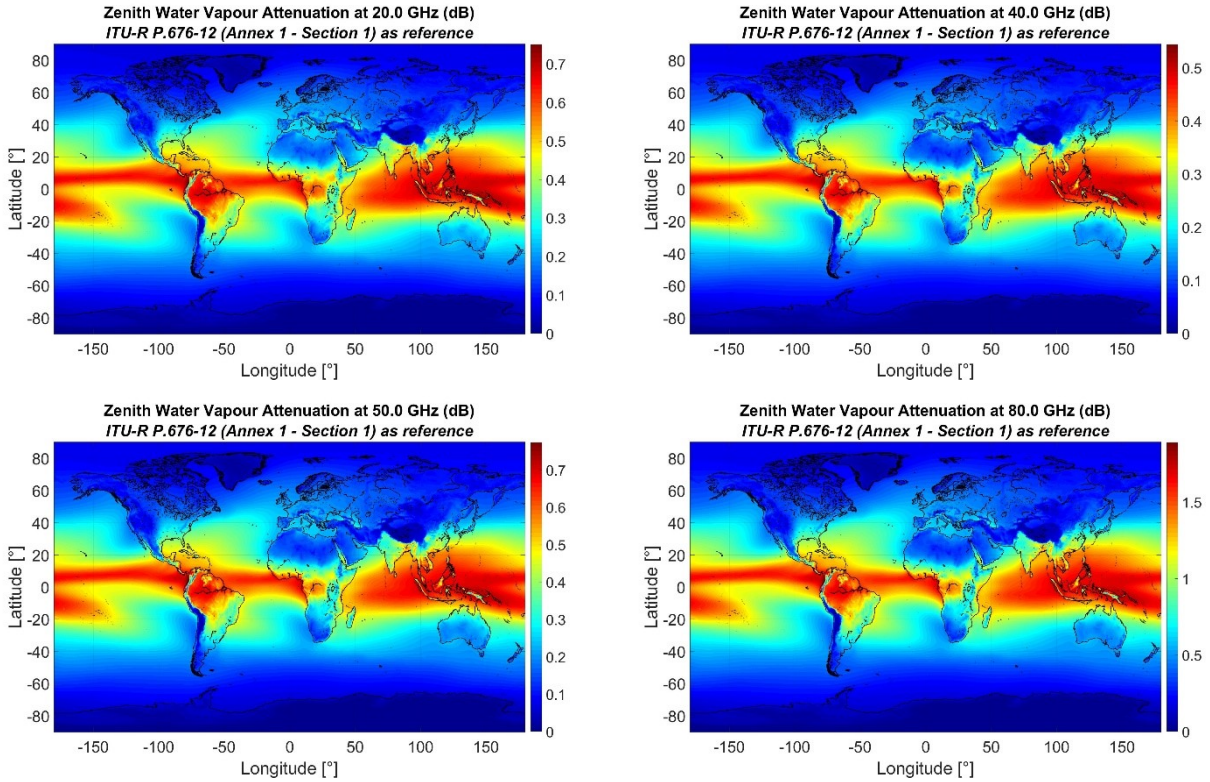

Figure 5-6 : Zenith Water Vapour Attenuation at 20, 40, 50, and 80 GHz derived from the integration of the water vapour specific attenuation along the new ERA5 annual profiles by using Annex 1 of ITU-R P.676-12

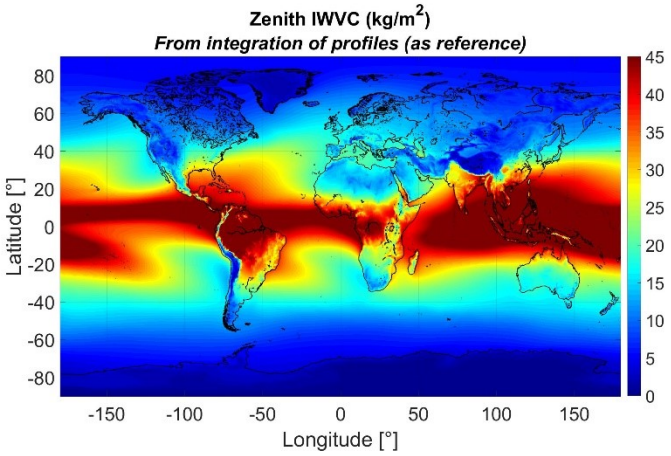

Figure 5-7 : Mean annual zenith Integrated Water Vapour Content (IWVC) derived from the ERA5 monthly averaged database (1991-2020)

5.2.2 NEW MODEL OF THE WATER VAPOUR EQUIVALENT HEIGHT

5.2.2.1 DESCRIPTION

The idea is to propose a new model to compute the water vapour equivalent height, h_w (in km), such that water vapour attenuation can be easily derived from:

$$A_W = \frac{\gamma_{w_S} \cdot h_w}{\sin\theta}$$

where γ_{w_S} (in dB/km) is the water vapour specific attenuation at the surface of the Earth and θ is the elevation angle (θ>5°).

The new proposed model has been derived by applying the following step-by-step procedure:

1. for each frequency, *f*, between 1 and 350 GHz, an optimal value of $h_w(f)$ to retrieve the reference zenith water vapour attenuation, called $h_{w_{opt}}(f)$, is derived from the scatterplot of $A_{W_{ref}}(f)$ vs γ_{w_S}. Note that $\gamma_{w_S} = \gamma_w(f, P_s, T_s, \rho_{w_S})$, where P_s (hPa), T_s (K), and ρ_{w_S} (g/m^3) are the surface total pressure, temperature and water vapour density, respectively.

   It has to be noticed that the retrieval has been performed by weighting each grid point (pixel) by the area on the surface of the Earth as explained in Section 3 of this document. Examples of the retrieval of the water vapour equivalent height are given below:

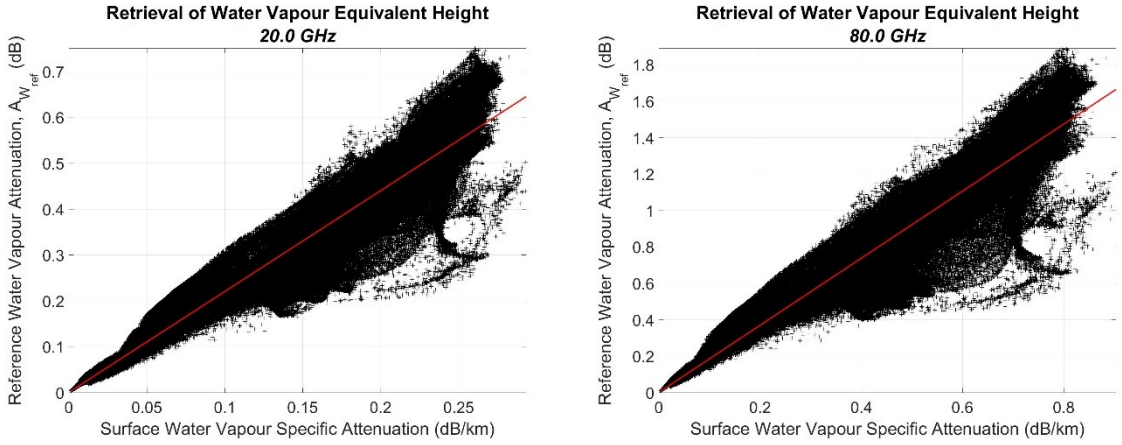

2. $h_{w_{opt}}(f)$ is fitted by the best following function:

$$h_{w_{opt}}(f) = A \cdot f + B + \sum_{i=1}^{3} \frac{a_i}{(f - f_i)^2 + b_i}$$

The results of the fitting procedure and the relative error on the modelling of the water vapour equivalent height are shown in Figure 5-8 and Figure 5-9, respectively.

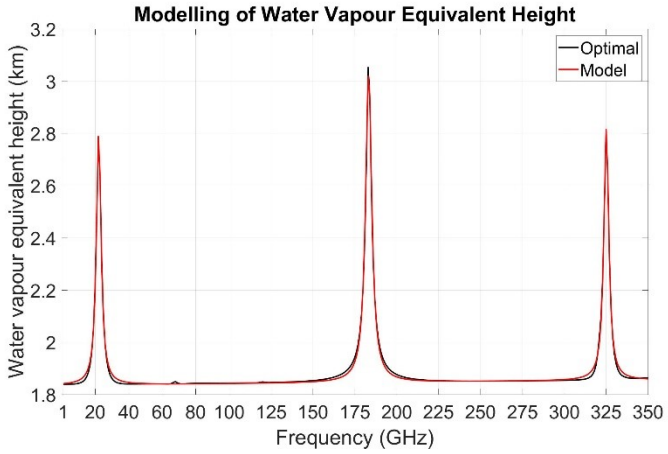

Figure 5-8 : Modelling of the water vapour equivalent height

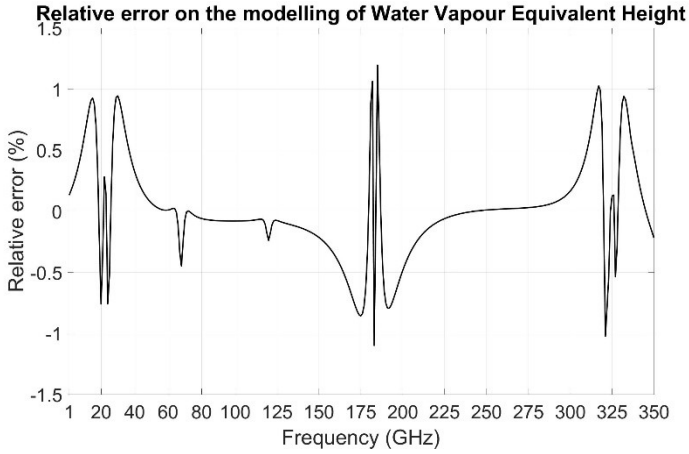

Figure 5-9 : Relative error on the modelling of the water vapour equivalent height

Finally, for a given frequency, *f*, the final new prediction method of the instantaneous water vapour attenuation based on the water vapour equivalent height is:

$$A_W(f, P_s, T_s, \rho_{w_s}) = \frac{\gamma_w(f, P_s, T_s, \rho_{w_s}) \cdot h_w(f)}{\sin\theta}$$

with $h_w(f) = A \cdot f + B + \sum_{i=1}^{3} \frac{a_i}{(f-f_i)^2+b_i}$ and for which the coefficients are given in the table below:

A	5.6485×10^{-5}	B	1.8348
i	f_i (GHz)	a_i	b_i
1	22.235080	2.6846	2.7649
2	183.310087	5.8905	4.9219
3	325.152888	2.9810	3.0748

5.2.2.2 VERIFICATION USING THE NEW MEAN ANNUAL VERTICAL PROFILES

The two prediction methods of Sections 2.2 of Annex 2 of ITU-R P.676-11 and ITU-R P.676-12 and the new model have been tested using the new mean annual maps provided in Section 2.2 of this document. First, the worldwide absolute and relative errors for the selected frequencies between 1 and 350 GHz are computed. Some illustrations of the relative errors at 20, 40, 50 and 80 GHz are shown in Figure 5-10. Finally, Figure 5-11 highlights the relative mean and RMS errors from 1 to 350 GHz. It can be observed that for both metrics, the new model performs a bit better than Sections 2.2 of Annex 2 of ITU-R P.676-11 and ITU-R P.676-12 over the full range of frequency from 1 to 350 GHz. Indeed, the relative RMS errors for ITU-R P.676-11 and ITU-R P.676-12 are around 16% and 21%, respectively, while for the new model, it is around 15%.

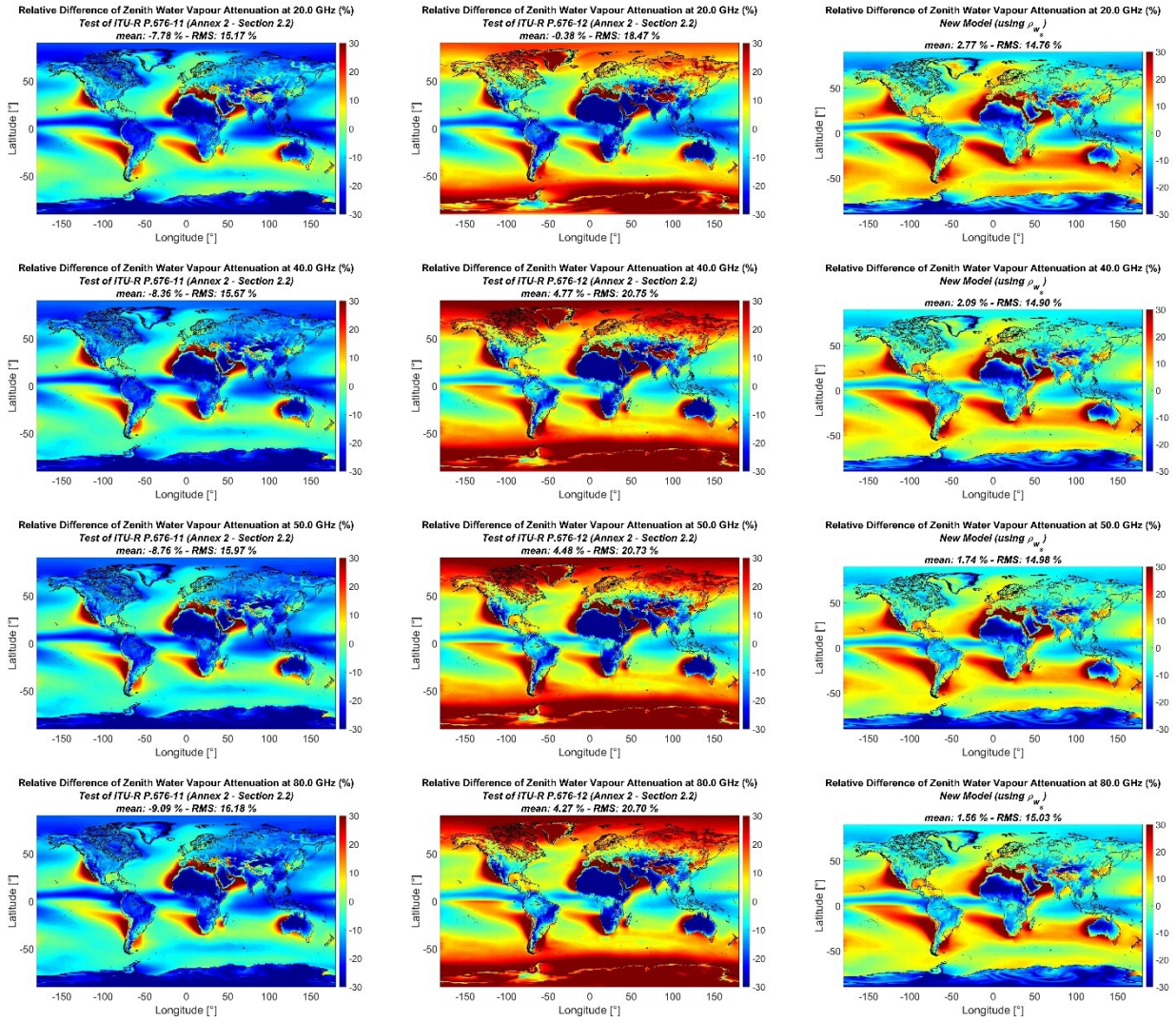

Figure 5-10 : Relative error of zenith water vapour attenuation
1st line: 20 GHz, 2nd line: 40 GHz, 3rd line: 50 GHz, 4th line: 80 GHz
1st column: ITU-R P.676-11, 2nd column: ITU-R P.676-12, 3rd column: new model

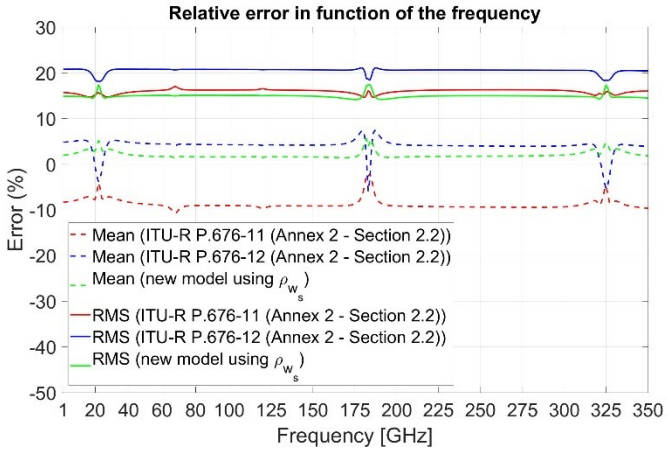

Figure 5-11 : Relative mean and RMS errors in function of the frequency

5.2.2.3 TEST USING RADIOSOUNDING OBSERVATIONS (RAOBS)

To test the performances of the new instantaneous water vapour attenuation prediction method with respect to Section 2.2 of Annex 2 of both ITU-R P.676-11 and ITU-R P.676-12, concurrent surface total pressure, surface temperature, surface water vapour density and water vapour attenuation have been extracted from radiosounding observations (RAOBS) data. Ten years (2011-2020) of RAOBS on 24 different locations have been taken into account (same data than in Section 4.1.2.3). As these RAOBS data were also used to test oxygen attenuation prediction methods, only RAOBS for which the highest altitude level is above 25 km have been considered. The table below recalls the main information on the RAOBS dataset. The total number of RAOBS used is 80698.

Country (NOAA ID)	Site	Latitude (°N)	Longitude (°E)	Altitude (m)	Total number of RAOBS	Number of RAOBS with the highest level above 25 km
AR	BUENOS-AIRES-EZEIZA	-34.82	-58.53	20	4930	3635
AT	GRAZ	47.00	15.43	347	3106	1254
BR	GALEAO-RIO	-22.82	-43.25	6	6650	1980
CI	ABIDJAN-PORT-BOUET	5.25	-3.93	8	5569	1713
CN	BEIJING-PEKING	39.93	116.28	55	6558	677
ES	MADRID-BARAJAS	40.47	-3.58	638	6449	5637
FR	BORDEAUX-MERIGNAC	44.83	-0.70	45	6413	3267
GA	LIBREVILLE-LEON-MBA	0.45	9.42	15	2206	1037
GF	CAYENNE-ROCHAMBEAU	4.83	-52.37	9	6851	2728
GP	POINTE-A-PITRE-RAIZET	16.27	-61.52	8	4667	2247
GR	ATHENS-HELLENKION	37.90	23.73	14	2479	853
IN	CALCUTTA-DUM-DUM	22.65	88.45	6	8056	3774
IN	DELHI-SAFDARJUNG	28.58	77.20	216	9499	1537
IT	MILANO-LINATE	45.43	9.28	103	7447	6946
MX	MEXICO-CITY	19.43	-99.07	2309	7353	5073
NO	NY-ALESUND-II	78.92	11.93	8	4615	4292
PT	LISBON-GAGO-COUTINHO	38.77	-9.13	105	3208	1808
RE	SAINT-DENIS	-20.88	55.52	20	3221	1408
SG	SINGAPORE-CHANGI	1.37	103.98	16	11635	3993
US	DENVER	39.77	-104.88	1611	7270	6772
US	FAIRBANKS	64.82	-147.87	135	7264	6888
US	LAS-VEGAS	36.05	-115.18	693	7209	6553
US	MCMURDO-USA-BASE	-77.85	166.67	34	5270	225
US	MIAMI-INTL-UNIV	25.75	-80.38	4	7455	6401

First, the relative mean (Figure 5-12) and RMS (Figure 5-13) errors have been computed for each site and each frequency from 1 to 350 GHz with a frequency step of 1 GHz. It is hard to say from these figures which model performs better but ITU-R P.676-11 seems to give the best performances.

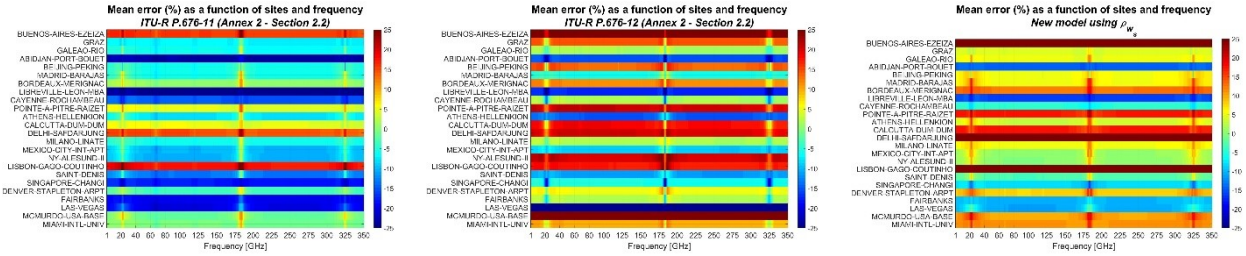

Figure 5-12 : Relative mean errors as a function of sites and frequency

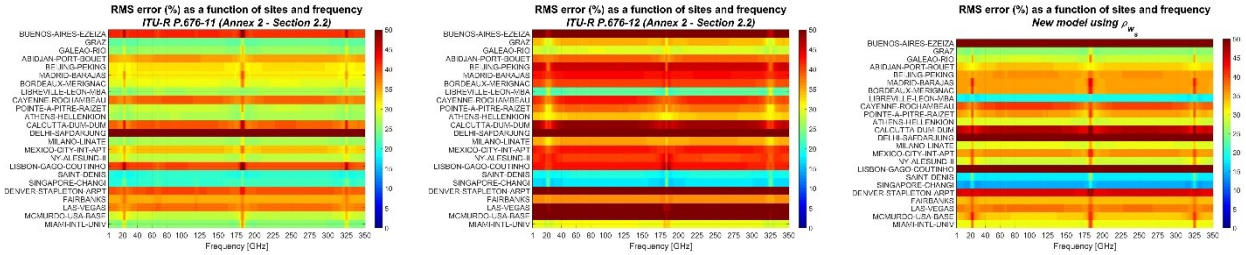

Figure 5-13 : Relative RMS errors as a function of sites and frequency

Second, the combined (for all sites) relative mean and RMS errors have been computed from 1 to 350 GHz. The results are highlighted in Figure 5-14. As previously mentioned, it can be observed that Section 2.2 of Annex 2 of ITU-R P.676-11 (so not the in-force recommendation) is the best model over the full range of frequency from 1 to 350 GHz followed very closely by the new model.

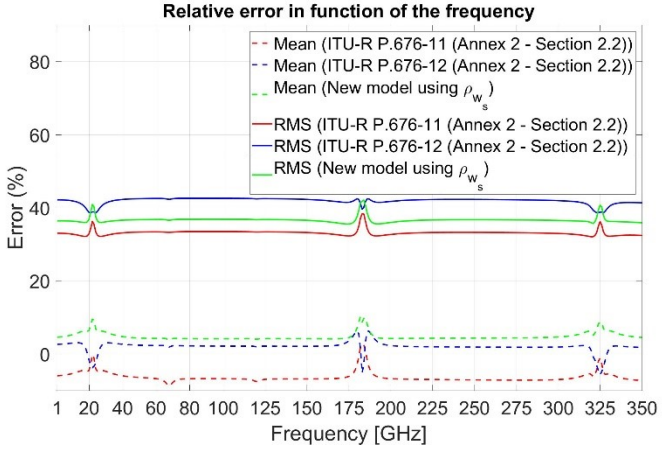

Figure 5-14 : Relative mean and RMS errors in function of the frequency

Third, the scatterplot of the retrieved water vapour attenuation vs. the reference water vapour attenuation is also a good performance indicator. The results at 20, 40, 80, and 150 GHz are shown in Figure 5-15. The straight black line represents the curve y=x. It can be then observed that the performances of the three models are quite moderate.

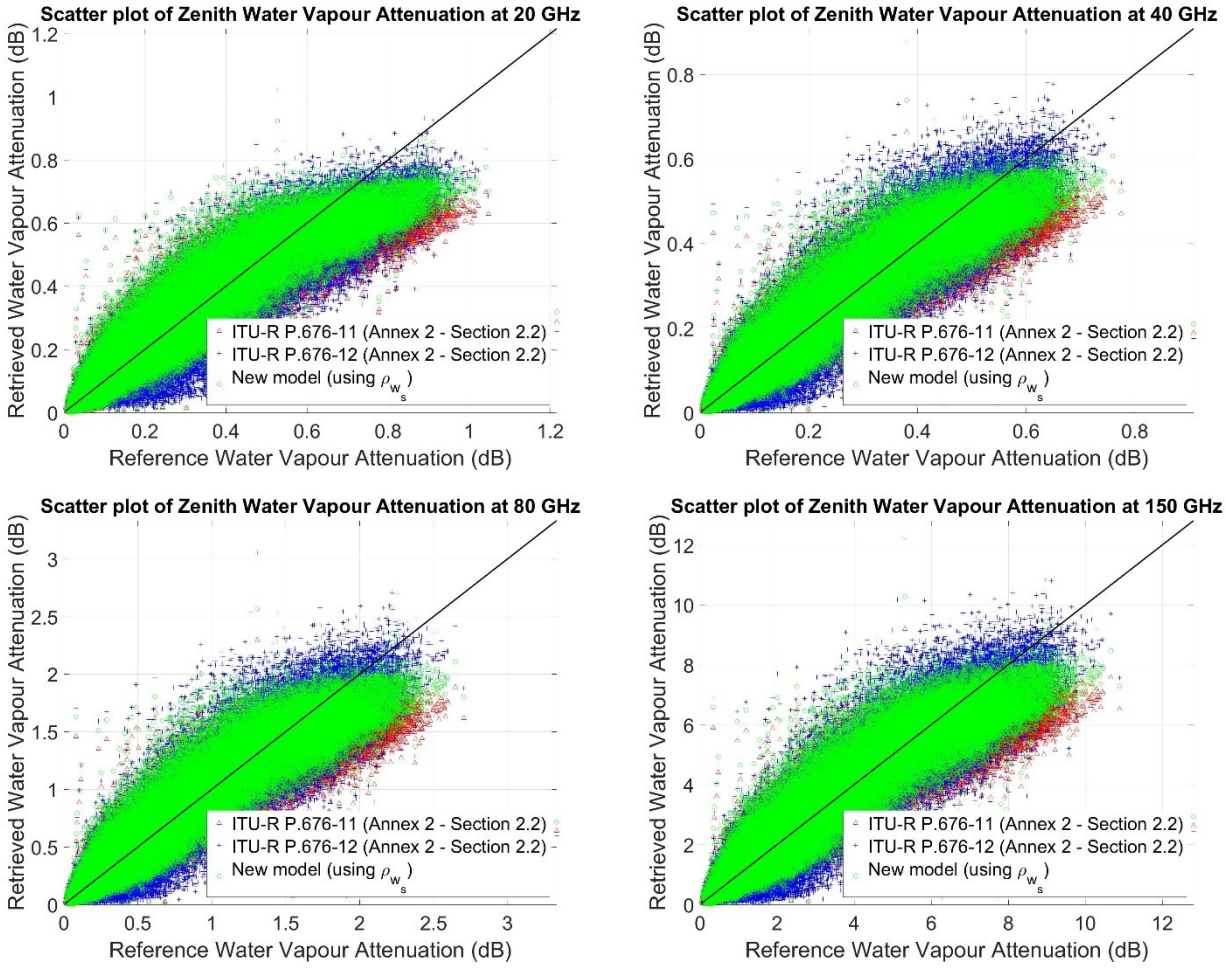

Figure 5-15 : Scatterplot of zenith water vapour attenuation

Finally, CCDF of water vapour attenuation (taking into account the full dataset, so disregarding the locations) have been computed. The results at 20, 40, 80, and 150 GHz are given in Figure 5-16. This time, it can be observed that, at least for probability of exceedance below 10%, the best model seems to be Section 2.2 of Annex 2 of ITU-R P.676-12 (so the in-force recommendation) followed by the new model.

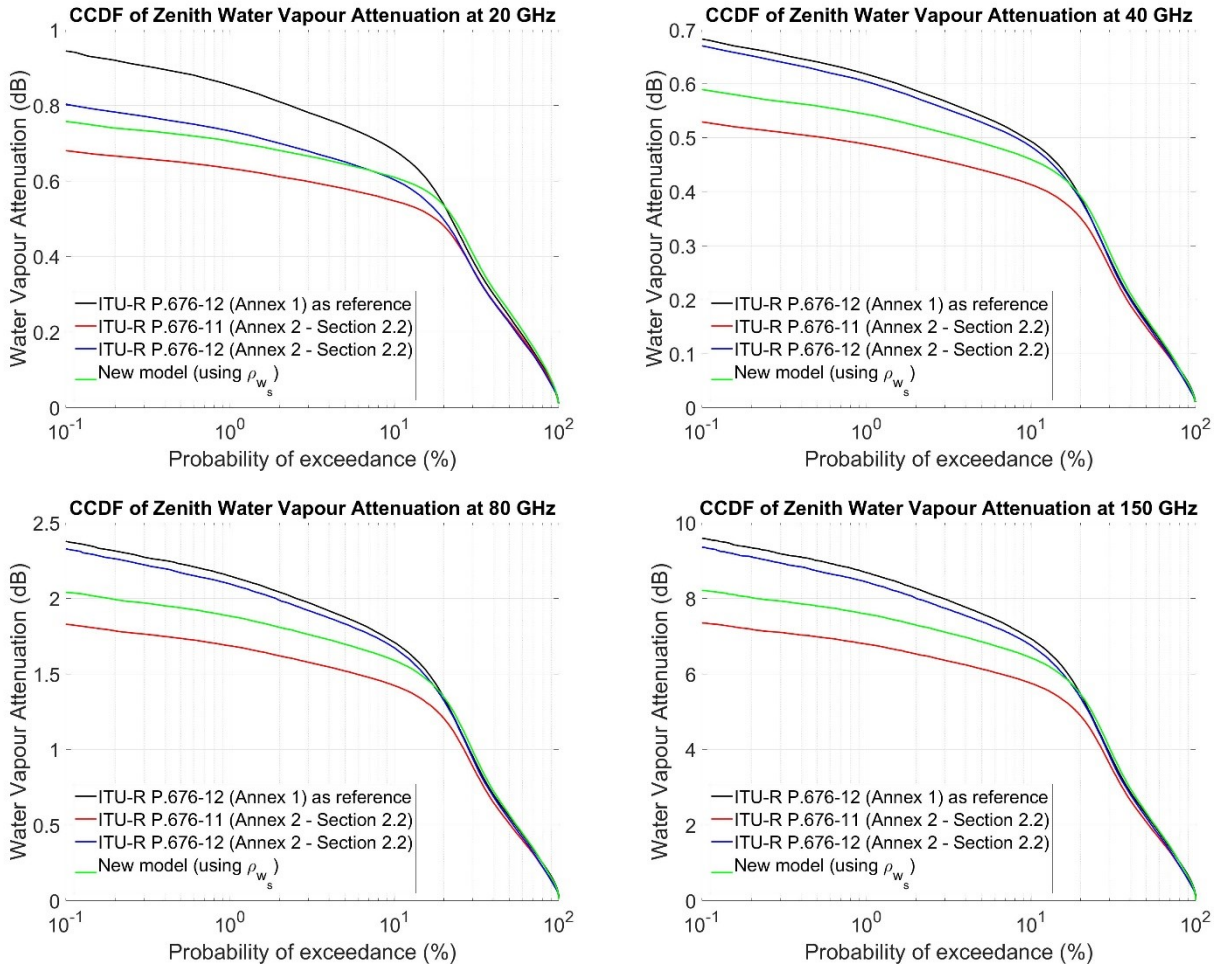

Figure 5-16 : CCDF of zenith water vapour attenuation

5.2.3 NEW MODEL OF THE WATER VAPOUR ABSORPTION COEFFICIENT

5.2.3.1 DESCRIPTION

The idea is to propose a new model to compute the water vapour absorption coefficient, K_V, in dB/mm, such that the water vapour attenuation can be easily derived from the total columnar content of water vapour, *V*, in mm, with the following relationship:

$$A_W = \frac{K_V \cdot V}{\sin\theta}$$

where θ is the elevation angle (θ>5°).

The new proposed model has been derived by applying the following step-by-step procedure:

1. for each frequency, *f*, between 1 and 350 GHz, a global map of optimal values of $K_V(f)$, called $K_{V_{opt}}(f)$, is computed by dividing the reference zenith water vapour attenuation map $A_{W_{ref}}(f)$ by reference integrated water vapour content map, V_{ref}. It means that the following computation is performed:

$$K_{V_{opt}}(f) = \frac{A_{W_{ref}}(f)}{V_{ref}}$$

Examples at 20 GHz and 80 GHz are given below:

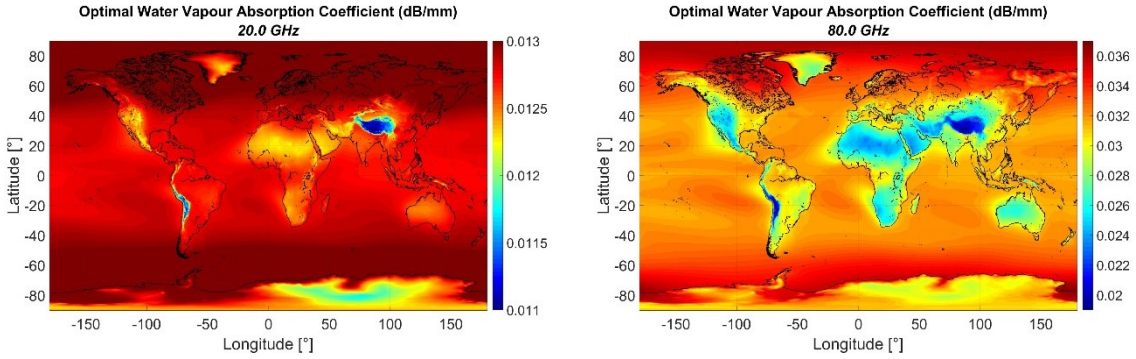

2. for each frequency, *f*, between 1 and 350 GHz, a linear relationship between $K_{V_{opt}}(f)$ and the surface total pressure, temperature and water vapour density is found. Four different models are tested:

   a. $K_{V_{opt}}(f) = K_{V_{opt}}(f, \rho_{w_S}) = a_V(f) + b_V(f) \cdot \rho_{w_S}$

   b. $K_{V_{opt}}(f) = K_{V_{opt}}(f, \rho_{w_S}, T_s) = a_V(f) + b_V(f) \cdot \rho_{w_S} + c_V(f) \cdot T_s$

   c. $K_{V_{opt}}(f) = K_{V_{opt}}(f, \rho_{w_S}, P_s) = a_V(f) + b_V(f) \cdot \rho_{w_S} + d_V(f) \cdot P_s$

   d. $K_{V_{opt}}(f) = K_{V_{opt}}(f, \rho_{w_S}, T_s, P_s) = a_V(f) + b_V(f) \cdot \rho_{w_S} + c_V(f) \cdot T_s + d_V(f) \cdot P_s$

It has to be noticed that the linear regression has been performed by weighting each grid point (pixel) by the area on the surface of the Earth as explained in Section 3 of this document. Examples of the retrieval of the water vapour absorption coefficient (using model d.) are given below:

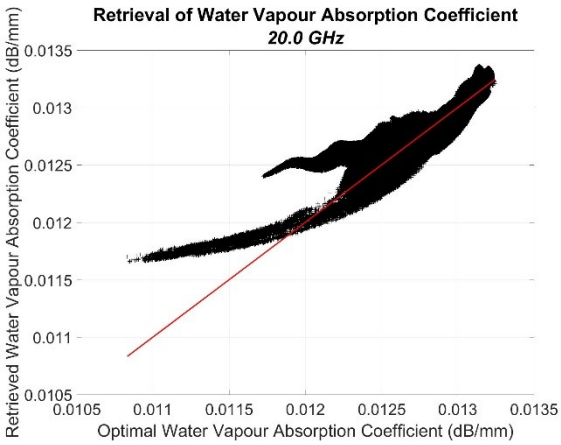

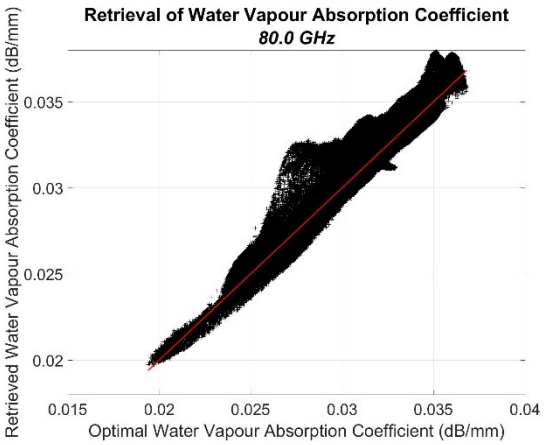

3. The absolute (in dB/mm) and relative (in %) RMS errors between the optimal water vapour absorption coefficient and the proposed models are computed.

The results of the linear regressions are given in Figure 5-17 where the specific values of the coefficients a_V, b_V, c_V and d_V are highlighted.

The absolute and relative RMS errors between the optimal water vapour equivalent height and the proposed models are shown in Figure 5-18. It can be observed that adding more surface parameters improves the global performances of the model.

Finally, for a given frequency, *f*, the final new prediction method of the instantaneous water vapour attenuation based on the total columnar content of water vapour is:

$$A_W(f, \rho_{w_S}, T_s, P_s) = \frac{K_V(f, \rho_{w_S}, T_s, P_s) \cdot V}{\sin\theta}$$

with $K_V(f, \rho_{w_S}, T_s, P_s) = a_V(f) + b_V(f) \cdot \rho_{w_S} + c_V(f) \cdot T_s + d_V(f) \cdot P_s$.

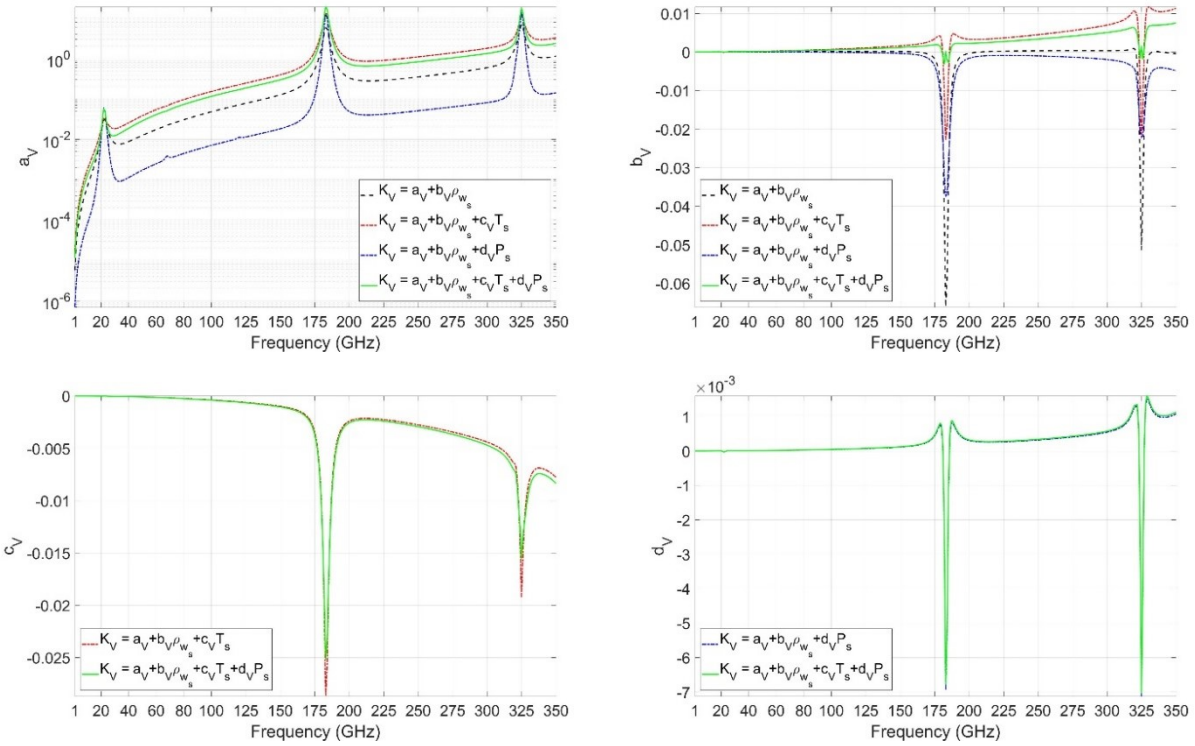

Figure 5-17 : *av*, *bv*, *cv*, and *dv* coefficients of the new model of the water vapour absorption coefficient

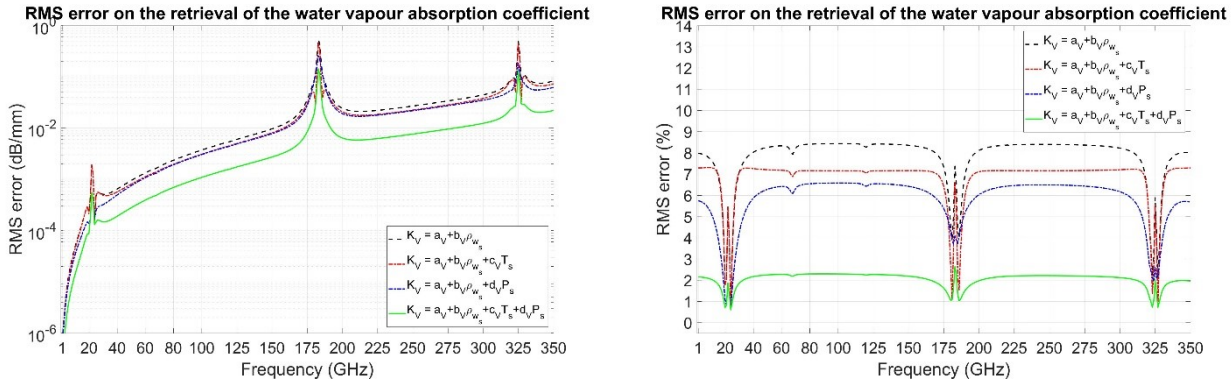

Figure 5-18 : Absolute (left) and relative (right) RMS errors of the new model of the water vapour absorption coefficient

5.2.3.2 VERIFICATION USING THE NEW MEAN ANNUAL VERTICAL PROFILES

The two prediction methods of Sections 2.3 of Annex 2 of ITU-R P.676-11 and ITU-R P.676-12 and the new model have been tested using the new mean annual maps provided in Section 2.2 of this document. First, the worldwide absolute and relative errors for the selected frequencies between 1 and 350 GHz are computed. Some illustrations of the relative errors at 20, 40, 50 and 80 GHz are shown in Figure 5-19. Finally, Figure 5-20 highlights the relative mean and RMS errors from 1 to 350 GHz. It can be observed that for both metrics, the new model performs largely better than Sections 2.3 of Annex 2 of ITU-R P.676-11 and ITU-R P.676-12 over the full range of frequency from 1 to 350 GHz. Indeed, the relative RMS errors for ITU-R P.676-11 and ITU-R P.676-12 are around 7% and 12%, respectively, while for the new model, it is around 2%.

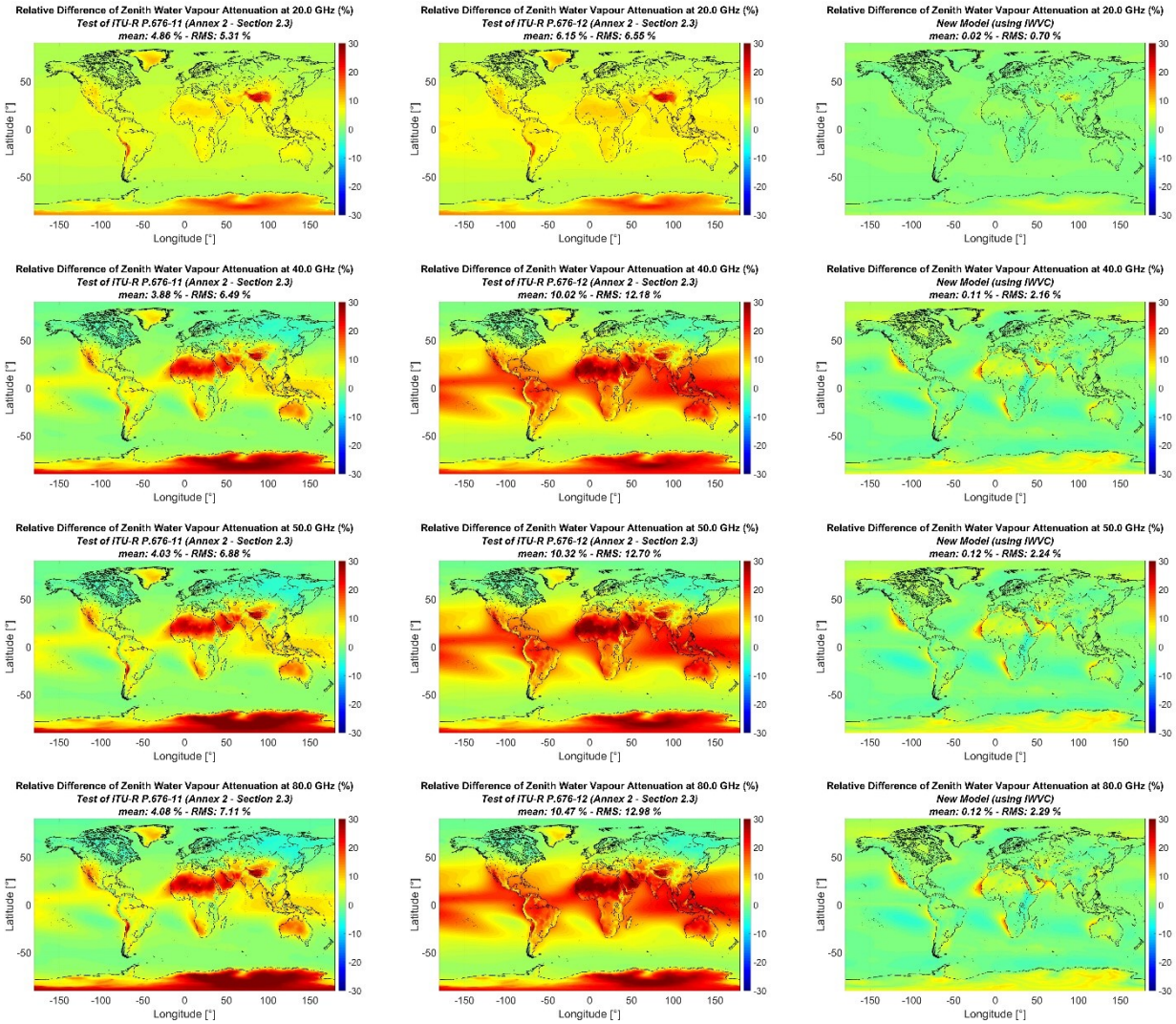

Figure 5-19 : Relative error of zenith water vapour attenuation
1st line: 20 GHz, 2nd line: 40 GHz, 3rd line: 50 GHz, 4th line: 80 GHz
1st column: ITU-R P.676-11, 2nd column: ITU-R P.676-12, 3rd column: new model

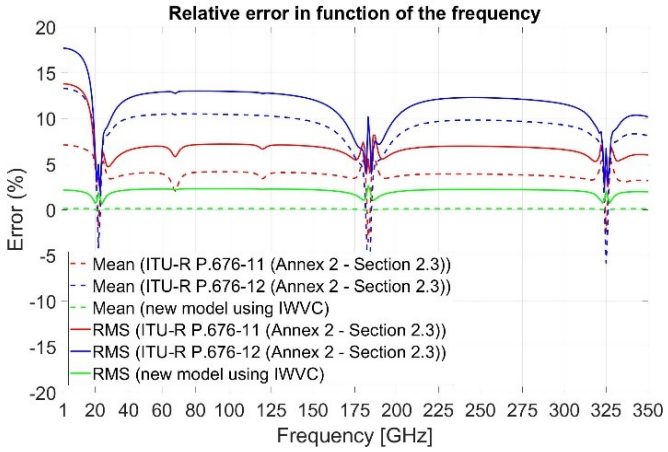

Figure 5-20 : Relative mean and RMS errors in function of the frequency

5.2.3.3 TEST USING RADIOSOUNDING OBSERVATIONS (RAOBS)

To test the performances of the new instantaneous water vapour attenuation prediction method with respect to Section 2.3 of Annex 2 of both ITU-R P.676-11 and ITU-R P.676-12, concurrent IWVC and water vapour attenuation have been extracted from radiosounding observations (RAOBS) data. Ten years (2011-2020) of RAOBS on 24 different locations have been taken into account (same data than in Section 4.1.2.3). As these RAOBS data were also used to test oxygen attenuation prediction methods, only RAOBS for which the highest altitude level is above 25 km have been considered. The table below recalls the main information on the RAOBS dataset. The total number of RAOBS used is 80698.

Country (NOAA ID)	Site	Latitude (°N)	Longitude (°E)	Altitude (m)	Total number of RAOBS	Number of RAOBS with the highest level above 25 km
AR	BUENOS-AIRES-EZEIZA	-34.82	-58.53	20	4930	3635
AT	GRAZ	47.00	15.43	347	3106	1254
BR	GALEAO-RIO	-22.82	-43.25	6	6650	1980
CI	ABIDJAN-PORT-BOUET	5.25	-3.93	8	5569	1713
CN	BEIJING-PEKING	39.93	116.28	55	6558	677
ES	MADRID-BARAJAS	40.47	-3.58	638	6449	5637
FR	BORDEAUX-MERIGNAC	44.83	-0.70	45	6413	3267
GA	LIBREVILLE-LEON-MBA	0.45	9.42	15	2206	1037
GF	CAYENNE-ROCHAMBEAU	4.83	-52.37	9	6851	2728
GP	POINTE-A-PITRE-RAIZET	16.27	-61.52	8	4667	2247
GR	ATHENS-HELLENKION	37.90	23.73	14	2479	853
IN	CALCUTTA-DUM-DUM	22.65	88.45	6	8056	3774
IN	DELHI-SAFDARJUNG	28.58	77.20	216	9499	1537
IT	MILANO-LINATE	45.43	9.28	103	7447	6946
MX	MEXICO-CITY	19.43	-99.07	2309	7353	5073
NO	NY-ALESUND-II	78.92	11.93	8	4615	4292
PT	LISBON-GAGO-COUTINHO	38.77	-9.13	105	3208	1808
RE	SAINT-DENIS	-20.88	55.52	20	3221	1408
SG	SINGAPORE-CHANGI	1.37	103.98	16	11635	3993
US	DENVER	39.77	-104.88	1611	7270	6772
US	FAIRBANKS	64.82	-147.87	135	7264	6888
US	LAS-VEGAS	36.05	-115.18	693	7209	6553
US	MCMURDO-USA-BASE	-77.85	166.67	34	5270	225
US	MIAMI-INTL-UNIV	25.75	-80.38	4	7455	6401

First, the relative mean (Figure 5-21) and RMS (Figure 5-22) error have been computed for each site and each frequency from 1 to 350 GHz with a frequency step of 1 GHz. In both cases, the new model seems to perform better than Section 2.3 of Annex 2 of both ITU-R P.676-11 and ITU-R P.676-12.

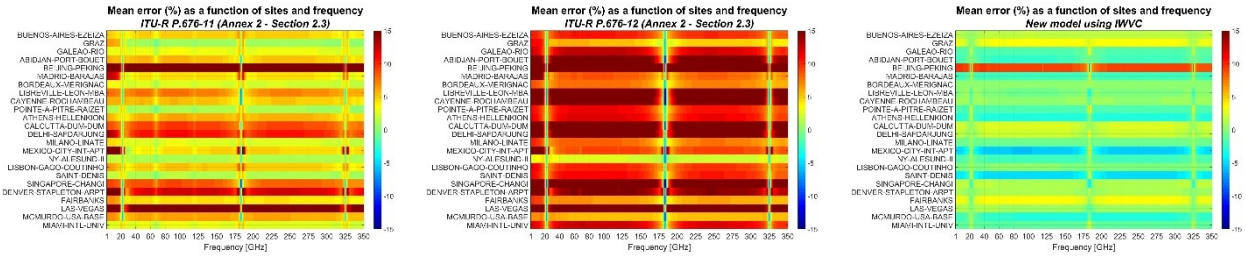

Figure 5-21 : Relative mean errors as a function of sites and frequency

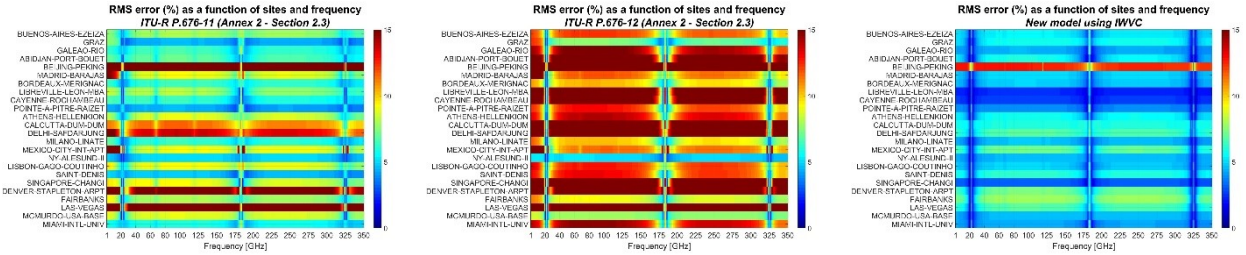

Figure 5-22 : Relative RMS errors as a function of sites and frequency

Second, the combined (for all sites) relative mean and RMS errors have been computed from 1 to 350 GHz. The results are highlighted in Figure 5-23. It can be observed that for both metrics, the new model performs better than Section 2.3 of Annex 2 of both ITU-R P.676-11 and ITU-R P.676-12 over the full range of frequency from 1 to 350 GHz.

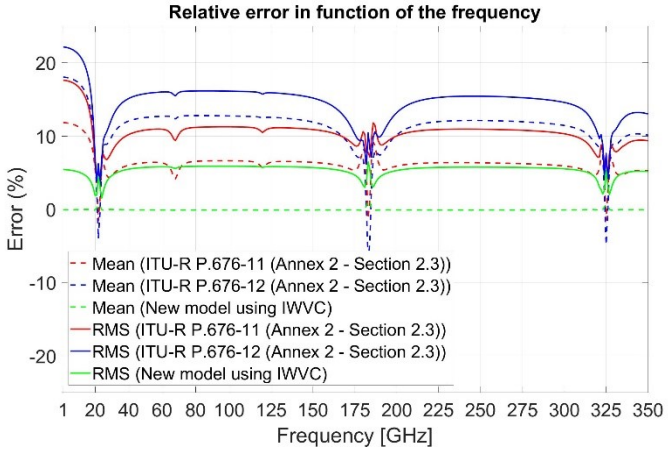

Figure 5-23 : Relative mean and RMS errors in function of the frequency

Third, the scatterplot of the retrieved water vapour attenuation vs. the reference water vapour attenuation is also a good performance indicator. The results at 20, 40, 80, and 150 GHz are shown in Figure 5-24. The straight black line represents the curve y=x. It can be then observed that the new model performs better than the ITU-R prediction methods which is in agreement with the results of Figure 5-23.

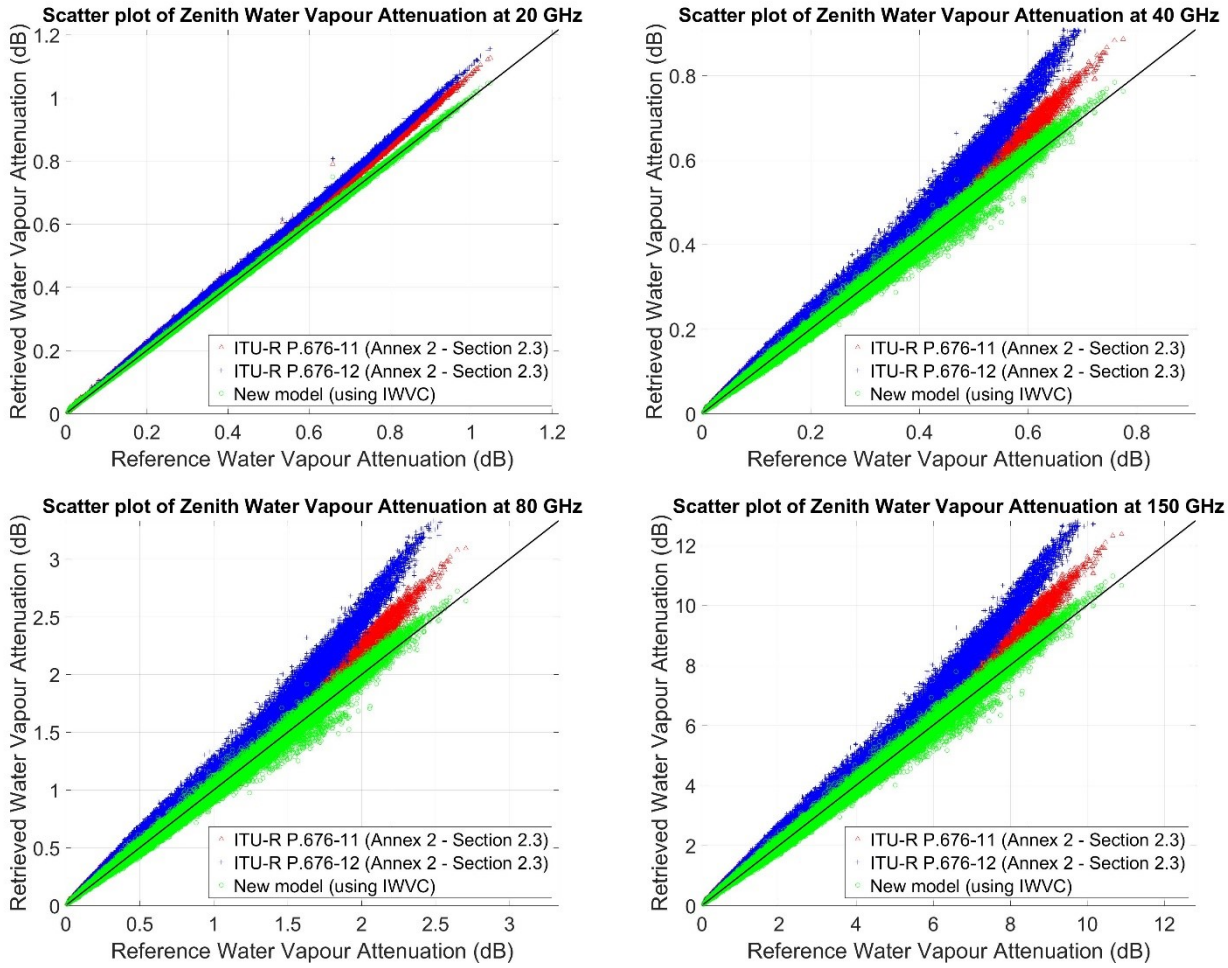

Figure 5-24 : Scatterplot of zenith water vapour attenuation

Finally, CCDF of water vapour attenuation (taking into account the full dataset, so disregarding the locations) have been computed. The results at 20, 40, 80, and 150 GHz are given in Figure 5-25. It can be observed a very good agreement of the new proposed model.

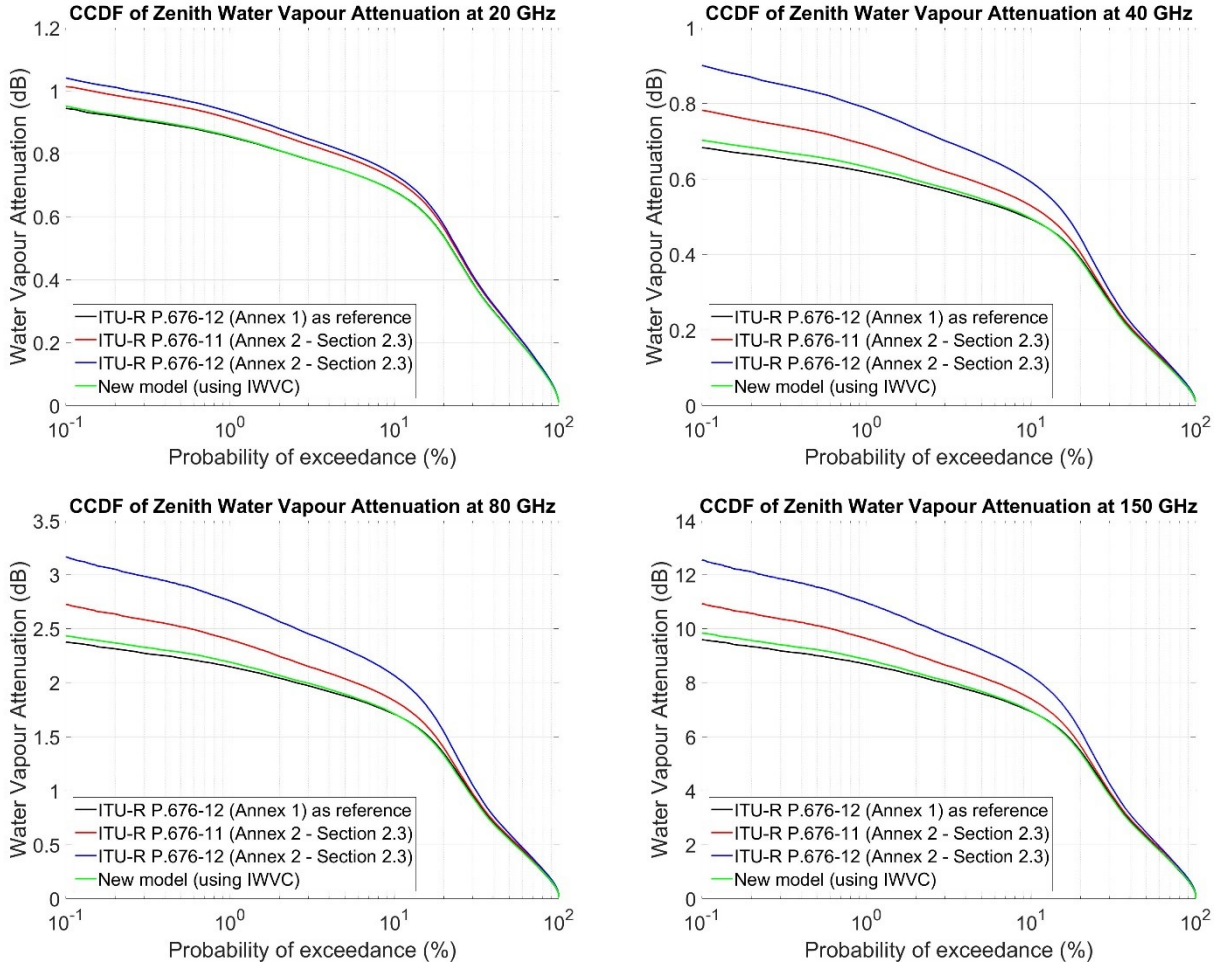

Figure 5-25 : CCDF of zenith water vapour attenuation

5.3 NEW PREDICTION METHOD OF THE STATISTICAL DISTRIBUTION OF WATER VAPOUR ATTENUATION

5.3.1 DESCRIPTION

Recalling that the new prediction method of the instantaneous water vapour attenuation based on the total columnar content of water vapour is (section 5.2.3.1):

$$A_W(f, \rho_{w_s}, T_s, P_s) = \frac{K_V(f, \rho_{w_s}, T_s, P_s) \cdot V}{\sin\theta}$$

with $K_V(f, \rho_{w_s}, T_s, P_s) = a_V(f) + b_V(f) \cdot \rho_{w_s} + c_V(f) \cdot T_s + d_V(f) \cdot P_s$, it is not necessarily straightforward to define a new prediction method of the statistical distribution (CCDF) of water vapour attenuation $A_W(f, p)$ where *p* is the probability of exceedance (in %).

The proposed modelling of $A_W(f, p)$ is the following

$$A_W(f, p) = \frac{K_V(f, \overline{\rho_{w_s}}, \overline{T_s}, \overline{P_s}) \cdot V(p)}{\sin\theta}$$

with $K_V(f, \overline{\rho_{w_s}}, \overline{T_s}, \overline{P_s}) = a_V(f) + b_V(f) \cdot \overline{\rho_{w_s}} + c_V(f) \cdot \overline{T_s} + d_V(f) \cdot \overline{P_s}$.

$\overline{P_s}$, $\overline{T_s}$, and $\overline{\rho_{w_s}}$ are respectively the mean of surface pressure, surface temperature and surface water vapour density over the period of interest (e.g. annual or monthly mean). $V(p)$ represents the CCDF of the total columnar content of water vapour over the same period of interest (e.g. annual or monthly CCDF), i.e. the values of V exceeded for *p* % of the time.

Examples for some RAOBS sites are given in Figure 5-26 where the results coming from the instantaneous prediction method are compared with the results coming from the statistical prediction method. The black curve is the reference coming from the integration of the water vapour specific attenuation along the RAOBS profiles. It can be observed a very good agreement between the instantaneous and the statistical prediction methods.

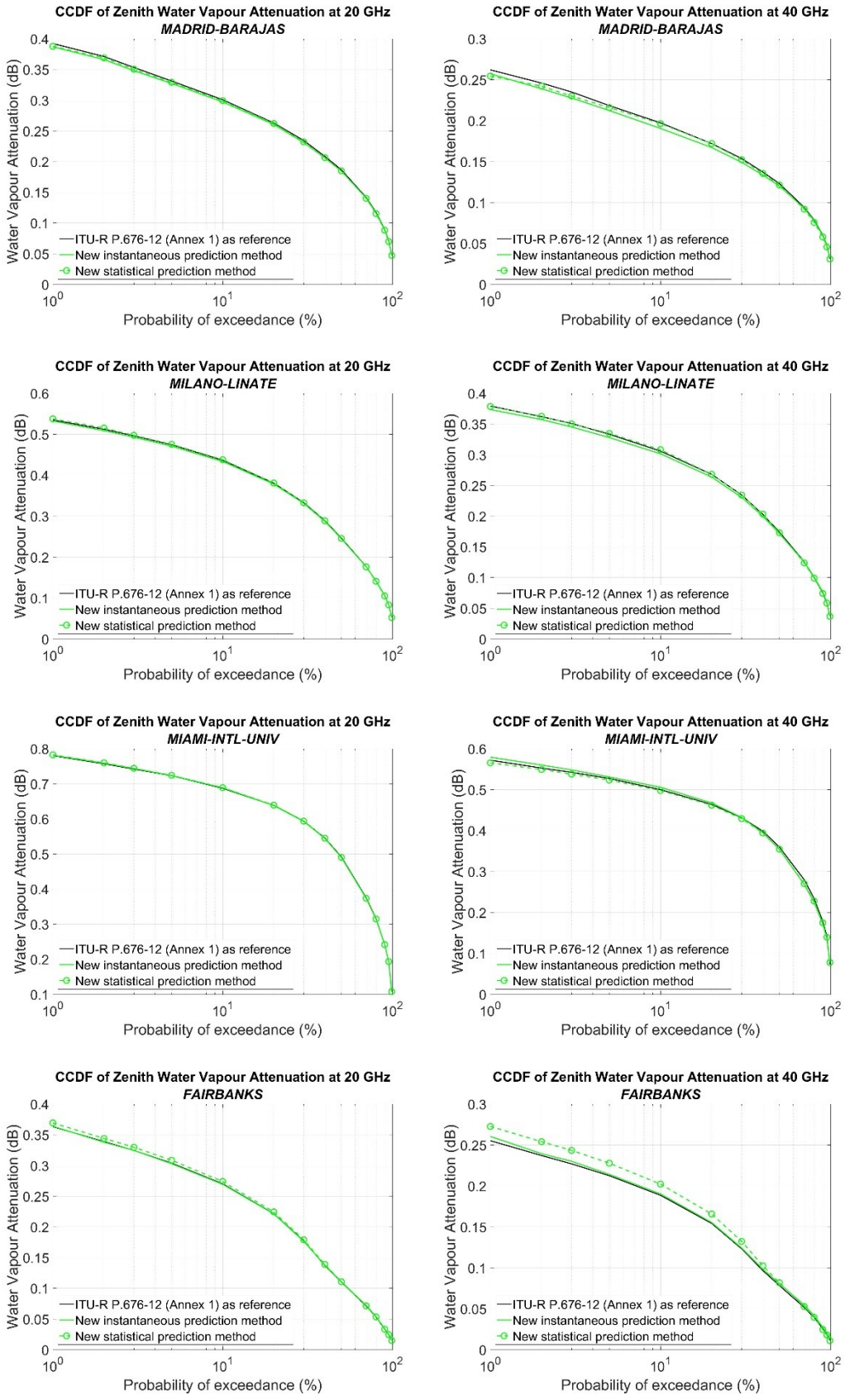

Figure 5-26 : Comparisons of instantaneous and statistical prediction methods of water vapour attenuation left: 20 GHz, right: 40 GHz

5.3.2 DERIVATION OF NEW MAPS OF IWVC

In addition to the monthly averaged pressure level data described in Section 2, ERA5 also contains hourly reanalysis data on single level. As for pressure level data, the spatial resolution is 0.25° in both latitude and longitude. Among all the available parameters, the **total column water vapour** might be of interest as it seems to be equivalent to the integrated Water Vapour Content, IWVC (and so equivalent to the total columnar content of water vapour, *V*).

Extract from ERA5 website:

Total column water vapour	$kg.m^{-2}$	This parameter is the total amount of water vapour in a column extending from the surface of the Earth to the top of the atmosphere. This parameter represents the area averaged value for a grid box.

Several new reference maps have then been derived from 30 years (1991-2020 that defines new climate normals) of ERA5 **hourly** data:

- The annual and monthly mean values of IWVC (in kg/m^2 equivalent to mm),
- The annual and monthly standard deviation values of IWVC (in kg/m^2 equivalent to mm),
- The annual values of IWVC (in kg/m^2 equivalent to mm) exceeded for the probability levels of 0.001, 0.002, 0.003, 0.005, 0.01, 0.02, 0.03, 0.05, 0.1, 0.2, 0.3, 0.5, 1, 2, 3, 5, 10, 20, 30, 50, 60, 70, 80, 90, 95, and 99% of an average year,
- The monthly values of IWVC (in kg/m2 equivalent to mm) exceeded for the probability levels of 0.01, 0.02, 0.03, 0.05, 0.1, 0.2, 0.3, 0.5, 1, 2, 3, 5, 10, 20, 30, 50, 60, 70, 80, 90, 95, and 99% of each average month.

The latitude grid is from −90° N to +90° N in 0.25° steps, and the longitude grid is from −180° E to +180° E in 0.25° steps.

As examples, Figure 5-27 shows the annual mean and standard deviation of IWVC (equivalent to the total columnar content of water vapour as previously indicated) derived from 30 years (1991-2020) of ERA5 hourly reanalysis data.

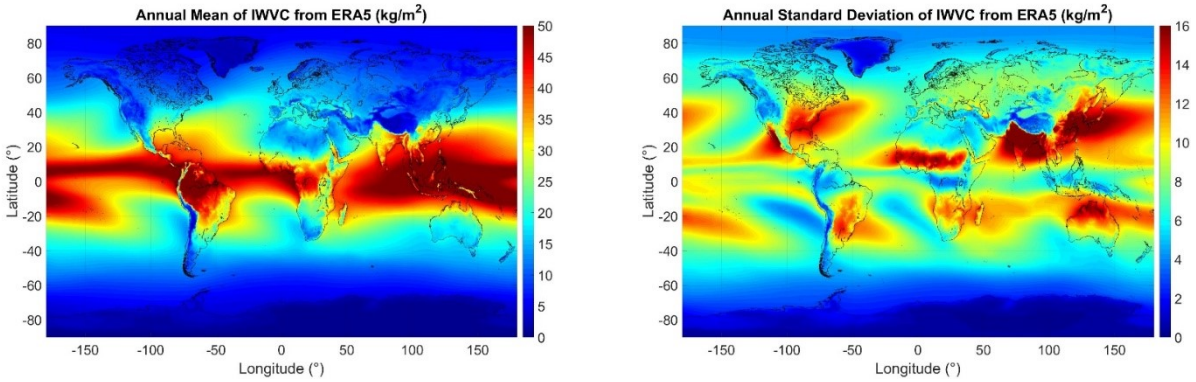

Figure 5-27 : Annual mean (left) and standard deviation (right) of Integrated Water Vapour Content derived from ERA5 hourly reanalysis data (1991-2020)

The main differences between the digital maps provided by ITU-R P.836-6 and this document are summarized in the table below:

Parameters related to total column of water vapour		ITU-R P.836-6	This document
Spatial resolution		**1.125°**	**0.25°**
Mean	Annual	Unavailable	Available
	Monthly	Unavailable	Available
Standard deviation	Annual	Unavailable	Available
	Monthly	Unavailable	Available
CCDF	Annual	Maps from 0.1% to 99%	Maps from 0.001% to 99%
	Monthly	Maps from 1% to 99%	Maps from 0.01% to 99%

Some illustrations of the differences of annual IWVC between ITU-R P.836-6 and the new ERA5 maps are shown in Figure 5-28 and Figure 5-29 respectively on a worldwide basis and over Europe for probabilities of exceedance equal to 0.1%, 1%, and 10%. No major difference can be observed but the impact of the new spatial resolution is clearly visible.

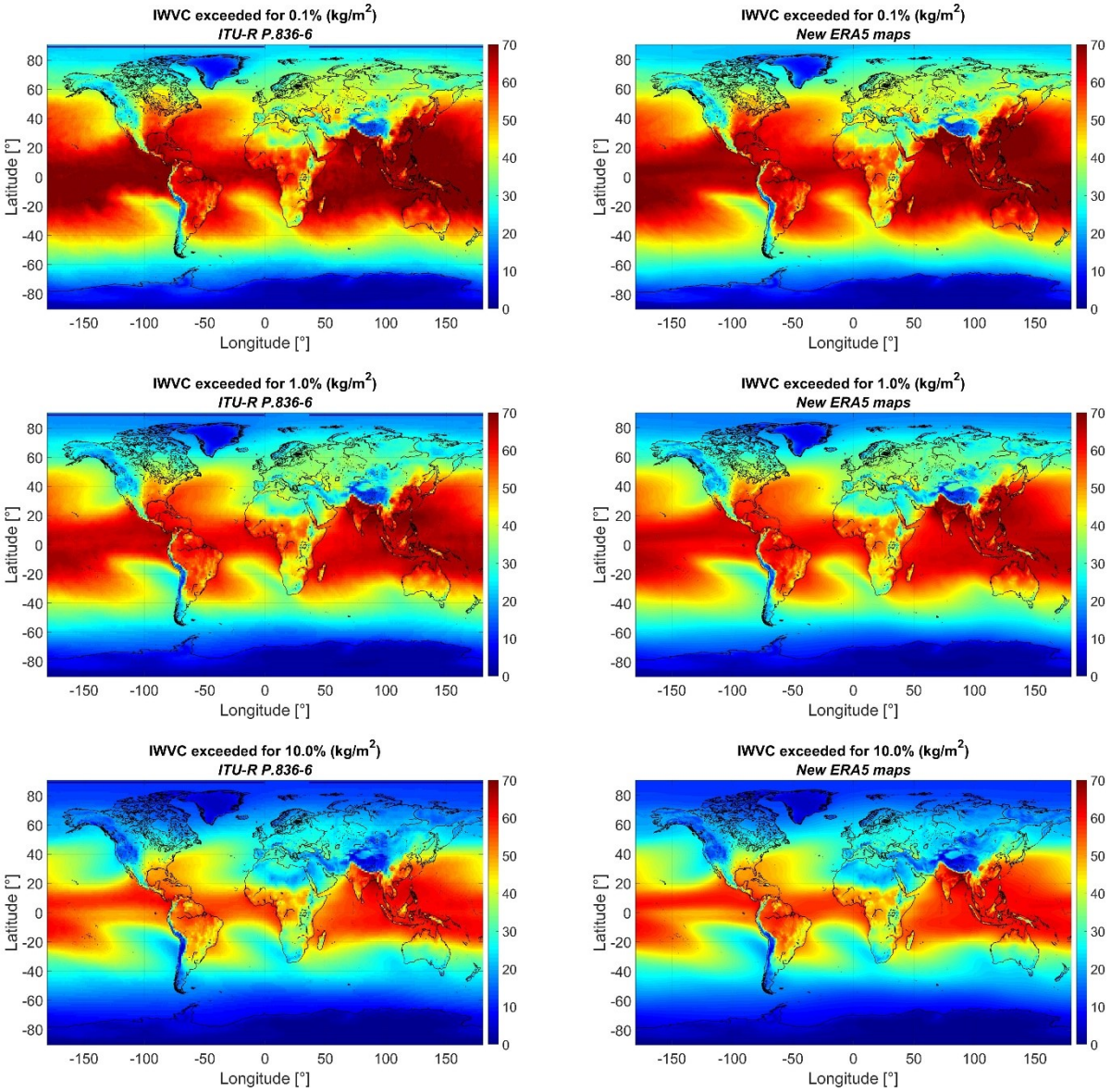

Figure 5-28 : Annual Integrated Water Vapour Content
1st line: 0.1%, 2nd line: 1%, 3rd line: 10%
left: ITU-R P.836-6, right: new ERA5 maps

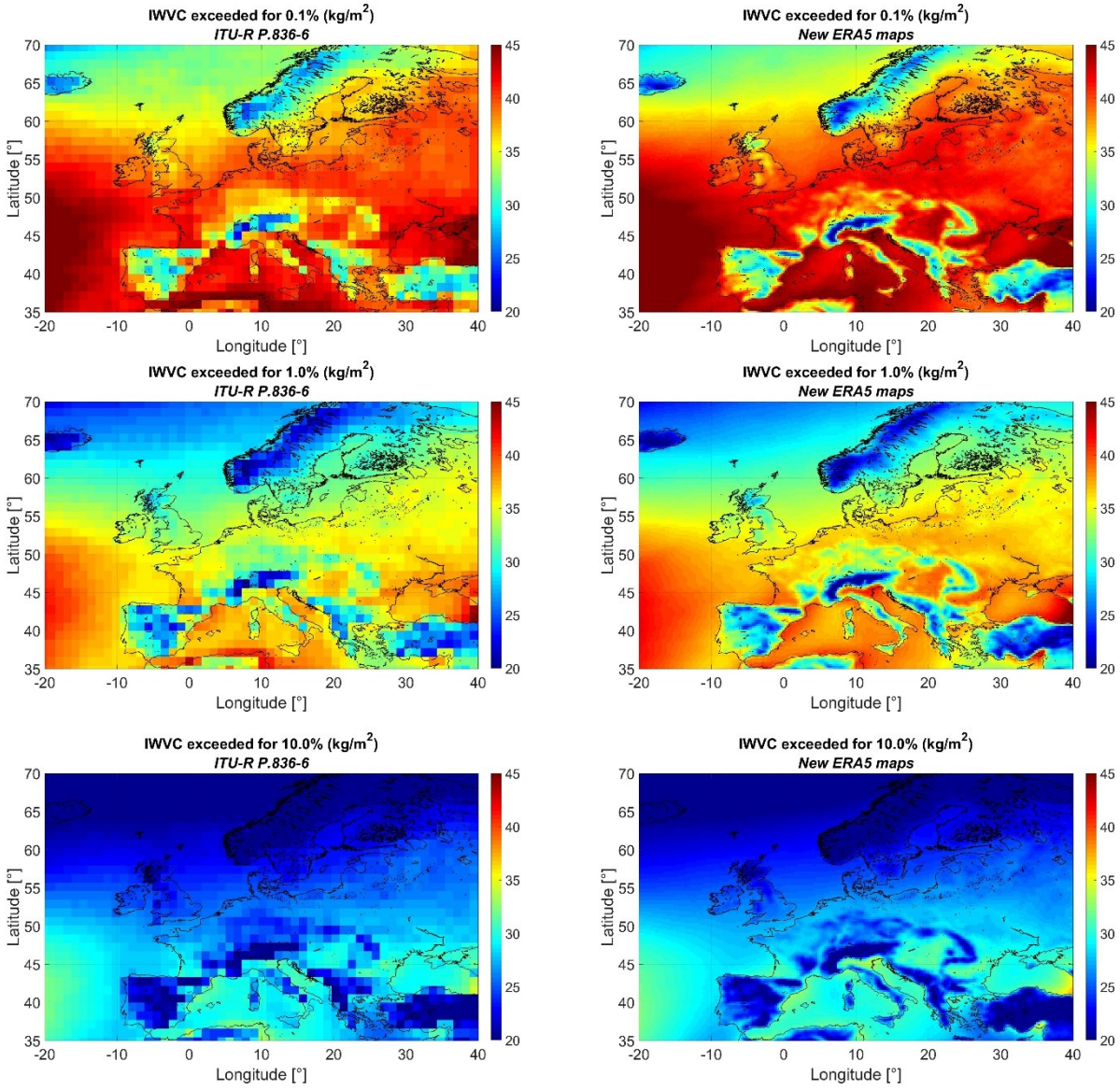

Figure 5-29 : Annual Integrated Water Vapour Content (over Europe)
1st line: 0.1%, 2nd line: 1%, 3rd line: 10%
left: ITU-R P.836-6, right: new ERA5 maps

Five specific sites have then been selected to highlight the differences of Integrated Water Vapour Content over the full distribution. The results are shown in Figure 5-30. It can be observed some differences especially for the sites close to mountains (Toulouse and Spino d'Adda) because the reference altitudes of the surface of the Earth are not necessarily the same (due to the poor spatial resolution of ITU-R P.836-6). Now, with ERA5 data, orographic effects are much better reproduced.

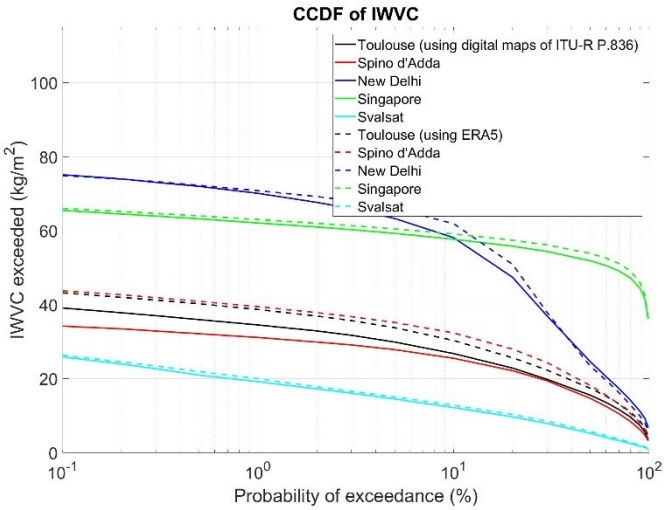

Figure 5-30 : CCDF of IWVC on the five specific locations

Finally, as explained in Section 5.1, the water vapour scale height, h_{VSC}, is a key parameter to scale in altitude the surface water vapour density and the total columnar content of water vapour. This is why, the annual and monthly mean of h_{VSC} (in km), $\overline{h_{VSC}}$, and the annual and monthly standard deviation values of h_{VSC} (in km) have been derived.

As examples, Figure 5-31 shows the annual mean and standard deviation of h_{VSC} derived from 30 years (1991-2020) of ERA5 hourly reanalysis data.

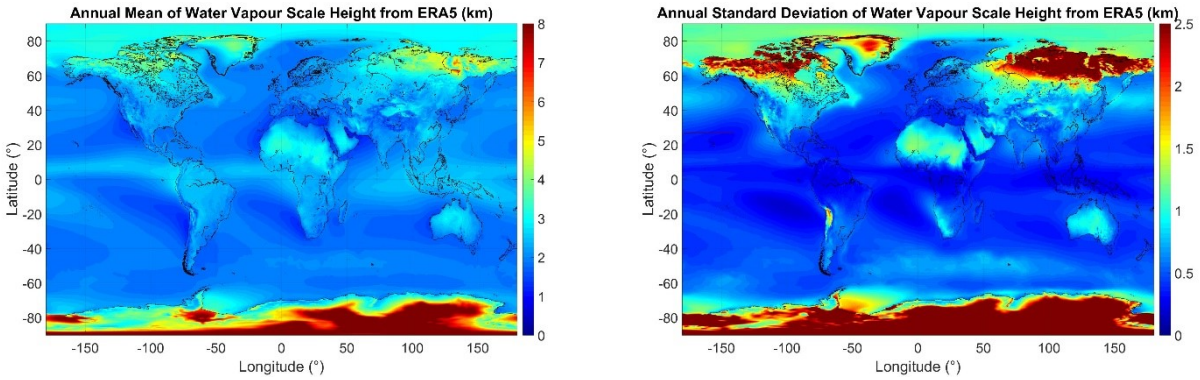

Figure 5-31 : Annual mean (left) and standard deviation (right) of water vapour scale height derived from ERA5 hourly reanalysis data (1991-2020)

5.3.3 DERIVATION OF NEW MAPS FOR THE APPROXIMATION OF THE STATISTICS OF IWVC BY A WEIBULL DISTRIBUTION

In Section 5.1, it has been proposed a new approach for the use of the water vapour scale height. For a given geometric height, Z, and a given probability of exceedance, *p*, the CCDF of the total columnar content of water vapour, $V(Z,p)$, is given by:

$$V(Z,p) = V_s(p) \cdot e^{-\frac{Z-h_s}{\overline{h_{VSC}}}}$$

Now it is assumed that, starting from data already well referenced in altitude (as this is the case for the new ERA5 data), the annual and monthly statistics of the total columnar content of water vapour, V_s, can be approximated by a Weibull distribution. Mathematically, it means that:

$$V_s(p) = \lambda_{V_s}\left(-ln\left(\frac{p}{100}\right)\right)^{\frac{1}{k_{V_s}}}$$

where, λ_{V_s} and k_{V_s} are respectively the scale and shape parameters of the Weibull distribution. Under this assumption, for any given geometric height, Z, the CCDF of the total columnar content of water vapour, $V(Z,p)$, can also be approximated by a Weibull distribution :

$$V(Z,p) = V_s(p)\cdot e^{-\frac{Z-h_s}{h_{VSC}}} = \lambda_{V_s} e^{-\frac{Z-h_s}{h_{VSC}}}\left(-ln\left(\frac{p}{100}\right)\right)^{\frac{1}{k_{V_s}}}$$

So, the new scale, λ_V, and shape, k_V, parameters are then defined by:

$$\begin{cases} \lambda_V = \lambda_{V_s} e^{-\frac{Z-h_s}{h_{VSC}}} \\ k_V = k_{V_s} \end{cases}$$

New reference digital maps of λ_{V_s} and k_{V_s} have been derived from the best Weibull regression fitting of the data provided in Section 5.3.2 of this document. As for the original CCDF data, the latitude grid is from −90° N to +90° N in 0.25° steps, and the longitude grid is from −180° E to +180° E in 0.25° steps.

Figure 5-32 shows the two parameters for the approximation of the annual statistics of the total columnar content of water vapour by a Weibull distribution. Figure 5-33 highlights the absolute and relative RMS errors on the regression of the Weibull distribution.

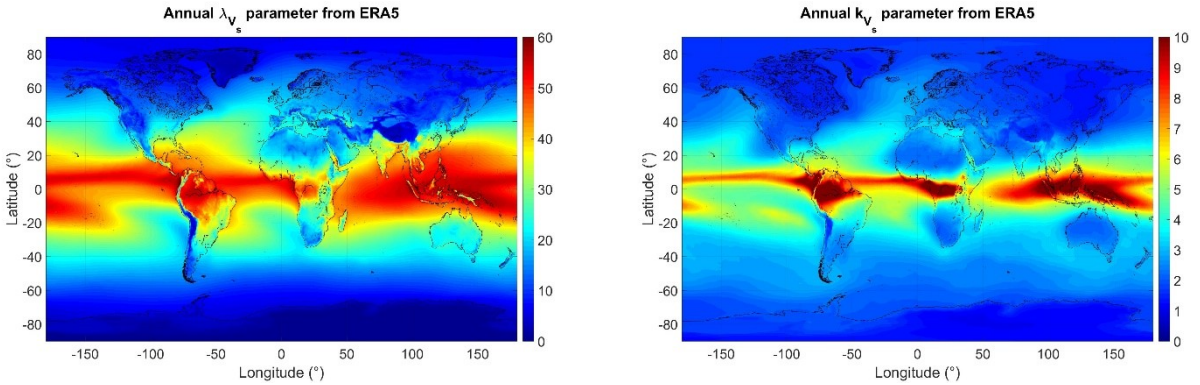

Figure 5-32 : Parameters for the approximation of the annual statistics of the total columnar content of water vapour by a Weibull distribution (left: λ_{V_s}, right: k_{V_s})

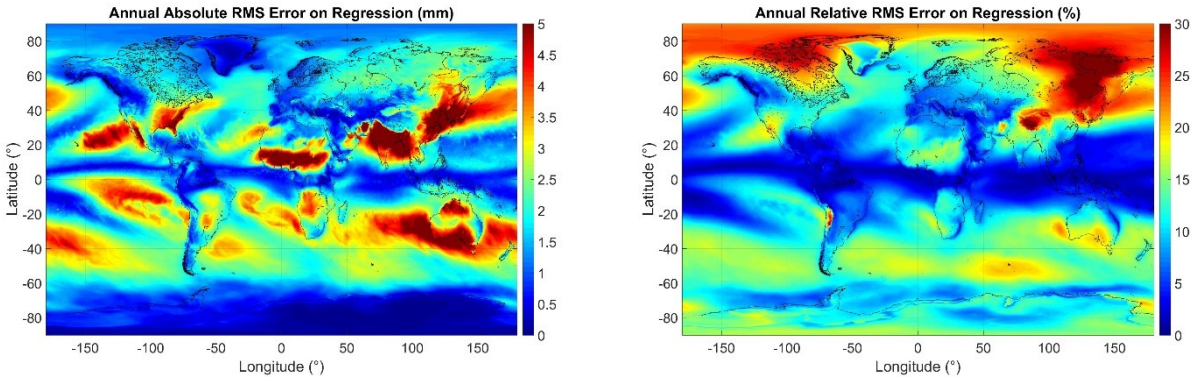

Figure 5-33 : Absolute (left) and relative (right) RMS errors on the regression of the Weibull distribution

Examples of the approximation of the Weibull distribution for the five specific sites (same than in the previous Section) are given in Figure 5-34.

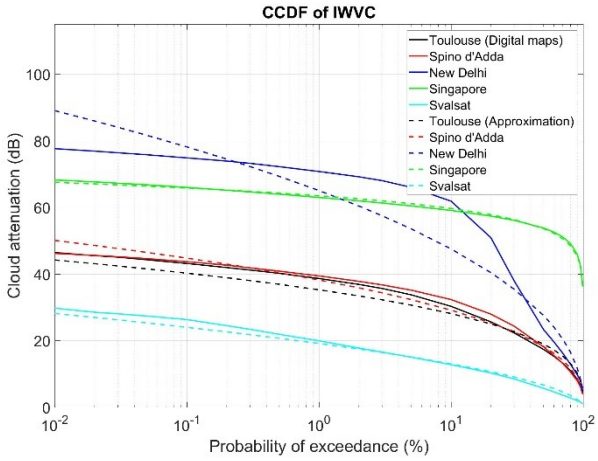

Figure 5-34 : CCDF of IWVC (digital maps and Weibull approximation)

In Section 5.3.1, a new statistical water vapour attenuation prediction method based on the CCDF of total columnar content of water vapour has been proposed:

$$A_W(f,p) = \frac{K_V\left(f,\overline{\rho_{w_S}},\overline{T}_S,\overline{P}_S\right)\cdot V(Z,p)}{\sin\theta}$$

Consequently,

$$A_W(f,p) = \lambda_{V_S}\frac{K_V\left(f,\overline{\rho_{w_S}},\overline{T}_S,\overline{P}_S\right)}{\sin\theta}\, e^{-\frac{Z-h_S}{\overline{h_{VSC}}}\left(-ln\left(\frac{p}{100}\right)\right)^{\frac{1}{k_{V_S}}}}$$

It is then straightforward that the distribution of water vapour attenuation can be approximated by a Weibull distribution:

$$A_W(f,p) = \lambda_W(f)\left(-ln\left(\frac{p}{100}\right)\right)^{\frac{1}{k_W}}$$

with

$$\begin{cases} \lambda_W(f) = \lambda_{V_s}\dfrac{K_V\left(f,\overline{\rho_{w_s}},\overline{T_s},\overline{P_s}\right)}{\sin\theta}e^{-\frac{Z-h_s}{\overline{h_{VSC}}}} \\ k_W = k_{V_s} \end{cases}$$

6 NEW PREDICTION METHODS OF CLOUD ATTENUATION

MAIN OBJECTIVES OF SECTION 6.1:

- Use of the new maps of the mean annual vertical atmospheric profiles to develop a new model of the **cloud liquid water absorption coefficient** for the prediction of cloud attenuation from the total columnar content of cloud liquid water
- Verification and comparison of the performances of the new model with the prediction method described in Section 3.2 of Recommendation ITU-R P.840-8
- Test of the new model using radiosounding observations

MAIN OBJECTIVES OF SECTION 6.2:

- Derivation of a new prediction method of the statistical distribution of cloud attenuation
- Derivation of new digital maps of the total columnar content of cloud liquid water for a worldwide application of the new prediction method in absence of local data
- Derivation of new digital maps for the approximation of the statistics of the total columnar content of cloud liquid water by a Dirac Log-normal distribution

A block diagram of this Section is proposed in Figure 6-1.

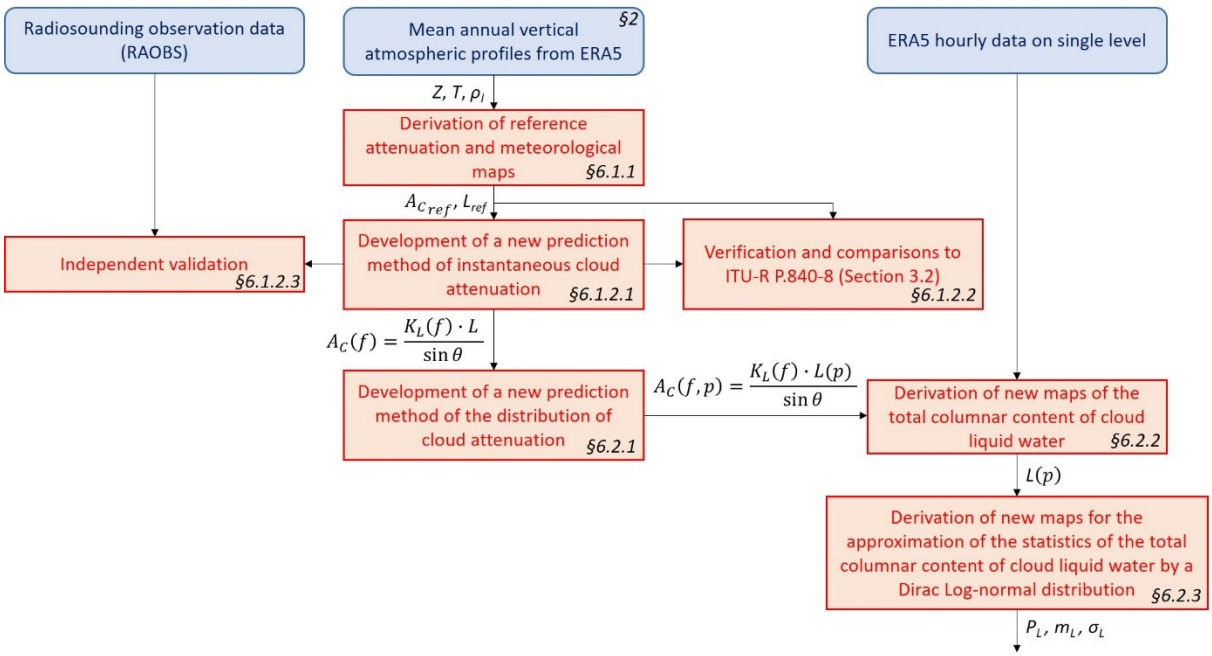

Figure 6-1 : Block diagram of Section 6

6.1 NEW PREDICTION METHOD OF THE INSTANTANEOUS CLOUD ATTENUATION

6.1.1 METHODOLOGY TO DERIVE REFERENCE MAPS

Section 1 of ITU-R P.840-8 [RD 4] is used to get the cloud liquid water specific attenuation profiles, $\gamma_c(Z) = K_l\big(T(Z)\big) \cdot \rho_l(Z)$ from the worldwide temperature, $T(Z)$, and cloud liquid water density, $\rho_l(Z)$, profiles given by the new maps of the mean annual vertical atmospheric profiles provided in Section 2.2 of this document. The cloud liquid water specific attenuation coefficient, K_l, is computed with the methodology described in Section 2 of ITU-R P.840-8 [RD 4].

Reference zenith cloud attenuation maps, $A_{C_{ref}}$, are then derived from the integration of $\gamma_c(Z)$ along the profiles. This process has been performed **from 1 to 200 GHz** (which is the validity range of ITU-R P.840-8) with a frequency step of 1 GHz. The reference zenith cloud attenuation maps at 20, 40, 50, and 80 GHz (frequencies currently used in SatCom systems) are shown in Figure 6-2.

The total columnar content of cloud liquid water, *L*, is derived from the integration of $\rho_l(Z)$ along the profiles. The reference map is then noted L_{ref} and shown in Figure 6-3. Note that the total columnar content of cloud liquid water is also known as the Integrated Liquid Water Content, *ILWC*.

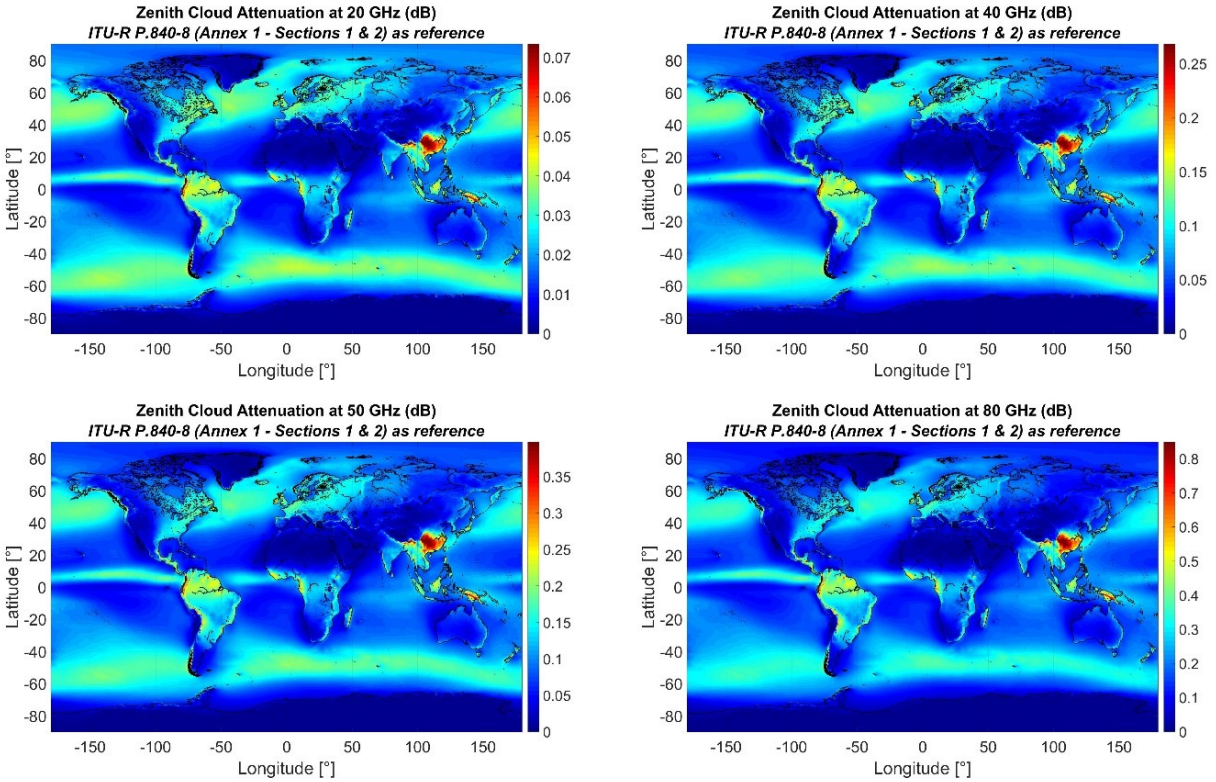

Figure 6-2 : Zenith Cloud Attenuation at 20, 40, 50, and 80 GHz derived from the integration of the cloud liquid water specific attenuation along the new ERA5 annual profiles by using Sections 1 & 2 of Annex 1 of ITU-R P.840-8

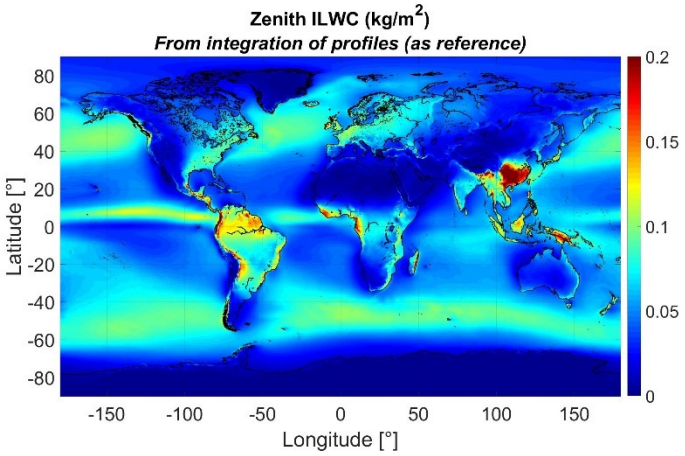

Figure 6-3 : Mean annual zenith Integrated cloud Liquid Water Content (ILWC) derived from the ERA5 monthly averaged database (1991-2020)

6.1.2 NEW MODEL OF THE CLOUD LIQUID WATER ABSORPTION COEFFICIENT

6.1.2.1 DESCRIPTION

The idea is to propose a new model to compute the cloud liquid water absorption coefficient, K_L, in dB/mm, such that the cloud attenuation can be easily derived from:

$$A_C = \frac{K_L \cdot L}{\sin\theta}$$

where θ the elevation angle (θ>5°).

The new proposed model has been derived by applying the following step-by-step procedure:

1. for each frequency, *f*, between 1 and 200 GHz, an optimal value of $K_L(f)$ to retrieve the reference zenith cloud attenuation, called $K_{L_{opt}}(f)$, is derived from the scatterplot of $A_{C_{ref}}(f)$ vs L_{ref}

   It has to be noticed that the retrieval has been performed by weighting each grid point (pixel) by the area on the surface of the Earth as explained in Section 3 of this document. Examples of the retrieval of the cloud liquid water absorption coefficient are given below:

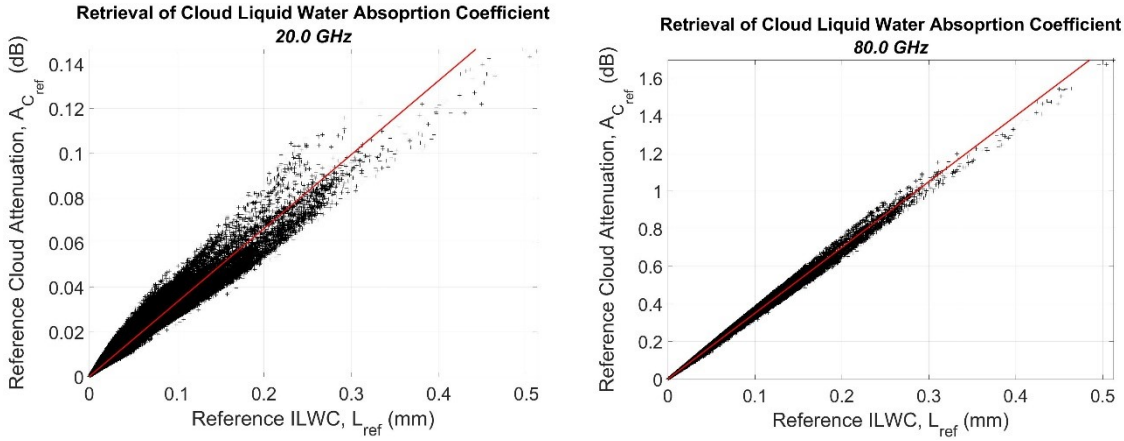

2. for each frequency, *f*, between 1 and 200 GHz and for temperatures, *T*, between -1°C and 2.5°C, the ratio $\frac{K_{L_{opt}}(f)}{K_l(f,T)}$ is computed, $K_l(f,T)$ being the cloud liquid water specific attenuation coefficient given in Section 2 of ITU-R P.840-8 [RD 4].

3. The resulting ratio $\frac{K_{L_{opt}}(f)}{K_l(f,T)}$ is fitted by the best following function:

$$\frac{K_{L_{opt}}(f)}{K_l(f,T)} = A_1 e^{-\frac{(f-\mu_1)^2}{\sigma_1}} + A_2 e^{-\frac{(f-\mu_2)^2}{\sigma_2}} + A_3$$

4. The mean RMS errors (over the full range of frequency from 1 to 200 GHz) between the optimal values of $K_L(f)$ and the model resulting from the fitting procedures are computed for

several temperature values T between -1°C and 2.5°C. The results of the fitting procedures are given in Figure 6-4.

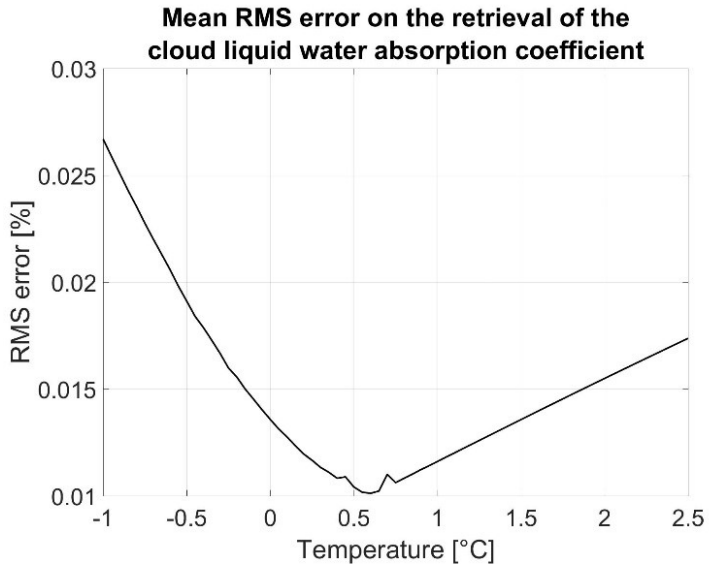

Figure 6-4 : Mean RMS error on the retrieval of cloud liquid water vapour absorption coefficient as a function of temperature

It seems that T=0.6°C is a good candidate to minimize the spread of the residual error over the full range of frequency from 1 to 200 GHz.

Figure 6-8 shows the results of the fitting procedure of the ratio $\frac{K_{Lopt}(f)}{K_l(f,T)}$ only for T=0.6°C.

Finally, for a given frequency, *f*, the final new prediction method of the instantaneous cloud attenuation based on the total columnar content of cloud liquid water is:

$$A_C(f) = \frac{K_L(f) \cdot L}{\sin\theta}$$

with

$$K_L(f) = K_l(f, T = 273.75K) \cdot \left(A_1 e^{-\frac{(f-\mu_1)^2}{\sigma_1}} + A_2 e^{-\frac{(f-\mu_2)^2}{\sigma_2}} + A_3 \right)$$

where

$$\begin{cases} A_1 = 0.1522, A_2 = 11.51, A_3 = -10.4912 \\ \mu_1 = -23.9589, \mu_2 = 219.2096 \\ \sigma_1 = 3.2991 \times 10^3, \sigma_2 = 2.7595 \times 10^6 \end{cases}$$

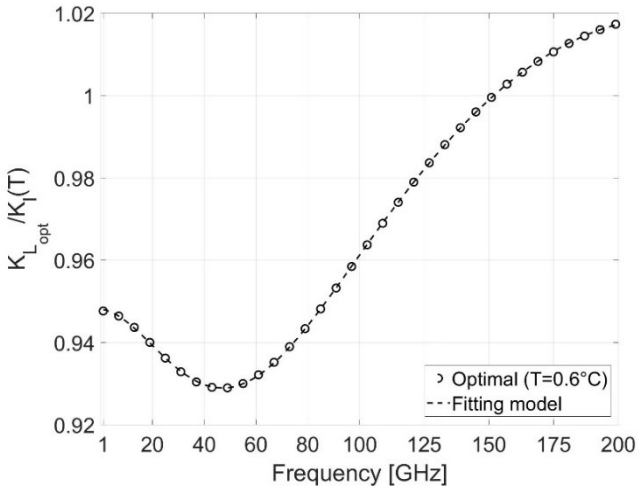

Figure 6-5 : Results of the fitting procedure of the ratio $\frac{K_{L_{opt}}(f)}{K_l(f,T)}$ for T=0.6°C

The comparison between the optimal cloud liquid water absorption coefficient and Section 3.2 of ITU-R P.840-8 and the new model is shown in Figure 6-6 while the absolute and relative errors are shown is Figure 6-7. The agreement of the new model is almost perfect.

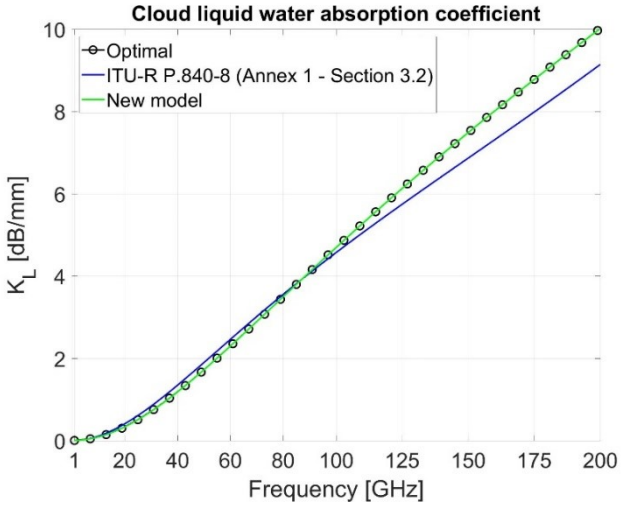

Figure 6-6 : Comparison between the optimal cloud liquid water absorption coefficient and Section 3.2 of ITU-R P.840-8 and the new model

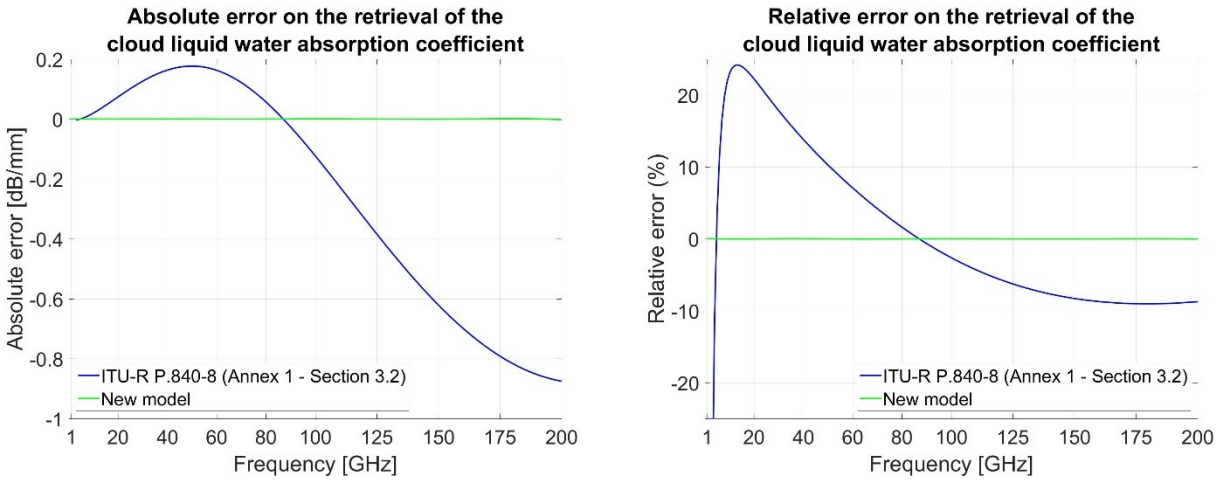

Figure 6-7 : Absolute (left) and relative (right) errors between the optimal cloud liquid water absorption coefficient and Section 3.2 of ITU-R P.840-8 and the new model

6.1.2.2 VERIFICATION AND COMPARISONS TO ITU-R P.840-8

Both Section 3.2 of ITU-R P.840-8 and the new model have been tested using the new mean annual maps provided in Section 2.2 of this document. First, the worldwide absolute and relative errors for the selected frequencies between 1 and 200 GHz are computed. Note that only points for which L_{ref} are higher than 0.01 mm have been taken into account. Some illustrations of the relative errors at 20, 40, 50 and 80 GHz are shown in Figure 6-8. Finally, Figure 6-9 highlights the absolute and relative mean and RMS errors from 1 to 200 GHz. It can be observed that for both metrics, the new model performs largely better than Sections 3.2 of ITU-R P.840-8 over the full range of frequency from 1 to 200 GHz.

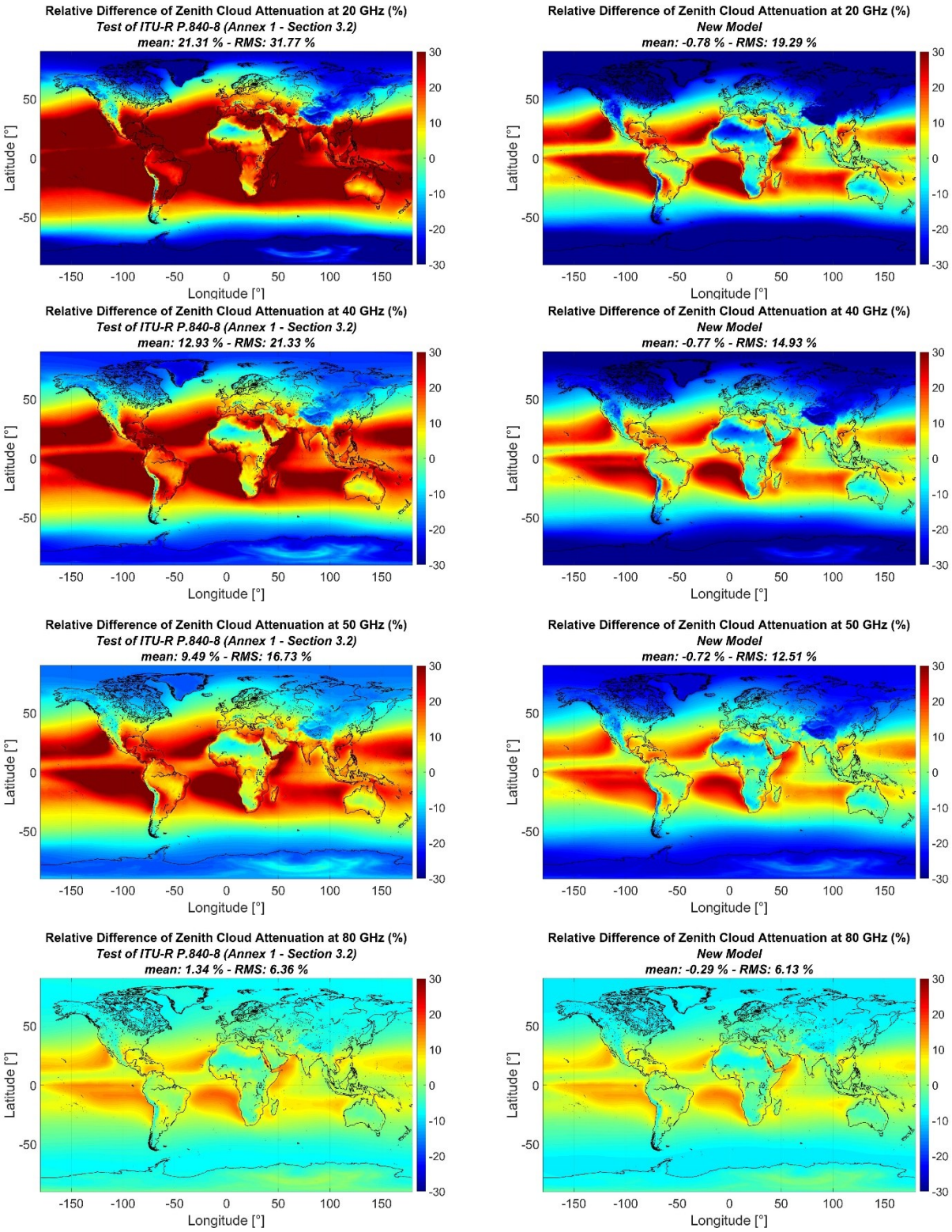

Figure 6-8 : Relative error of zenith cloud attenuation
1st line: 20 GHz, 2nd line: 40 GHz, 3rd line: 50 GHz, 4th line: 80 GHz
1st column: Section 3.2 of ITU-R P.840-8, 2nd column: new model

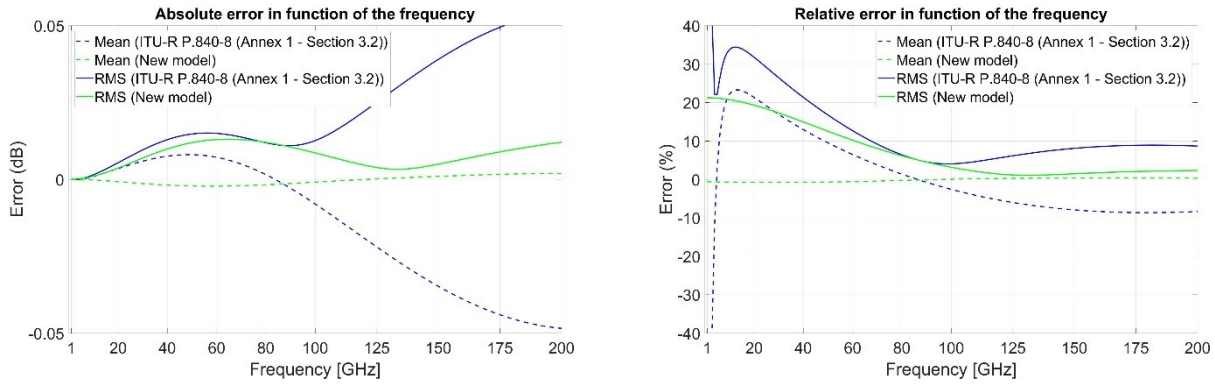

Figure 6-9 : Absolute and relative mean and RMS errors in function of the frequency

NB: Below a frequency of approximatively 2.01 GHz, the prediction method in Section 3.2 of ITU-R P.840-8 is unworkable because the values of the cloud liquid water absorption coefficient, $K_l^*(f, 273.15)$, become negative and consequently the cloud attenuation values become negative too.

6.1.2.3 TEST USING RADIOSOUNDING OBSERVATIONS (RAOBS)

To test the performances of the new instantaneous cloud attenuation prediction method with respect to Section 3.2 of ITU-R P.840-8, concurrent ILWC and attenuation due to clouds have been extracted from radiosounding observations (RAOBS) data. Ten years (2011-2020) of RAOBS on 24 different locations have been taken into account (same data than in Sections 4.1.2.3 and 0). As these RAOBS data were also used to test oxygen and water vapour attenuation prediction methods, only RAOBS for which the highest altitude level is above 25 km have been considered. The table below recalls the main information on the RAOBS dataset. The total number of RAOBS used is 80698.

Country (NOAA ID)	Site	Latitude (°N)	Longitude (°E)	Altitude (m)	Total number of RAOBS	Number of RAOBS with the highest level above 25 km
AR	BUENOS-AIRES-EZEIZA	-34.82	-58.53	20	4930	3635
AT	GRAZ	47.00	15.43	347	3106	1254
BR	GALEAO-RIO	-22.82	-43.25	6	6650	1980
CI	ABIDJAN-PORT-BOUET	5.25	-3.93	8	5569	1713
CN	BEIJING-PEKING	39.93	116.28	55	6558	677
ES	MADRID-BARAJAS	40.47	-3.58	638	6449	5637
FR	BORDEAUX-MERIGNAC	44.83	-0.70	45	6413	3267
GA	LIBREVILLE-LEON-MBA	0.45	9.42	15	2206	1037
GF	CAYENNE-ROCHAMBEAU	4.83	-52.37	9	6851	2728
GP	POINTE-A-PITRE-RAIZET	16.27	-61.52	8	4667	2247
GR	ATHENS-HELLENKION	37.90	23.73	14	2479	853
IN	CALCUTTA-DUM-DUM	22.65	88.45	6	8056	3774
IN	DELHI-SAFDARJUNG	28.58	77.20	216	9499	1537
IT	MILANO-LINATE	45.43	9.28	103	7447	6946
MX	MEXICO-CITY	19.43	-99.07	2309	7353	5073
NO	NY-ALESUND-II	78.92	11.93	8	4615	4292
PT	LISBON-GAGO-COUTINHO	38.77	-9.13	105	3208	1808
RE	SAINT-DENIS	-20.88	55.52	20	3221	1408
SG	SINGAPORE-CHANGI	1.37	103.98	16	11635	3993
US	DENVER	39.77	-104.88	1611	7270	6772
US	FAIRBANKS	64.82	-147.87	135	7264	6888
US	LAS-VEGAS	36.05	-115.18	693	7209	6553
US	MCMURDO-USA-BASE	-77.85	166.67	34	5270	225
US	MIAMI-INTL-UNIV	25.75	-80.38	4	7455	6401

As the cloud liquid water density profiles are not directly available from RAOBS, cloud detection algorithms must then be used. In the following analysis, the one described in the fascicle 3J/FAS/6 has been chosen.

First, the relative mean (Figure 6-10) and RMS (Figure 6-11) error have been computed for each site and each frequency from 1 to 200 GHz with a frequency step of 1 GHz. In both cases, the new model seems to perform better than Section 3.2 of ITU-R P.840-8.

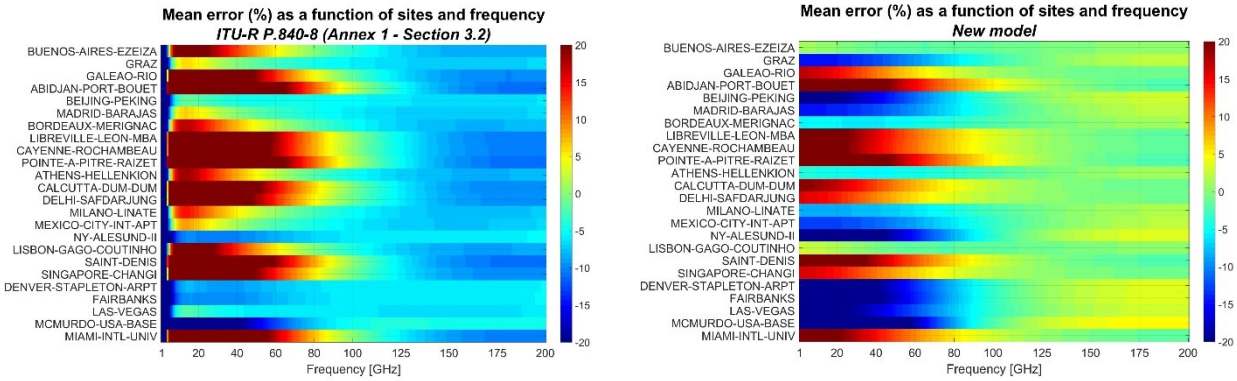

Figure 6-10 : Relative mean errors as a function of sites and frequency

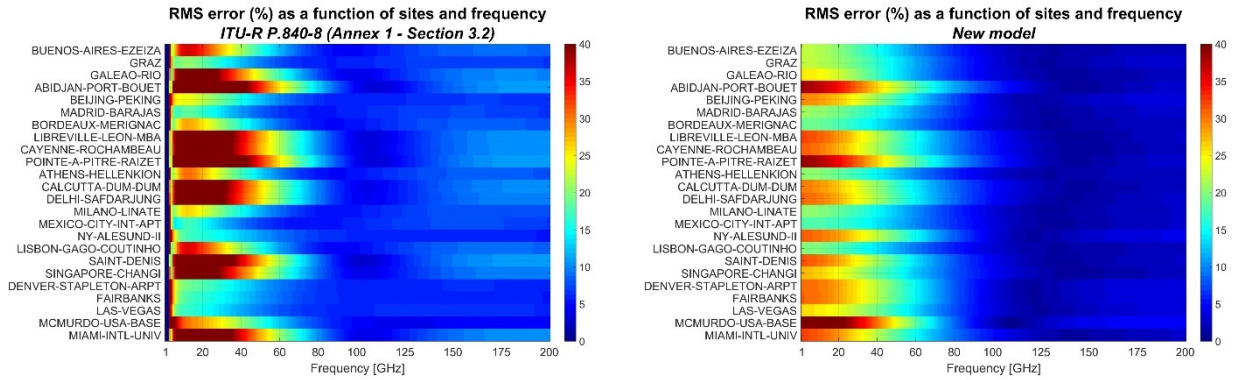

Figure 6-11 : Relative RMS errors as a function of sites and frequency

Second, the combined (for all sites) absolute and relative mean and RMS errors have been computed from 1 to 200 GHz with a frequency step of 1 GHz. The results are highlighted in Figure 6-12. It can be observed that for both metrics, the new model performs better than Section 3.2 of ITU-R P.840-8 over the full range of frequency from 1 to 200 GHz.

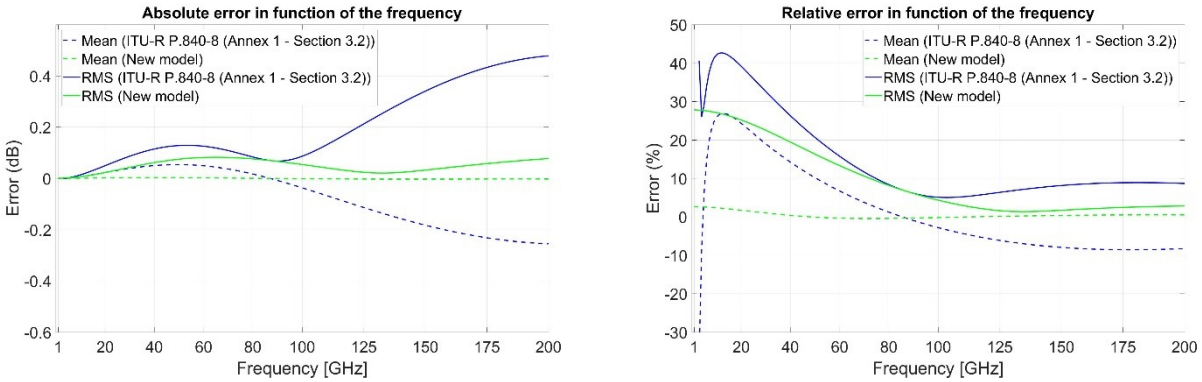

Figure 6-12 : Absolute and relative mean and RMS errors in function of the frequency

Third, the scatterplot of the retrieved cloud attenuation vs. the reference cloud attenuation is also a good performance indicator. The results at 20, 40, 80, and 150 GHz are shown in Figure 6-13. The straight black line represents the curve y=x. It can be then observed that the new model performs better than the in-force ITU-R prediction method which is in agreement with the results of Figure 6-12.

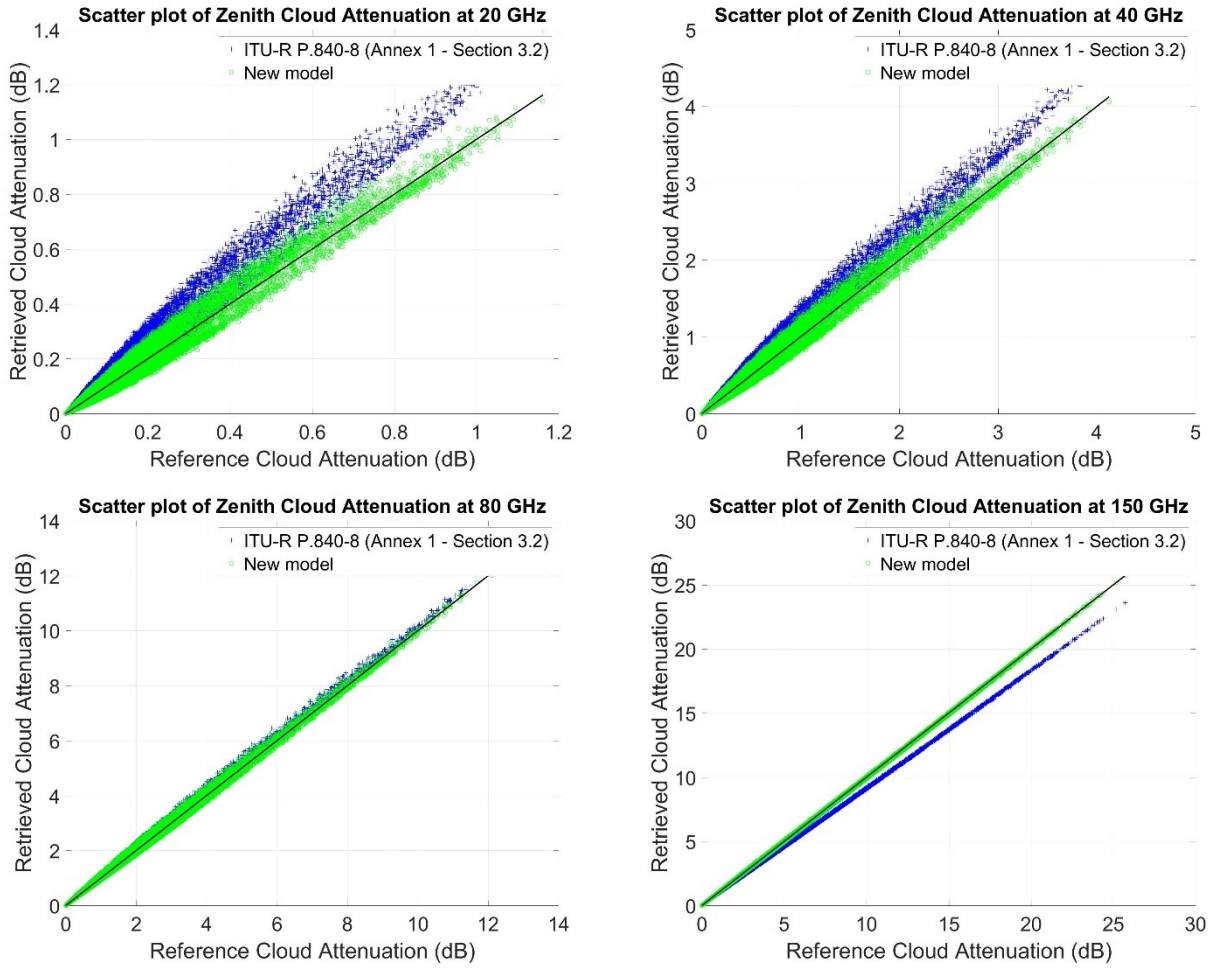

Figure 6-13 : Scatterplot of zenith cloud attenuation

Finally, CCDF of cloud attenuation (taking into account the full dataset, so disregarding the locations) have been computed. The results at 20, 40, 80, and 150 GHz are given in Figure 6-14. It can be observed a very good agreement of the new proposed model.

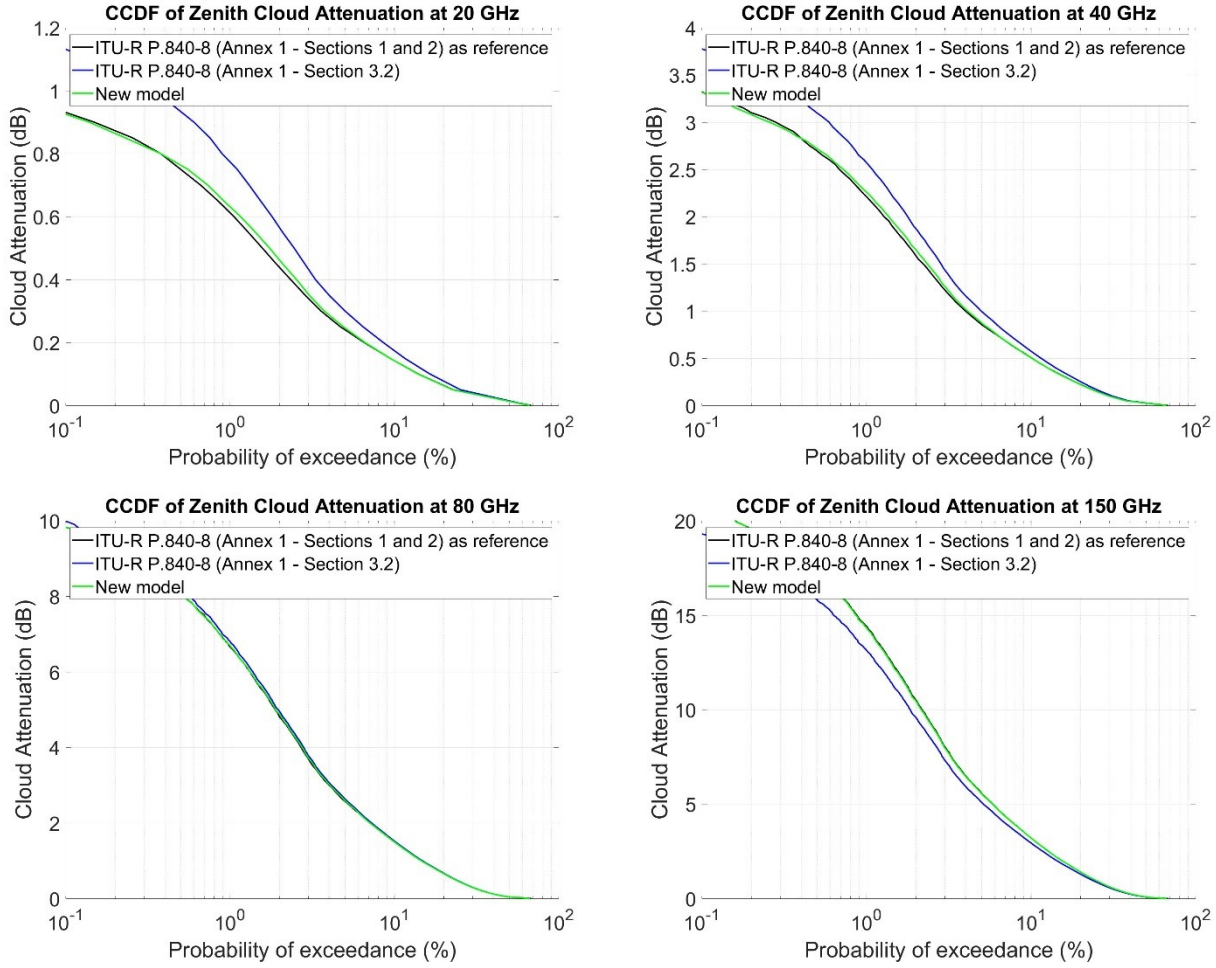

Figure 6-14 : CCDF of zenith water vapour attenuation

6.2 NEW PREDICTION METHOD OF THE STATISTICAL DISTRIBUTION OF CLOUD ATTENUATION

6.2.1 DESCRIPTION

Recalling that the new prediction method of the instantaneous cloud attenuation based on the total columnar content of cloud liquid water is (section 6.1.2.1):

$$A_C(f) = \frac{K_L(f) \cdot L}{\sin\theta}$$

it is straightforward to define a new prediction method of the statistical distribution (CCDF) of cloud attenuation based on the CCDF of the total columnar content of cloud liquid water, *L(p)*, where *p* is the probability of exceedance (in %). Indeed, as the cloud liquid water absorption coefficient depends only on the frequency of interest, the CCDF of cloud attenuation can be estimated by:

$$A_C(f,p) = \frac{K_L(f) \cdot L(p)}{\sin\theta}$$

When local data of *L(p)* is not available, the idea is now to provide to the user digital tabulated worldwide maps of *L(p)* to be able to predict the CCDF of cloud attenuation anywhere in the world. This is the goal of the next section.

6.2.2 DERIVATION OF NEW MAPS OF ILWC

In addition to the monthly averaged pressure level data described in Section 2, ERA5 also contains hourly reanalysis data on single level. As for pressure level data, the spatial resolution is 0.25° in both latitude and longitude. Among all the available parameters, the **total column of cloud liquid water** might be of interest as it seems to be equivalent to the integrated cloud Liquid Water Content, ILWC (and so equivalent to the total columnar content of cloud liquid water, *L*).

Extract from ERA5 website:

Total column cloud liquid water	$kg.m^{-2}$	This parameter is the amount of liquid water contained within cloud droplets in a column extending from the surface of the Earth to the top of the atmosphere. Rain water droplets, which are much larger in size (and mass), are not included in this parameter. This parameter represents the area averaged value for a model grid box. Clouds contain a continuum of different sized water droplets and ice particles. The ECMWF Integrated Forecasting System (IFS) cloud scheme simplifies this to represent a number of discrete cloud droplets/particles including: cloud water droplets, raindrops, ice crystals and snow (aggregated ice crystals). The processes of droplet formation, phase transition and aggregation are also highly simplified in the IFS.

Several new reference maps have then been derived from 30 years (1991-2020 that defines new climate normals) of ERA5 **hourly** data:

- The annual and monthly mean values of ILWC (in kg/m^2 equivalent to mm),
- The annual and monthly standard deviation values of ILWC (in kg/m^2 equivalent to mm),
- The annual values of ILWC (in kg/m^2 equivalent to mm) exceeded for the probability levels of 0.001, 0.002, 0.003, 0.005, 0.01, 0.02, 0.03, 0.05, 0.1, 0.2, 0.3, 0.5, 1, 2, 3, 5, 10, 20, 30, 50, 60, 70, 80, 90, 95, 99 and 100% of an average year,
- The monthly values of ILWC (in kg/m2 equivalent to mm) exceeded for the probability levels of 0.001, 0.002, 0.003, 0.005, 0.01, 0.02, 0.03, 0.05, 0.1, 0.2, 0.3, 0.5, 1, 2, 3, 5, 10, 20, 30, 50, 60, 70, 80, 90, 95, 99 and 100% of each average month.

The latitude grid is from −90° N to +90° N in 0.25° steps, and the longitude grid is from −180° E to +180° E in 0.25° steps.

As examples, Figure 6-15 shows the annual mean and standard deviation of ILWC (equivalent to the total columnar content of cloud liquid water as previously indicated) derived from 30 years (1991-2020) of ERA5 hourly reanalysis data.

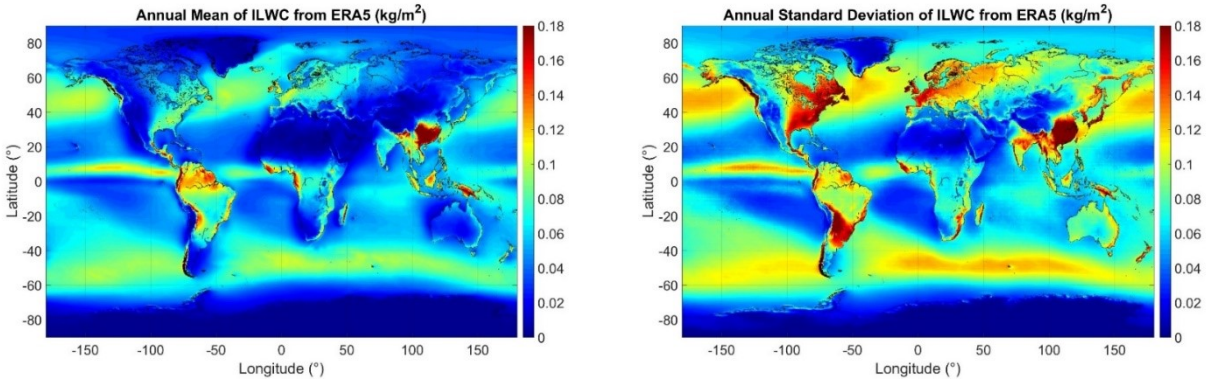

Figure 6-15 : Annual mean (left) and standard deviation (right) of Integrated cloud Liquid Water Content derived from ERA5 hourly reanalysis data (1991-2020)

The main differences between the digital maps provided by ITU-R P.840-8 and this document are summarized in the table below:

Parameters related to total column of cloud liquid water		ITU-R P.840-8	This document
Spatial resolution		**1.125°**	**0.25°**
Mean	Annual	Unavailable	Available
	Monthly	Unavailable	Available
Standard deviation	Annual	Unavailable	Available
	Monthly	Unavailable	Available
CCDF	Annual	Maps reduced to 0°C Maps from 0.1% to 99%	Maps not reduced to 0°C Maps from 0.001% to 100%
	Monthly	Maps reduced to 0°C Maps from 1% to 99%	Maps not reduced to 0°C Maps from 0.01% to 100%

Finally, some illustrations of the differences of annual zenith cloud attenuation between ITU-R P.840-8 (Annex 1 – Section 3.1) and the new prediction method (new model + new digital maps) are shown in Figure 6-16 and Figure 6-17 respectively at 20 GHz and 40 GHz for probabilities of exceedance equal to 0.1%, 1%, and 10%. It can be observed major differences especially between the tropics.

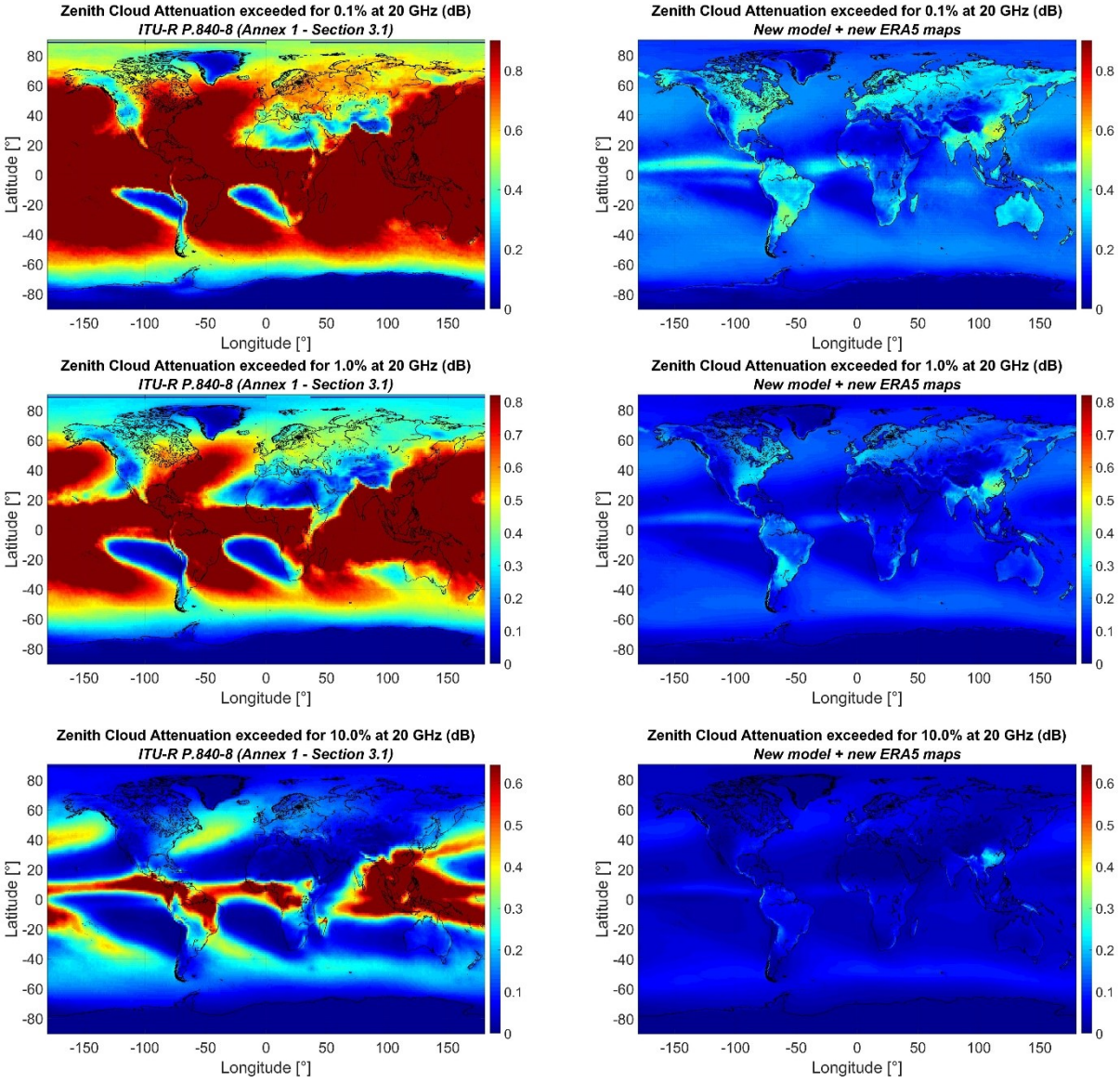

Figure 6-16 : Annual zenith cloud attenuation at 20 GHz
1st line: 0.1%, 2nd line: 1%, 3rd line: 10%
left: Section 3.1 of ITU-R P.840-8, right: new model

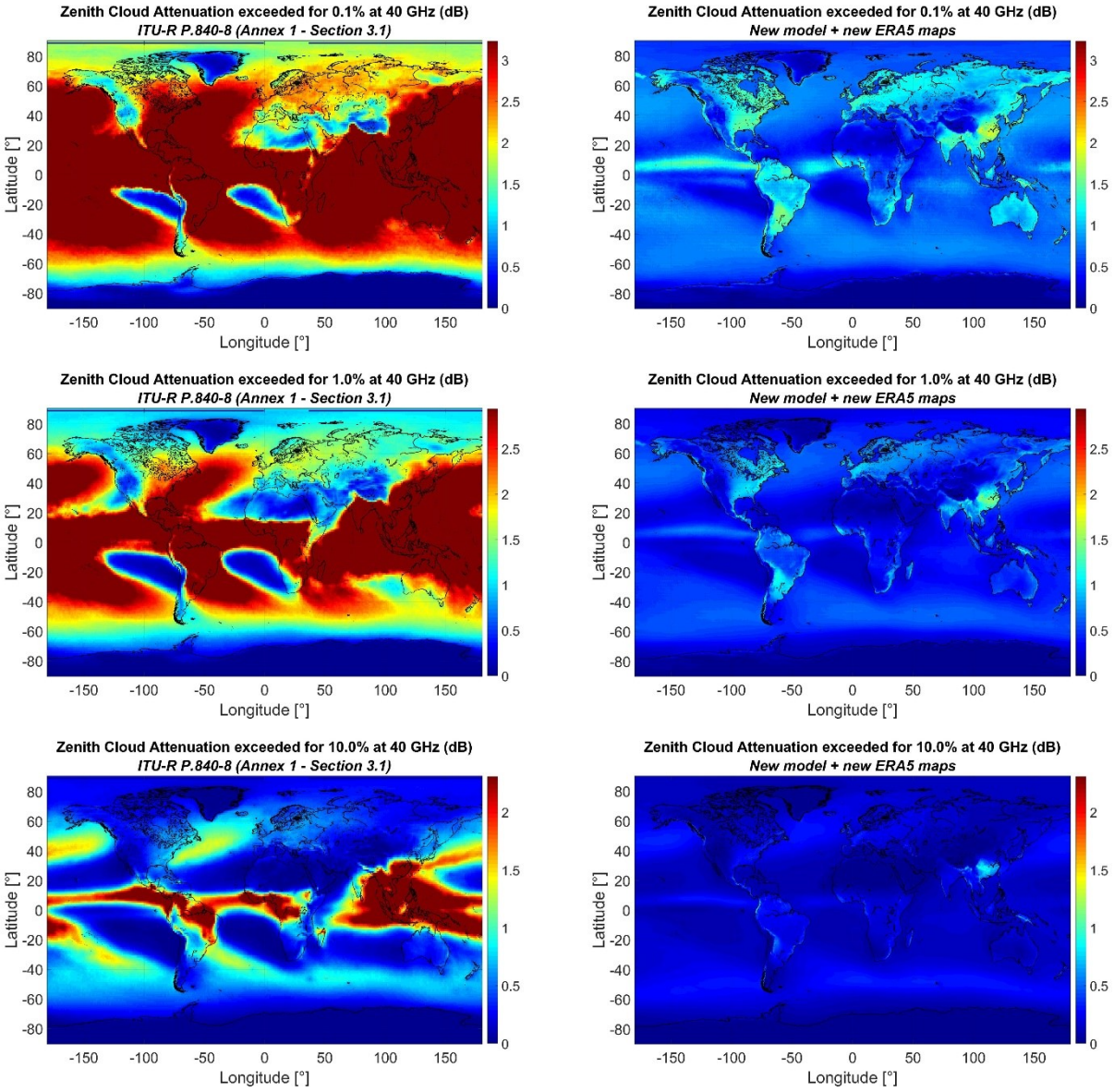

Figure 6-17 Annual zenith cloud attenuation at 20 GHz
1st line: 0.1%, 2nd line: 1%, 3rd line: 10%
left: Section 3.1 of ITU-R P.840-8, right: new model

Five specific sites have then been selected to highlight the differences of zenith cloud attenuation over the full distribution. The results are shown in Figure 6-18. As previously observed, the differences over Singapore and New Delhi (between the tropics) are very large.

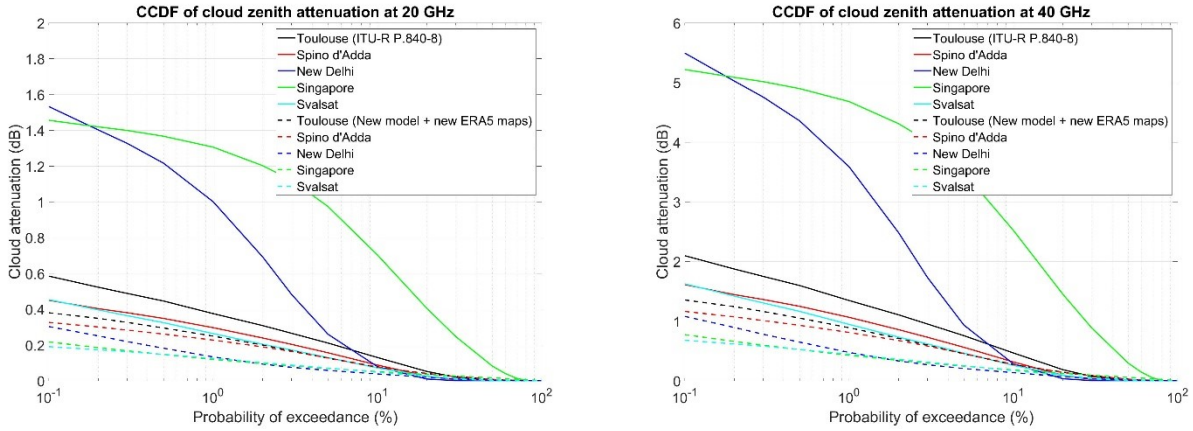

Figure 6-18 : CCDF of zenith cloud attenuation at 20 GHz (left) and 40 GHz (right)

6.2.3 DERIVATION OF NEW MAPS FOR THE APPROXIMATION OF THE STATISTICS OF ILWC BY A DIRAC LOG-NORMAL DISTRIBUTION

The annual and monthly statistics of the total columnar content of liquid water, L, can be approximated by a Dirac log-normal distribution. Mathematically, it means that:

$$\begin{cases} L(p) = e^{m_L + \sigma_L Q^{-1}\left(\frac{p}{P_L}\right)} & if \quad p < P_L \\ L(p) = 0 & if \quad p \geq P_L \end{cases}$$

where, m_L and σ_L are respectively the mean and standard deviation distribution parameters and P_L is the probability of non-zero total columnar content of liquid water. $Q^{-1}(x)$ is the inverse standard normal complementary cumulative distribution function defined in Recommendation ITU-R P.1057.

New reference digital maps of m_L, σ_L, and P_L, have then been derived from the best Dirac Log-normal regression fitting of the data provided in Section 6.2.2 of this document. To avoid numerical artefact, the probability of non-zero total columnar content of cloud liquid water actually represents the probability to exceed 0.01 mm, P_L=P(L>0.01). As for the original CCDF data, the latitude grid is from −90° N to +90° N in 0.25° steps, and the longitude grid is from −180° E to +180° E in 0.25° steps.

Figure 6-19 shows the three parameters for the approximation of the annual statistics of the total columnar content of cloud liquid water by a Dirac log-normal distribution. Figure 6-20 highlights the absolute and relative RMS errors on the regression of the Dirac Log-normal distribution.

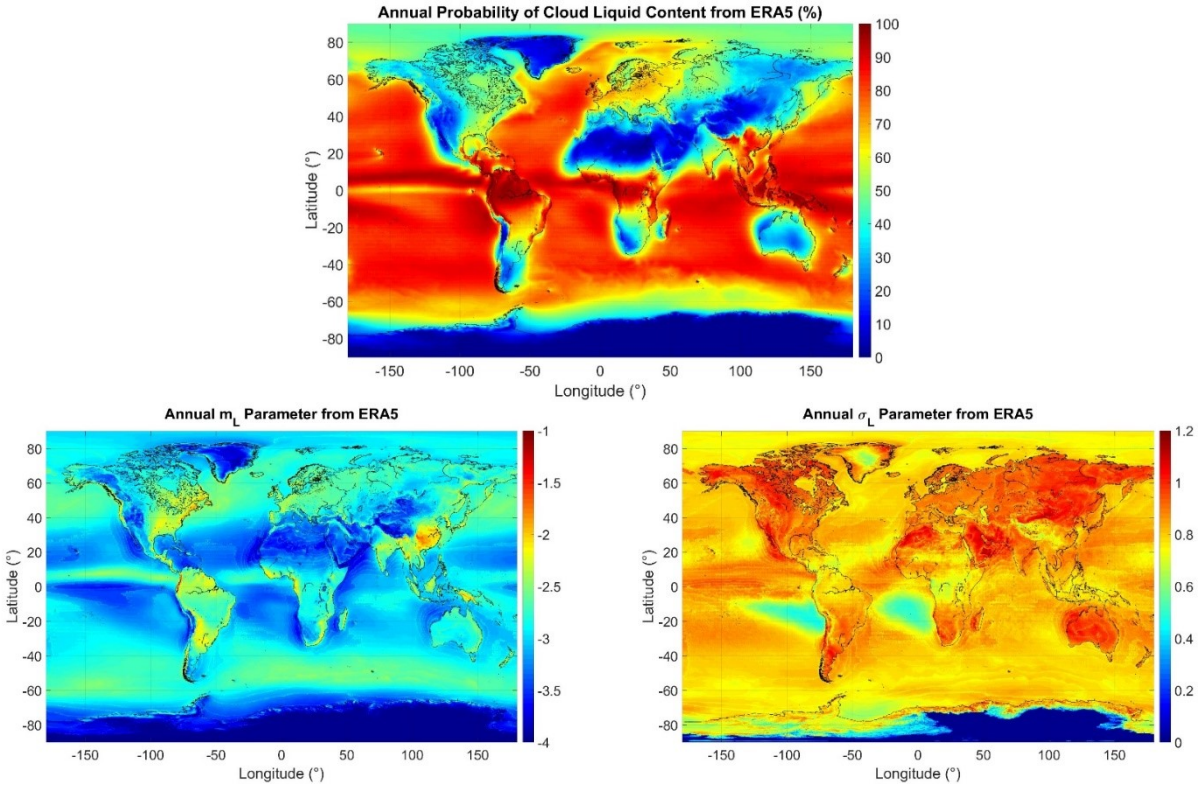

Figure 6-19 : Parameters for the approximation of the annual statistics of the total columnar content of cloud liquid water by a log-normal distribution (top: P_L, bottom left: m_L, bottom right: σ_L)

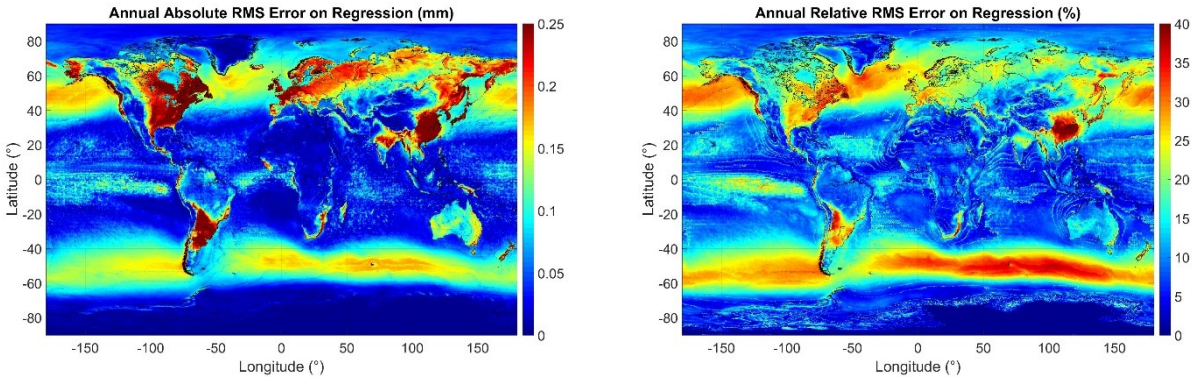

Figure 6-20 : Absolute (left) and relative (right) RMS errors on the regression of the Dirac Log-normal distribution

Examples of the approximation of the Dirac Log-normal distribution for the five specific sites (same than in the previous Section) are given in Figure 6-21.

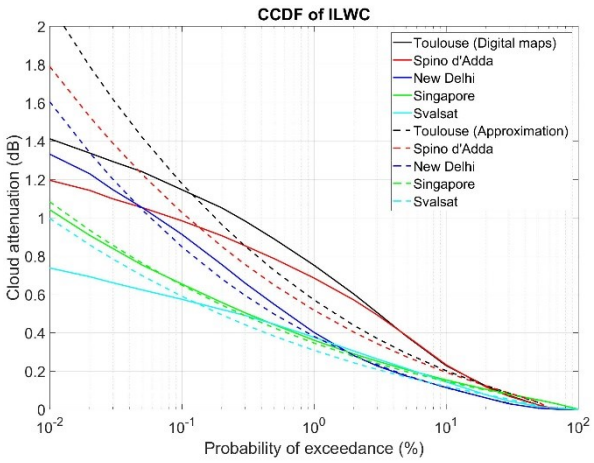

Figure 6-21 : CCDF of ILWC (digital maps and Dirac Log-normal approximation)

In Section 6.2.1, a new statistical cloud attenuation prediction method based on the CCDF of total columnar content of cloud liquid water has been proposed:

$$A_C(f,p) = \frac{K_L(f) \cdot L(p)}{\sin\theta}$$

Consequently,

$$A_C(f,p) = \frac{K_L(f) \cdot e^{m_L + \sigma_L Q^{-1}\left(\frac{p}{P_L}\right)}}{\sin\theta} = e^{ln\left(\frac{K_L(f)}{\sin\theta}\right) + m_L + \sigma_L Q^{-1}\left(\frac{p}{P_L}\right)}$$

Assuming that, for any elevation angle, θ, the probability of cloud attenuation on the slant path, P_C, can be approximated by the probability of non-zero total columnar content of liquid water, P_L, it is straightforward that the distribution of cloud attenuation can be approximated by a Dirac log-normal distribution:

$$\begin{cases} A_C(f,p) = e^{m_C(f) + \sigma_C Q^{-1}\left(\frac{p}{P_C}\right)} & if \quad p < P_C \\ A_C(f,p) = 0 \quad if \quad p \geq P_C \end{cases}$$

with

$$\begin{cases} P_C = P_L \\ \sigma_C = \sigma_L \\ m_C(f) = m_L + ln\left(\frac{K_L(f)}{\sin\theta}\right) \end{cases}$$

7 CONCLUSIONS

In this document, a synthesis of the CNES internal research activities on tropospheric instantaneous and statistical models for Earth-Space paths between 1 and 350 GHz has been given.

As far as the oxygen component is concerned:

- First, a new model to compute the **oxygen equivalent height** as a linear combination of surface meteorological parameters has been proposed. It allows the **instantaneous oxygen attenuation** to be retrieved only from **surface meteorological parameters**. It shows better performances than the equivalent prediction method recommended in ITU-R P.676-12.
- Second, a new model to compute the **statistical distribution of the oxygen attenuation** has been derived. It shows a fair agreement when compared with the performances of the new instantaneous prediction method. Note that no prediction method of the statistical distribution of oxygen attenuation is currently proposed in an ITU-R Recommendation.
- Finally, **new annual and monthly digitals maps of the surface meteorological parameters** (surface pressure, surface temperature and surface water vapour density) have been derived from 30 years (1991-2020) of the ECMWF ERA5 reanalysis database. The mean, the standard deviation and the full CCDF are now available.

As far as the water vapour component is concerned:

- First, a new model to compute the **water vapour equivalent height** has been proposed. It allows the **instantaneous water vapour attenuation** to be retrieved only from the **surface meteorological parameters**. It shows better performances than the equivalent prediction method recommended in ITU-R P.676-12 while being more simple as it only depends on the frequency.
- Second, a new model to compute the **water vapour absorption coefficient** has been proposed. It allows the **instantaneous water vapour attenuation** to be retrieved from the **total columnar content of water vapour (IWVC)**. It shows better performances than the equivalent prediction method recommended in ITU-R P.676-12. It is also more accurate than the prediction methods based on the water vapour equivalent height.
- Third, a new model to compute the **statistical distribution of the water vapour attenuation** has been derived. It shows a fair agreement when compared with the performances of the new instantaneous prediction method and better performances than the equivalent prediction method recommended in ITTU-R P.676-12.

- Fourth, **new annual and monthly digitals maps of the total columnar content of water vapour (IWVC)** have been derived from 30 years (1991-2020) of the ECMWF ERA5 reanalysis database. The mean, the standard deviation and the full CCDF are now available.
- Finally, **new annual and monthly digital maps for the approximation of the statistical distribution of IWVC by a Weibull distribution** have been derived. They can also be used for the approximation of the statistical distribution of water vapour attenuation by a Weibull distribution

As far as the cloud component is concerned:

- First, a new model to compute the **cloud liquid water absorption coefficient** has been proposed. It allows the **instantaneous cloud attenuation** to be retrieved from the **total columnar content of cloud liquid water (ILWC)**. It shows better performances than the equivalent prediction method recommended in ITU-R P.840-8.
- Second, a new model to compute the **statistical distribution of the cloud attenuation** has been straightforwardly derived.
- Third, **new annual and monthly digitals maps of the total columnar content of cloud liquid water (ILWC)** have been derived from 30 years (1991-2020) of the ECMWF ERA5 reanalysis database. The mean, the standard deviation and the full CCDF are now available.
- Finally, **new annual and monthly digital maps for the approximation of the statistical distribution of ILWC by a Dirac Log-normal distribution** have been derived. They can also be used for the approximation of the statistical distribution of cloud attenuation by a Dirac Log-normal distribution

The work will be presented during ITU-R SG3, WP3J and WP3M meetings. In particular, the work will be discussed within three ITU-R SG3 Correspondence Groups:

- CG 3J-11 (Reference standard atmospheres in Rec. ITU-R P.835)
- CG 3J-1 (Gaseous attenuation)
- CG 3J-3M-5 (Effect of clouds and precipitation on attenuation and depolarization on slant paths)

The following table summarizes all the new prediction methods of oxygen, water vapour and cloud attenuation proposed in this document.

	Instantaneous prediction method	Statistical prediction method	Approximation
Oxygen attenuation	$A_O(f) = \frac{\gamma_o(f, P_s, T_s, \rho_{w_s}) \cdot h_o(f, T_s, P_s, \rho_{w_s})}{\sin\theta}$ with $h_o(f, T_s, P_s, \rho_{w_s}) = a_o(f) + b_o(f) \cdot T_s + c_o(f) \cdot P_s + d_o(f) \cdot \rho_{w_s}$	$A_O(f,p) = \frac{\gamma_o(f, \overline{P_s}, \overline{T_s}, \overline{\rho_{w_s}}) \cdot h_o(f, T_s(p), P_s(p), \rho_{w_s}(p))}{\sin\theta}$ with $h_o\left(f, T_s(p), P_s(p), \rho_{w_s}(p)\right) = a_o(f) + b_o(f) \cdot T_s(p) + c_o(f) \cdot P_s(p) + d_o(f) \cdot \rho_{w_s}(p)$	
Water vapour attenuation	$A_W(f) = \frac{\gamma_w(f, P_s, T_s, \rho_{w_s}) \cdot h_w(f)}{\sin\theta}$ with $h_w(f) = A \cdot f + B + \sum_{i=1}^{3} \frac{a_i}{(f - f_i)^2 + b_i}$		
	$A_W(f) = \frac{K_V(f, \rho_{w_s}, T_s, P_s) \cdot V}{\sin\theta}$ with $K_V(f, \rho_{w_s}, T_s, P_s) = a_V(f) + b_V(f) \cdot \rho_{w_s} + c_V(f) \cdot T_s + d_V(f) \cdot P_s$	$A_W(f,p) = \frac{K_V(f, \overline{\rho_{w_s}}, \overline{T_s}, \overline{P_s}) \cdot V(p)}{\sin\theta}$ with $K_V(f, \overline{\rho_{w_s}}, \overline{T_s}, \overline{P_s}) = a_V(f) + b_V(f) \cdot \overline{\rho_{w_s}} + c_V(f) \cdot \overline{T_s} + d_V(f) \cdot \overline{P_s}$	$A_W(f,p) = \lambda_W(f) \left(-ln\left(\frac{p}{100}\right)\right)^{\frac{1}{k_W}}$ with $\begin{cases} \lambda_W(f) = \lambda_{V_s} \frac{K_V(f, \overline{\rho_{w_s}}, \overline{T_s}, \overline{P_s})}{\sin\theta} e^{-\frac{Z - h_S}{h_{VSC}}} \\ k_W = k_{V_s} \end{cases}$
Cloud attenuation	$A_C(f) = \frac{K_L(f) \cdot L}{\sin\theta}$ with $K_L(f) = K_l(f, T = 273.75K) \cdot \left(A_1 e^{-\frac{(f-\mu_1)^2}{\sigma_1}} + A_2 e^{-\frac{(f-\mu_2)^2}{\sigma_2}} + A_3\right)$	$A_C(f,p) = \frac{K_L(f) \cdot L(p)}{\sin\theta}$ with $K_L(f) = K_l(f, T = 273.75K) \cdot \left(A_1 e^{-\frac{(f-\mu_1)^2}{\sigma_1}} + A_2 e^{-\frac{(f-\mu_2)^2}{\sigma_2}} + A_3\right)$	$\begin{cases} A_C(f,p) = e^{m_C(f) + \sigma_C Q^{-1}\left(\frac{p}{P_C}\right)} & if \quad p < P_C \\ A_C(f,p) = 0 & if \quad p \geq P_C \end{cases}$ with $\begin{cases} P_C = P_L \\ \sigma_C = \sigma_L \\ m_C(f) = m_L + ln\left(\frac{K_L(f)}{\sin\theta}\right) \end{cases}$

8 REFERENCES

[1] https://cds.climate.copernicus.eu/cdsapp#!/dataset/reanalysis-era5-single-levels?tab=overview

[2] https://confluence.ecmwf.int/display/CKB/ERA5%3A+data+documentation

[3] Buck, Model CR-1A hygrometer with autofill. Operating manual. Buck Research Instruments, LLC. May 2012

9 ACKNOWLEDGEMENT

The author would like to thank the colleagues from the ITU-R SG3 Correspondence Groups CG 3J-1, CG 3J-11 and CG 3J-3M-5 and in particular Harvey Berger, Antonio Martellucci, Carlo Riva, Lorenzo Luini, and George Brost for their support in the CNES propagation activities. The author is also very grateful to the colleagues from ONERA for checking the work.

END OF DOCUMENT